Experiments were performed by MIC to compare the initiation of SCC on unpeened U-bend surfaces with SCC initiation in U-bends treated with ALP. Room temperature IGSCC tests were performed for Alloy 600 welded U-bends in three conditions: as-received (with no peening), sensitized (with no peening) and sensitized (with laser-peening). Without laser peening, the as-received coupon cracked within two days while the sensitized one cracked after immersion in the thiosulfate solution for one day. Both U-bends cracked near the center of the weld beads. Half of the second sensitized U-bend was peened on the top and side surfaces with an irradiance of 10 GW/cm^2 and 200% coverage (as in Figure A-99). Following the peening, the fixture bolt was tightened, further stressing the outer side of the U-bend. When the U-bend is tensioned by loading the laser peened region will remain in compression but the untreated region will go into tension due to the loading. The unpeened half of the specimen developed hairline cracks after two days of exposure in thiosulfate solution, while no cracks were observed on the laser peened surface. Cracks growing from the unpeened side appear to stop prior to reaching the laser peened area (Figure A-100). These results justify the importance of applying ALP to areas initially in a tensile stress state.

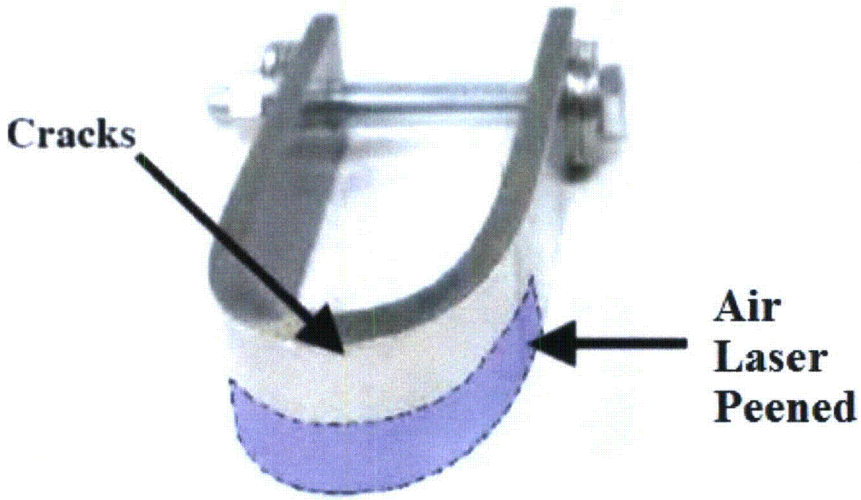

Figure A-99
Partial air laser peening of coupon subsequently loaded by tightening the fixture bolt

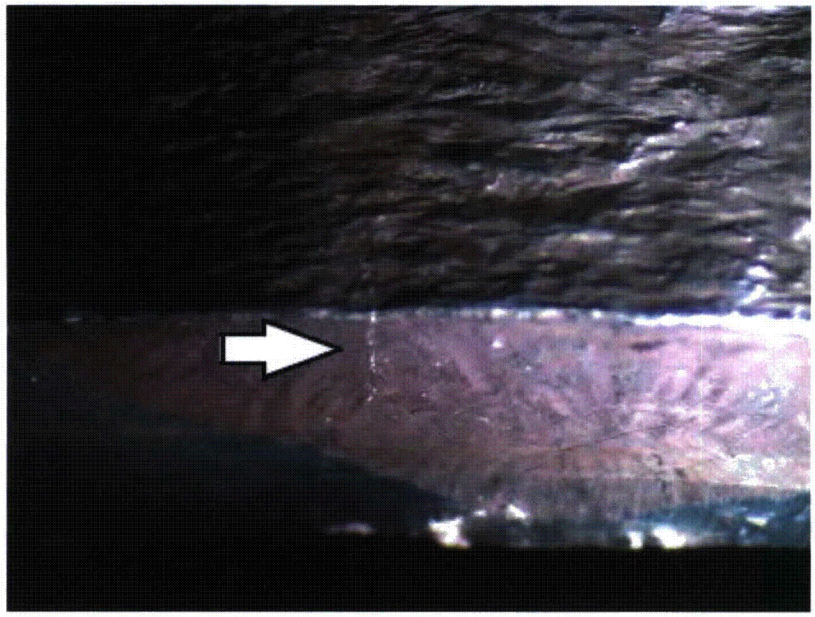

Figure A-100
IGSCC crack observed in the unpeened region arrests at the ALP-treated region

A.2.2 Effects of peening to metal surface with pre-existing flaws

All four vendors have performed a number of tests on effects of peening of surfaces with pre-existing flaws. There are two potential concerns to consider regarding peening of surfaces with flaws: 1) does the peening application process aggravate the existing flaws; and 2) with pre-existing flaws, is peening still effective at mitigating growth of the SCC? The section below describes the R&D work performed to address these two concerns.

A.2.2.1 Evaluation of the impact of the application process to existing cracks

Toshiba performed stress corrosion cracking tests on Alloy 600 and Type 304 stainless steel specimens, both of which had been heat treated. Specimens of both alloys were subjected to 0.5% tensile stress by setting them into jigs and then they were exposed to cracking fluids. The Alloy 600 samples were cracked in boiling tetrathionate solution, and the Type 304 stainless steel samples were cracked in boiling magnesium chloride solution. Then, one specimen of each alloy was treated with ULP, while another specimen of each alloy was left unpeened. The crack depths in all four specimens were measured, and, for each alloy, the crack depth distribution for the peened specimen was compared with that of the unpeened specimen by a t-test. For both specimens, there was no difference found between the peened and unpeened specimens, indicating that the ULP application process does not cause crack growth. The procedure and results for the Type 304 stainless steel and the Alloy 600 are shown in Figure A-101 and Figure A-102 respectively.

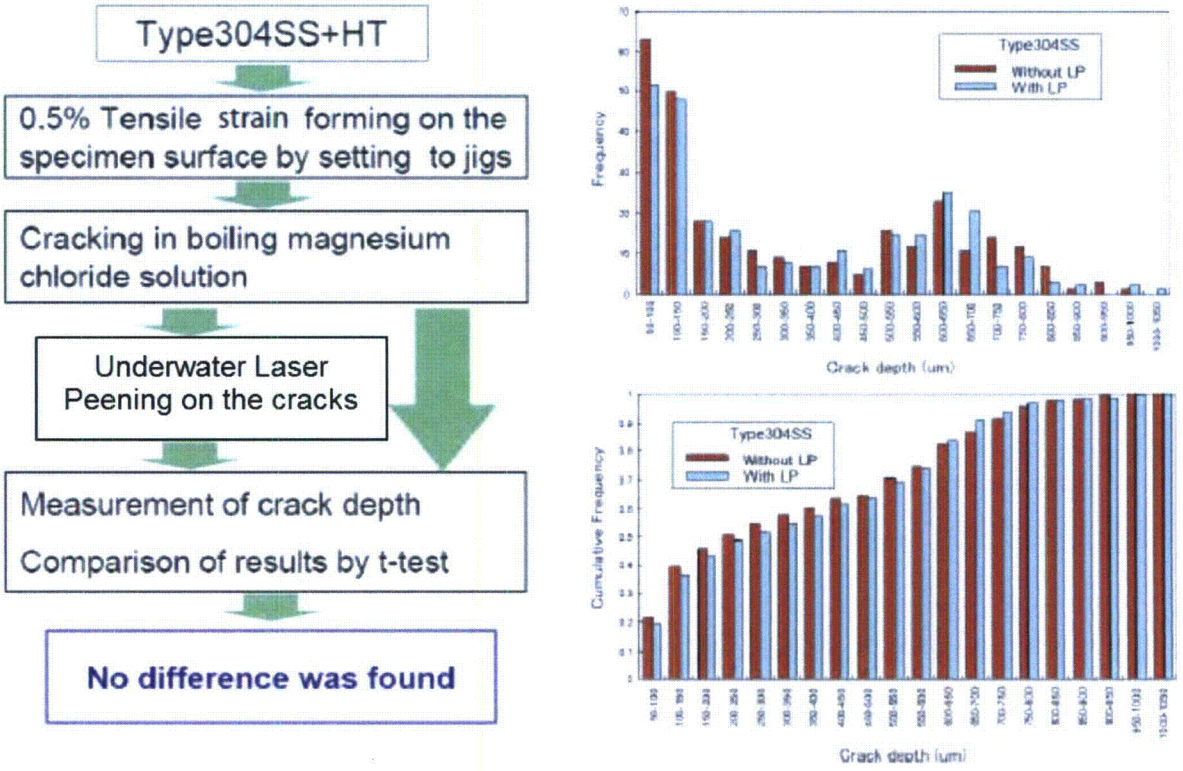

Figure A-101
Test procedure and crack depth distribution for SCC testing of Type 304 stainless steel

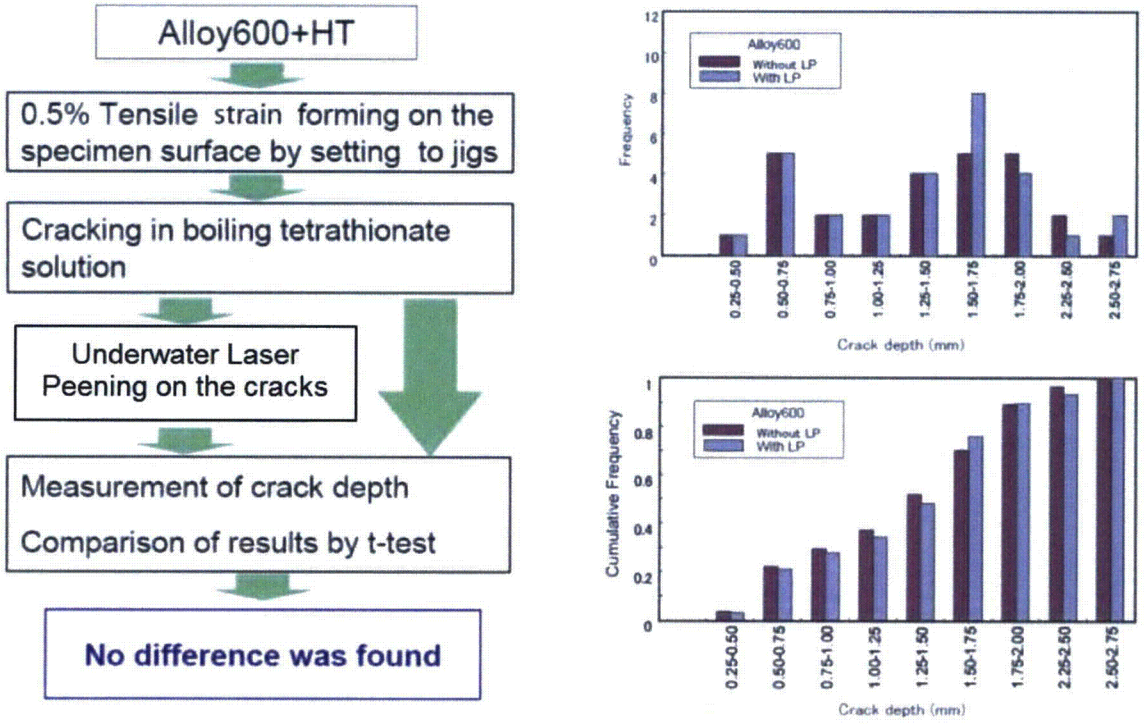

Figure A-102
Test procedure and crack depth distribution for SCC testing of Alloy 600

MHI has performed tests to ensure that the application process of WJP treatment causes no adverse effects on existing defects such as cracks. In order to demonstrate this, SCC cracks were induced in Alloy 600 test coupons prior to the application of the WJP process. SCC cracks of 0.6 mm, 0.8 mm, 1.2 mm and 2.0 mm in depth were produced for this study. These samples with SCC cracks were treated by WJP. After the WJP treatment, these samples were heat-tinted for temper coloring and then ruptured to open up the crack faces. Inspection of the fracture face was performed to determine if the crack had propagated due to the application process of WJP treatment. If the WJP process caused the crack to grow, a ductile fracture would be evident at the tinted fracture surface. Figure A-103 shows the test procedure that was used for this testing.

No crack propagation occurred as a result of WJP treatment in any of the test samples, Figure A-104 clearly shows no ductile cracking in front of the tip of a pre-existing 2.0 mm SCC crack. The lack of a ductile feature indicates that application process of WJP treatment did not cause crack propagation.

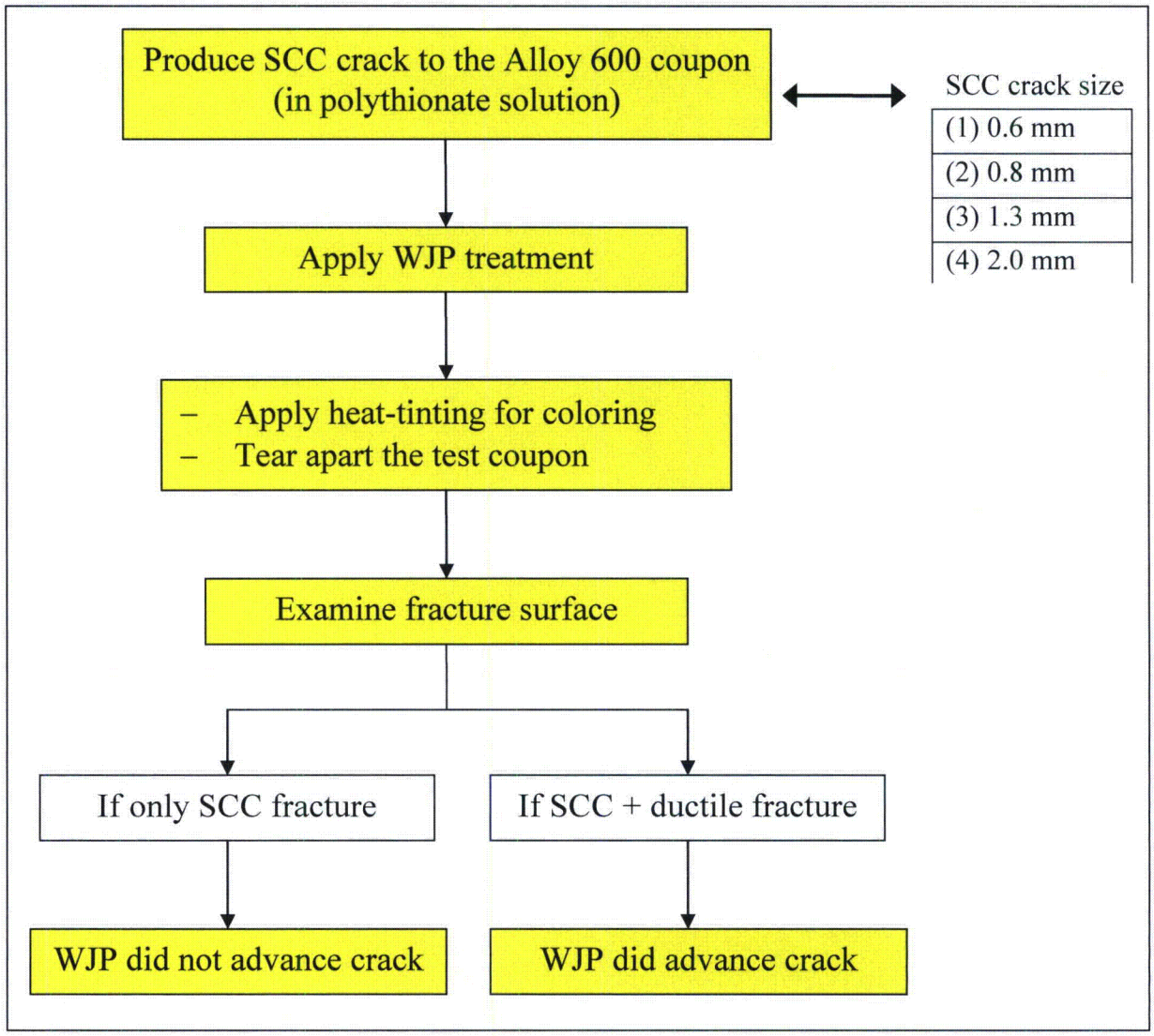

Figure A-103
Test procedure for testing WJP on existing defects, provided by Mitsubishi

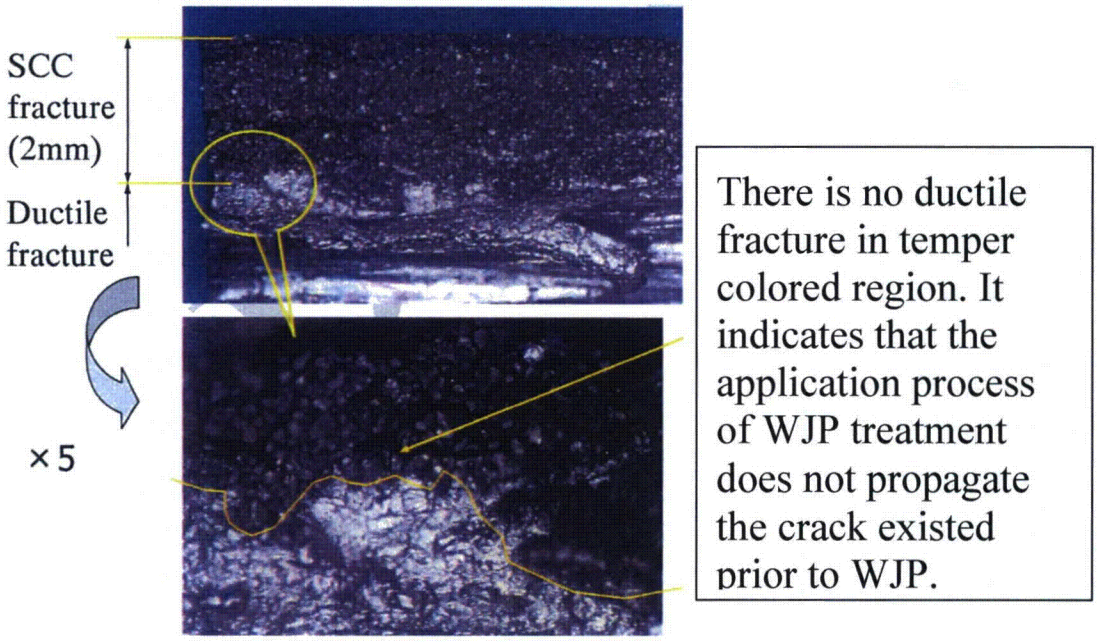

Figure A-104
Test results of investigation on the effect of WJP application process on existing defects, provided by Mitsubishi

A.2.2.2 Effectiveness of peening in mitigating further growth of pre-existing SCC cracks

Toshiba performed CBB SCC tests to verify the effectiveness of ULP on a surface with pre-existing defects. Sensitized Type 304 stainless steel with 20% cold work was used in Toshiba's verification test. SCC pre-cracks were generated in all CBB coupons prior to ULP treatment. These CBB coupons with SCC cracks were divided into three groups: TP-A, TP-B, and TP-C. TP-A included pre-crack coupons that were not subjected to further treatment or SCC testing. TP-B included pre-crack coupons that were treated with ULP, and then exposed to simulated BWR water for 500 hours. TP-C included pre-crack coupons that did not receive ULP treatment, but were exposed to simulated BWR water for 500 hours. The strain of the CBB coupons was 0.5%, and the simulated BWR water contained 8 ppm DO at 288°C. A summary of the CBB test results is shown in Figure A-105. Measurements of crack size were performed before and after the SCC test.

The SCC test results are summarized in Figure A-105, with measurement results of crack sizes plotted as "Cumulative Probability" versus "Crack Depth." Measurements of crack size in TP-A samples provided the size distribution before the 500 hour SCC test, and all SCC pre-cracks were shallower than 1 mm with an average at 0.40 mm. Measurements of TP-B and TP-C sample provided crack size distributions after 500 hours in the SCC test. Figure A-105 clearly indicates that with ULP treatment, pre-existing cracks did not advance during 500 hours in a simulated

BWR environment (TP-A vs. TP-B). Without ULP treatment, a noticeable increase in crack size was observed after 500 hours in a simulated BWR environment (TP-A vs. TP-C).

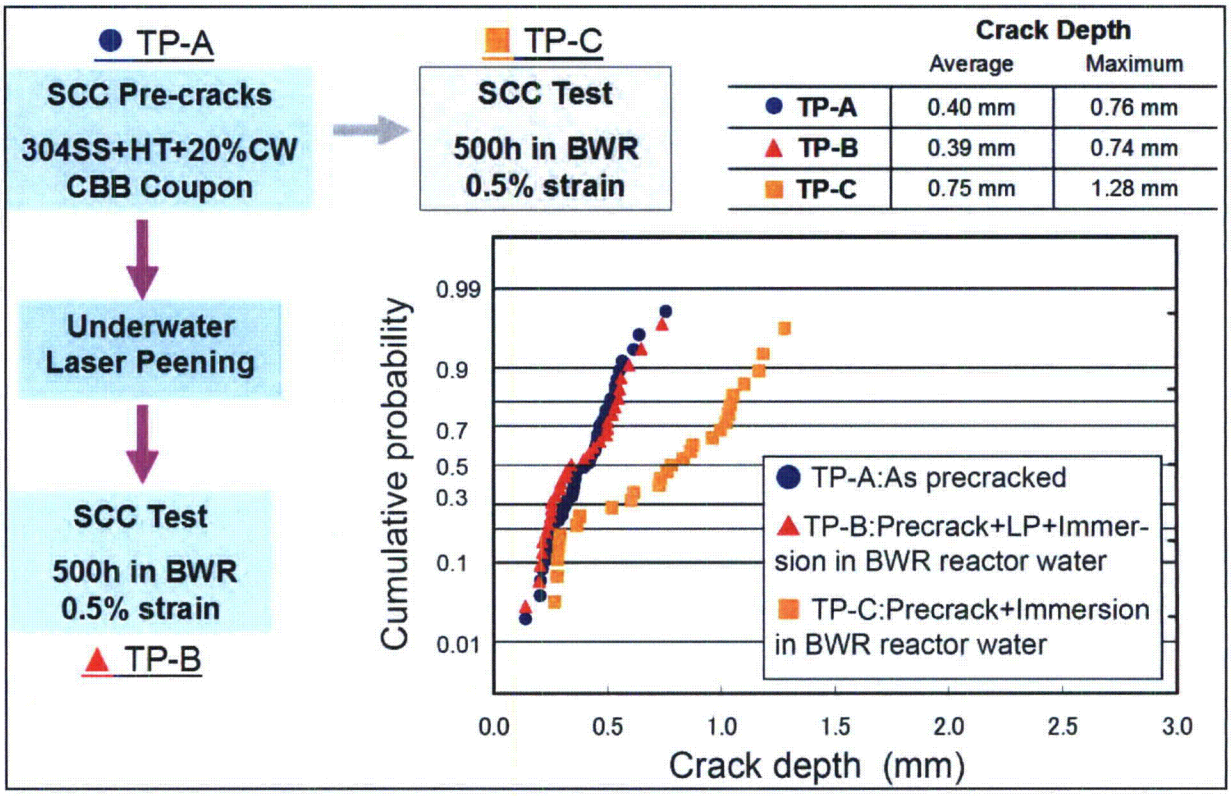

Figure A-105
Toshiba's CBB test for assessing the effectiveness of ULP to a surface with pre-existing defects—The final SCC test was performed in a simulated BWR environment with 8 ppm DO at 288°C for 500 hours. The strain applied in CBB test was 0.5%

Hitachi-GE also performed several SCC tests to verify the effectiveness of WJP treatment on surfaces with pre-existing defects. Figure A-106 shows the scheme and the result of a CBB test using Alloy 182 coupons. The pre-cracks were generated by fatigue, with crack sizes of 1.5 mm, 3.5 mm and 5.5 mm in depth. The pre-cracked coupons were fit into a CBB test jig, and WJP treatment was applied to the surfaces of the CBB coupons. After receiving the WJP treatment, the CBB coupons were exposed to high purity water with 2.0 ppm DO at 288°C for 1000 hours and a constant strain of 0.2%.

The test result indicated that for cracks sized at 1.5 mm and 3.5 mm in depth, WJP was effective at preventing SCC crack growth. When the crack size was too large (5.5 mm), i.e. deeper than the compressive stress layer, WJP became not effective at mitigating SCC growth, Figure A-106. The crack depths presented in Figure A-106 indicate the differences between the crack depth at the end of the stress corrosion cracking testing and the pre-crack depth. The crack growth rate for the deeper cracks in the peened case was similar to the crack growth rate in the unpeened case, showing that WJP does not significantly accelerate the growth of cracks deeper than the

compressive stress layer.[8] Furthermore, the results of this test show that no flaw growth was produced by the peening application itself.

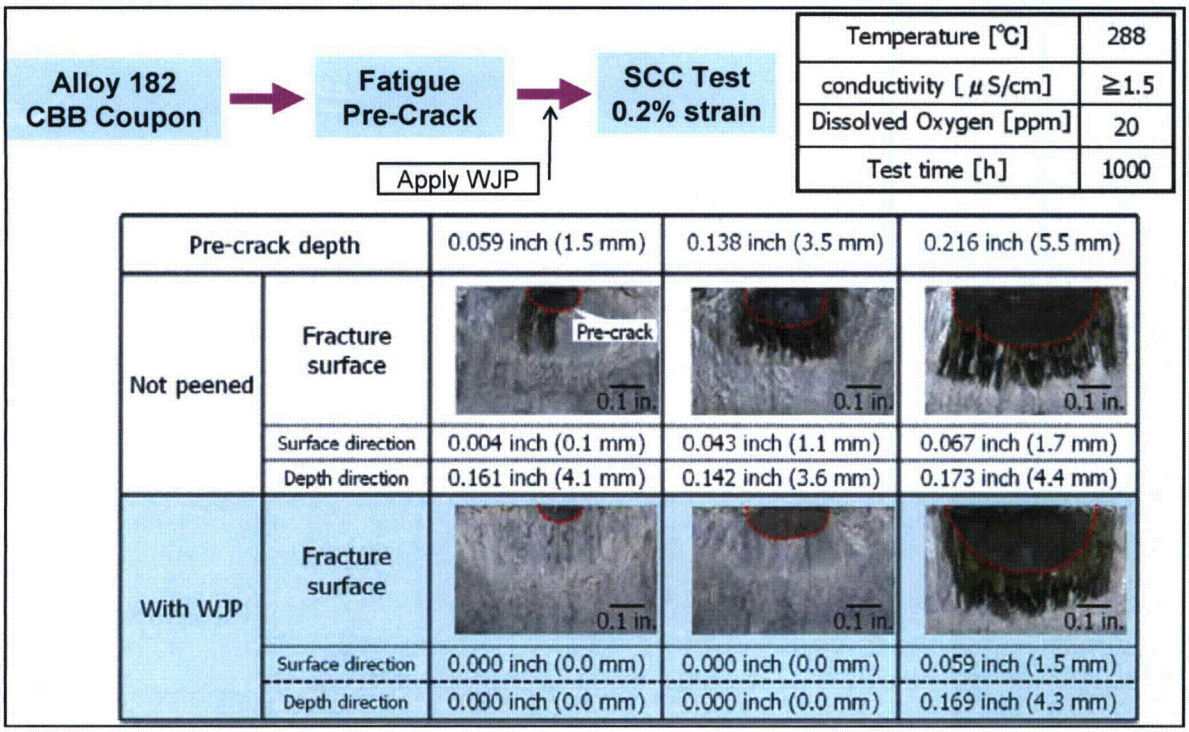

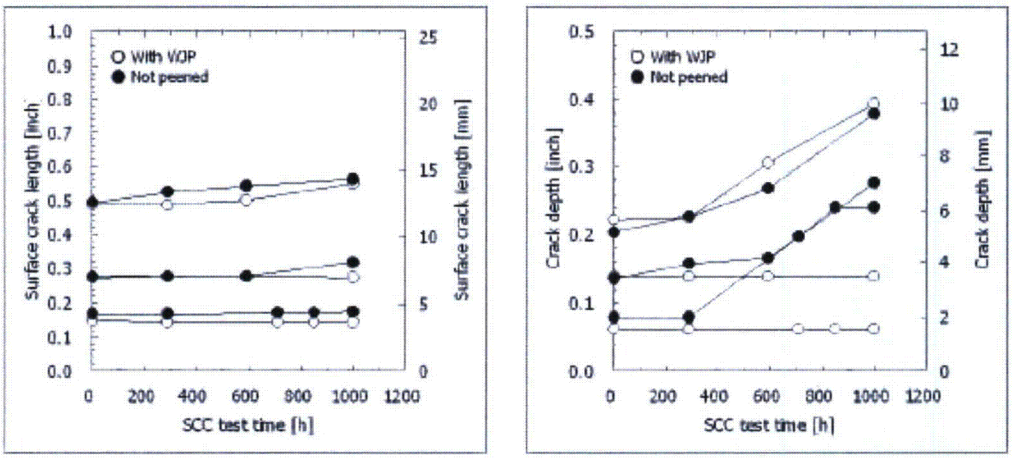

Figure A-106
Hitachi-GE investigation of effectiveness of WJP to a surface with pre-existing cracks, provided by Hitachi-GE

[8] The plot on the right side of Figure A 106 shows a single crack that may appear to have grown slightly faster than for the unpeened case. The data on the plot indicate that the peened crack was about 9% longer than the unpeened crack at the start of the test and was about 5% longer at the end of the test, indicating that it did not really grow faster than the unpeened crack over the full test time. In addition, it is noted that the difference in length at the end of the test, 5%, is well within the normal scatter for SCC crack growth rate tests, and is not significant.

Hitachi-GE performed experiments CBB testing on pre-cracked sensitized Type 304 stainless steel as another assessment of the effectiveness of WJP treatment on surfaces with pre-existing defects. Figure A-107 shows the scheme and the result of the CBB test using a maximum pre-crack depth 0.4 mm (0.016 in) in sensitized Type 304 S.S. material. The crack depths in the peened specimens did not exceed the crack depths measured in the unpeened specimens. The surface cracks did not propagate on the specimens treated with WJP both in a speed of 40 min/m (61 s/in) and in a speed of 60 min/m (91 s/in), to which CBB test was performed for 1500 h, as shown in Figure A-108. In this test, no crack propagation was found on the specimens. This result also shows that WJP does not accelerate crack propagation and has no adverse effect to the pre-existing crack.

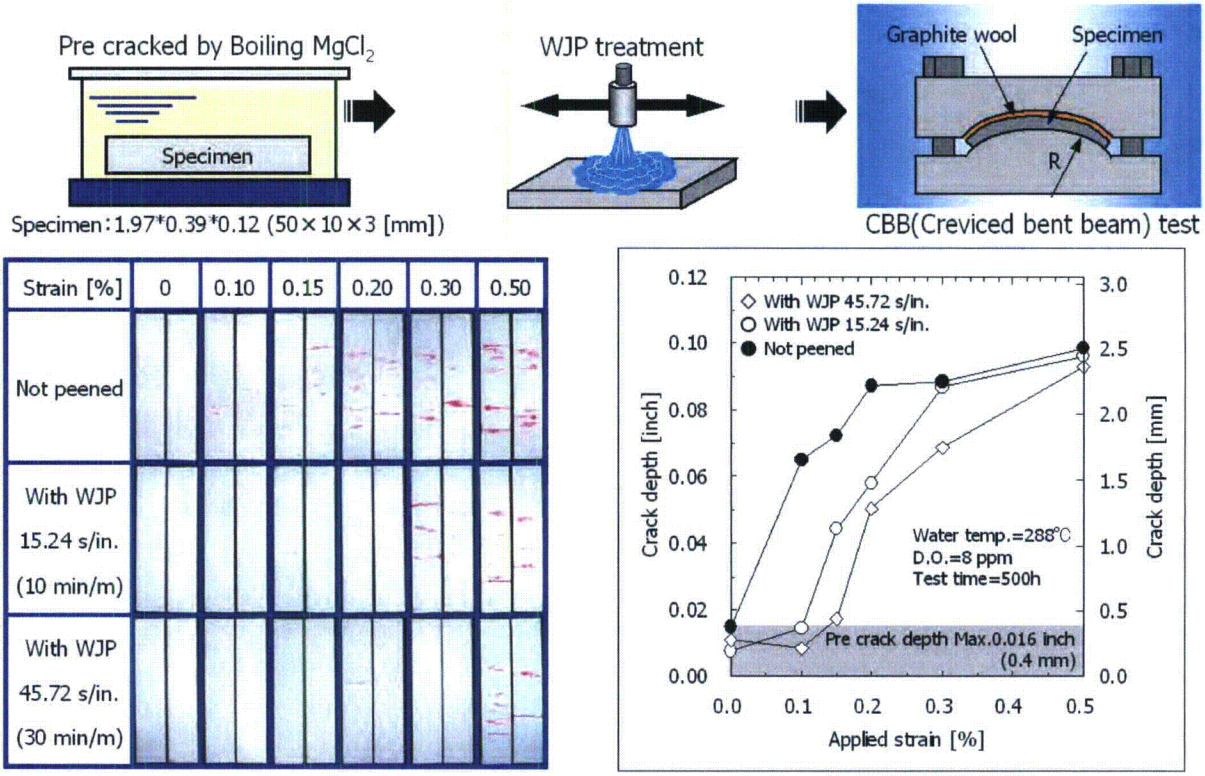

Figure A-107
Creviced Bent Beam (CBB) test on pre-cracked sensitized Type 304 stainless steel, provided by Hitachi-GE

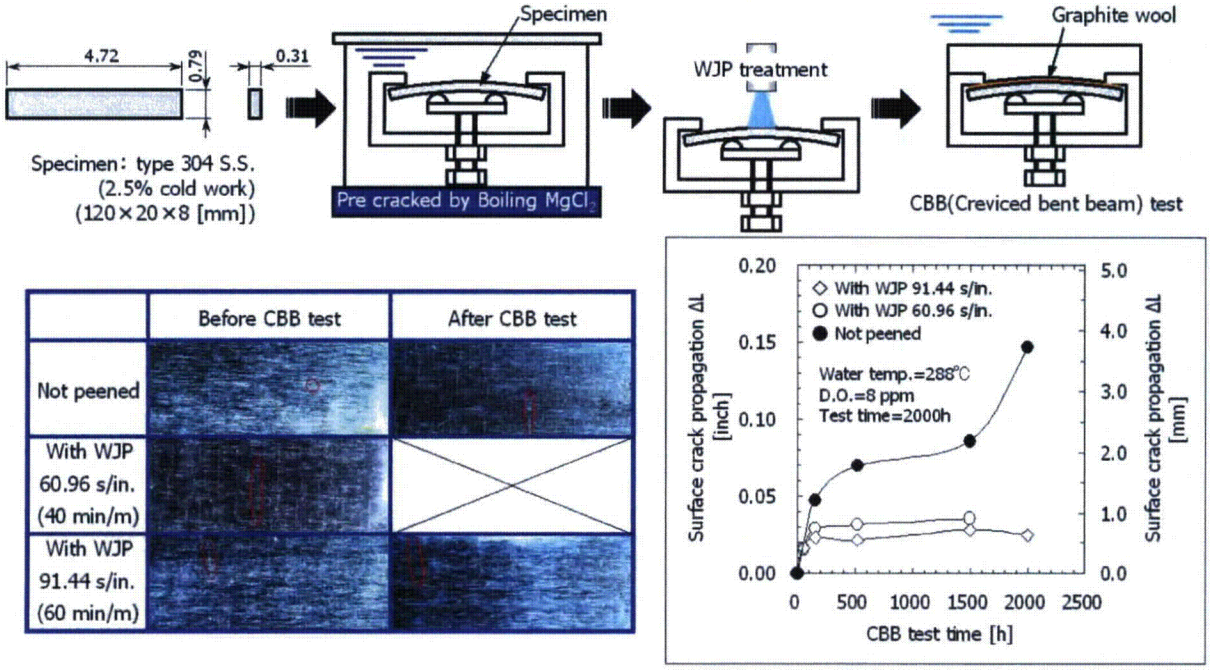

Figure A-108
Creviced Bent Beam (CBB) test on the effect of WJP on surface crack propagation, provided by Hitachi-GE

In order to assess how the growth behavior of pre-existing cracks is affected by WJP treatment, MHI performed SCC growth tests on WJP treated Alloy 600 tubes with SCC cracks on the OD surface. The experimental procedure is summarized in Figure A-109. Pre-WJP SCC cracks were produced by applying a pressure of 130 MPa to the inside of Alloy 600 tubes (inner diameter of 15 mm and wall thickness of 5 mm, similar to a BMN tube) and exposing the OD to polythionic acid. Pre-WJP SCC cracks were initiated with depths ranging between 0.5-1.0 mm. After receiving WJP treatment, the samples were re-exposed to the polythionic acid and the same internal pressure of 130 MPa. The WJP process was carried out under the same process parameters as for the BMN tube inner surface. The resulting stress profile from the peened surface of the BMN size pipe is shown in Figure A-110. The residual stress is compressive to at least 0.5 mm, and when the inside of the tube is pressurized, the effect of the operating stress probably decreased the depth of the compressive residual stress field to approximately 0.5 mm.

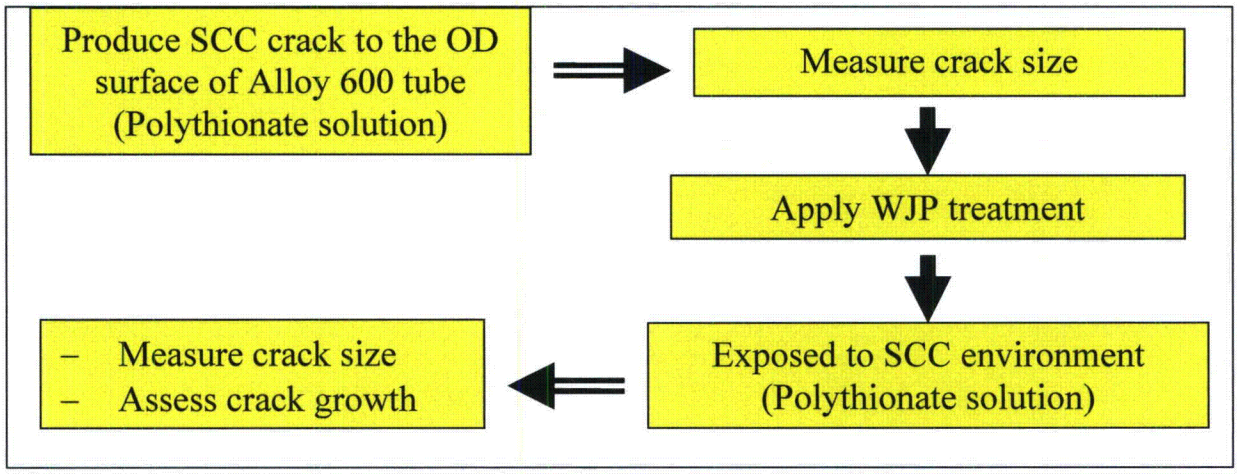

Figure A-109
Test procedure to investigate the effectiveness of WJP in mitigating further growth of pre-existing SCC cracks, provided by Mitsubishi

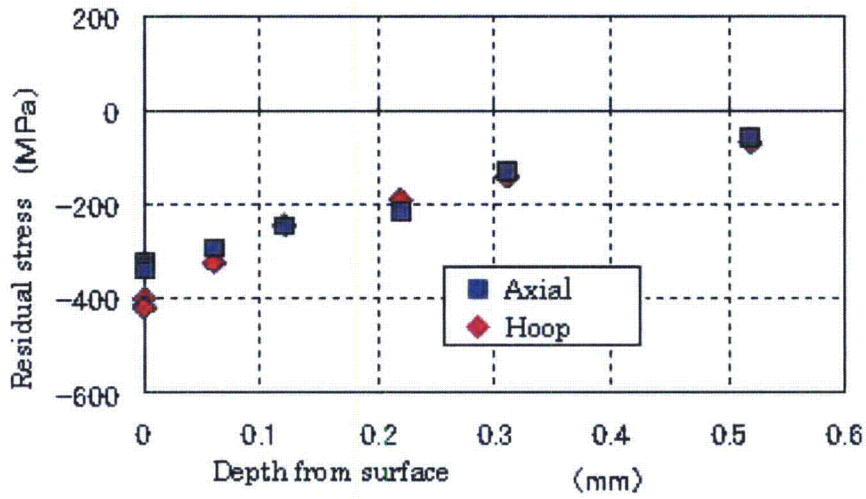

Figure A-110
Residual stress condition after WJP from the peened surface of the BMN size pipe used to assess further SCC growth of pre-existing flaws, provided by Mitsubishi

The results of the testing are summarized in Figure A-111. It is clearly shown that, for pre-WJP cracks with a depth less than 0.5 mm, WJP is effective at preventing further growth. For pre-WJP cracks with a depth greater than 0.5 mm but less than 1.0 mm, subsequent crack growth is prevented or at least significantly decreased. The test results also indicated that, for pre-existing defects deeper than the compressive stress layer, WJP was not effective to mitigate SCC growth. However, it is noteworthy to point out that WJP did not accelerate the growth of pre-existing SCC cracks.

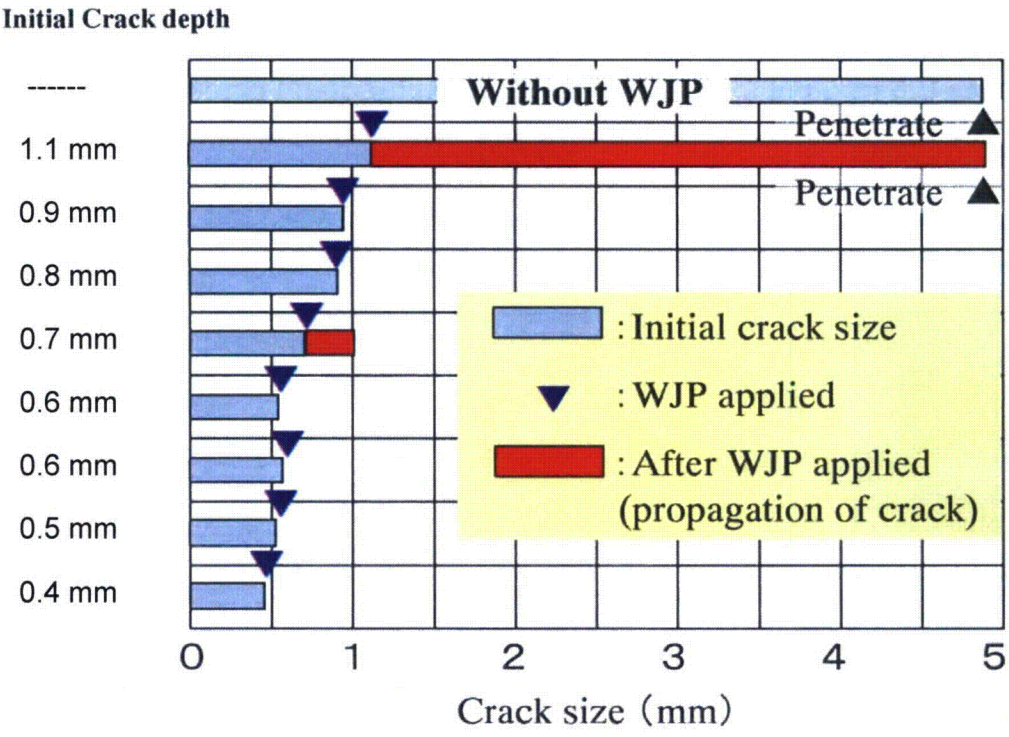

Figure A-111
SCC flaw depth following application of WJP and exposure to polythionate solution as a function of initial SCC flaw depth, provided by Mitsubishi

To experimentally confirm that latent defects subjected to WJP/USP do not develop into SCC during service, MHI prepared a test specimen (Alloy 600 and Type 316 stainless steel joined by Alloy 132 specimen 150 mm long × 40 mm wide × 10 mm thick), shown in Figure A-112. The specimen was cut off along the central line of the 40-mm width, and WJP or USP was applied to only one of the cut pieces. Then, SCC testing was carried out with the specimens immersed in polythionic acid under application of a stress equivalent to that encountered during operation by means of four-point bending to determine by destructive examination after testing whether SCC develops. A magnified observation was carried out on two cross sections for each test condition to measure the depth of all defects observed, and the result was graphed on a Weibull plot.

The test results obtained for SUS316 specimens are shown in Figure A-113 as a representative example. The depth of all defects identified by cross-sectional observation was measured. In the equation of the vertical axis, *Fx* is the cumulative frequency of a defect whose depth is less than the value in the horizontal axis. After peening was implemented, there was no significant difference in defect depth between the specimens with and without SCC testing, suggesting there was no development of SCC. In addition, a comparison between with and without WJP/USP showed a greater SCC progress in the specimens without WJP/USP, revealing that the SCC testing had been performed under appropriate conditions. These results suggest that the growth of pre-existing flaws, including those shallow enough to be missed by pre-peening inspection, is still mitigated.

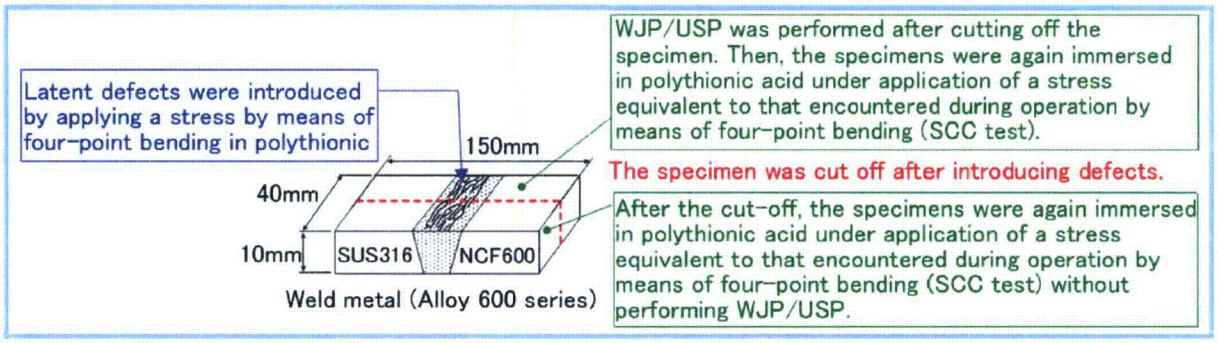

Figure A-112
Plate specimen for determining the effectiveness of inhibiting SCC progress, provided by Mitsubishi

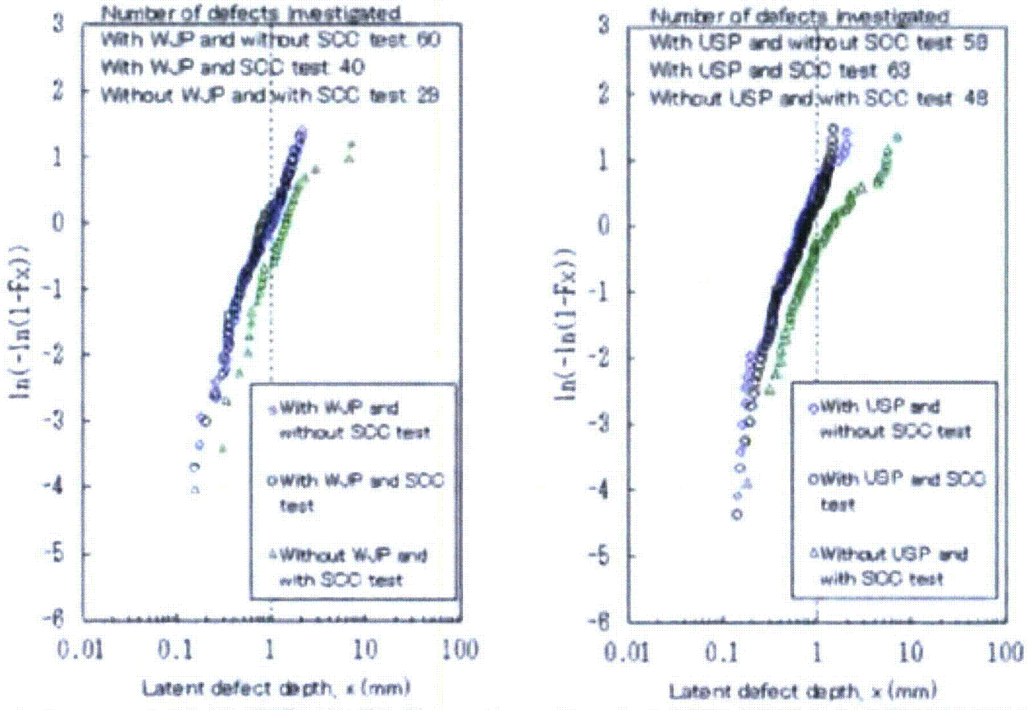

Figure A-113
Weibull plot of latent defect depth (in the case of SUS316) from WJP and USP, provided by Mitsubishi

The test data provided by vendors have verified the effectiveness of surface peening, either WJP or ULP, to mitigate SCC cracking not only of a surface with no pre-existing defects, but also of a surface with shallow defects.

MIC investigated the ability of air laser peening for applications in nuclear reactors to mitigate the potential of stress corrosion cracking in Alloy 600. Toward this end U-bend samples of Alloy 600 were fabricated, air laser peened with an ablative layer and then tested in a corrosive environment. Some samples were air laser peened with an ablative layer and others left unpeened

for baseline comparisons. Figure A-114 below shows an Alloy 600 U-bend used in the tests. The bolt in the base of the U-bend enables it to be tensioned to a desired stress level. A solution of thiosulfate is used to produce the corrosion environment and thereby accelerate stress corrosion cracking. Figure A-115 shows cracks that have initiated in the tensioned U-bends after 24 hours in the thiosulfate solution.

Figure A-116 shows the qualitative comparison of peened and unpeened U-bend samples. With continued exposure, the cracks in the unpeened samples propagate quickly toward the inner surface. For samples that are pre-cracked in the solution and then air laser peened, no additional crack growth is experienced upon further exposure. Finally, if samples are air laser peened prior to exposure, no cracks are seen to develop.

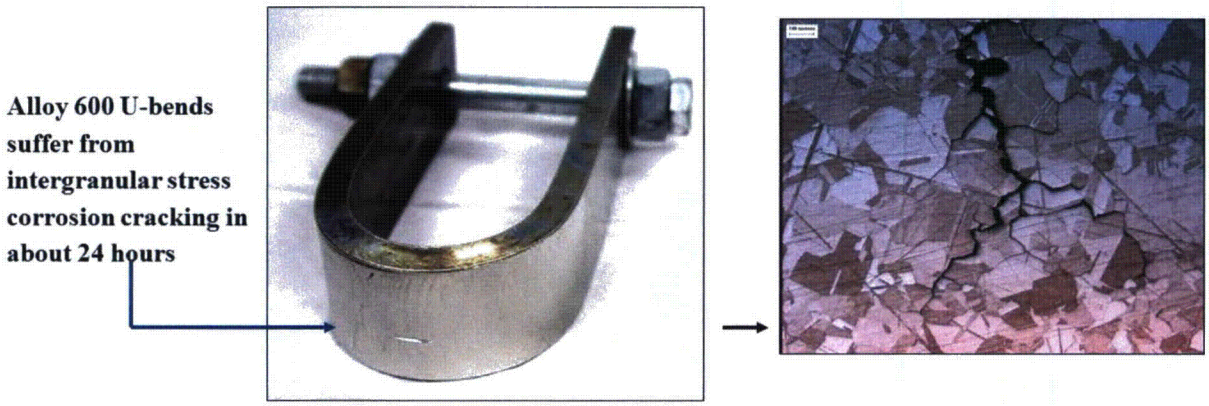

Figure A-114
U-Bend specimen

Hairline cracks develop on the outer surface after one day in the thiosulfate solution

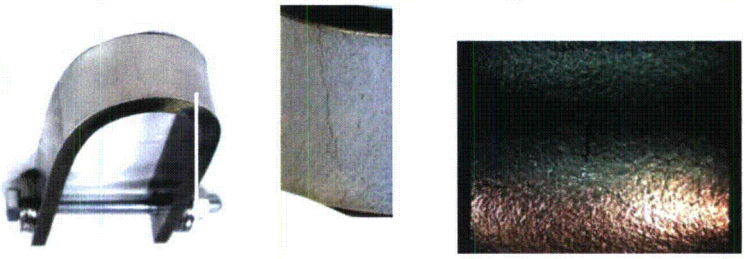

Cracks propagate quickly toward the inner surface with continued exposure

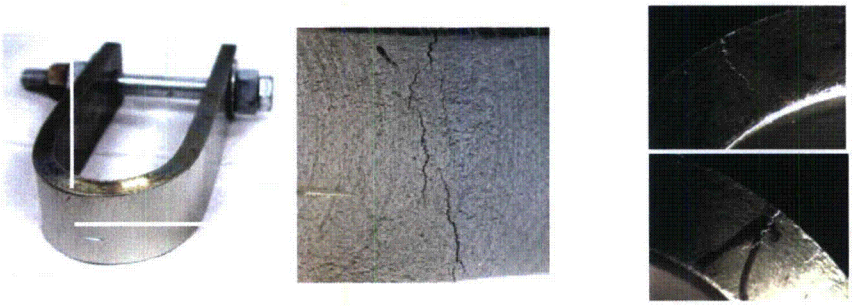

Figure A-115
Cracked U-Bend specimens

U-bend samples tensioned and exposed to Thiosulfate to enhance SCC

Figure A-116
By application of air laser peening, stress corrosion is arrested in tensioned U-bends of Alloy 600 exposed to corrosive thiosulfate

A.3 Independent testing to confirm the effectiveness of surface peening

To independently verify the effectiveness of surface remediation methods, EPRI commissioned AREVA NP to experimentally evaluate different measures for mitigating PWSCC in Alloy 182 welds. The study was performed in two phases. In the first phase, welds were treated with WJP

or ULP and subjected to simulated PWR primary water for 1000 h. In the second phase of testing, the welds from Phase 1 were subjected to another 2000 h (for a cumulative exposure of 3000 h), and new welds were treated with ALP, or other surface stress mitigation techniques, and subjected to simulated primary water for 3000 h. The study examined several different techniques, but only the part pertaining to ALP, ULP, and WJP is included in this technical basis document.

Spring-loaded Alloy 182 U-bends machined in the T-L direction relative to the weld passes were used to test resistance to PWSCC. The surfaces of the specimens were heavily ground prior to forming the U-bend, and were then bent with a sequence of -2% straining in the compressive direction followed by 6% strain in the tensile direction at the apex of the U-bend.

With this specimen preparation procedure, the longitudinal stress at the apex was about 1000/1100 MPa. The mitigation methods were applied after forming the U-bend specimens, which were then exposed to simulated PWR primary water at 360°C for a total of 3000 h (see above). Reference Alloy 182 U-bends with "heavily ground" surfaces suffered extensive PWSCC, as discussed in the following sections.

The main goal of this experimental study was to test the efficacy of the surface remediation treatments to prolong the life of PWSCC-susceptible welds of Alloy 182. The focus of this report is on ULP, ALP, and WJP, as explained in previous sections. Please note that the first phase of this experimental study performed by AREVA is more fully documented in MRP-265 [64].

A.3.1 Experimental Procedure

The experimental program consisted of testing U-bend specimens made from ground Alloy 182 flat rectangular coupons. The remedial surface treatments were applied after the specimens had been formed into their PWSCC U-bend test configuration. Sections A.3.1.1 to A.3.1.3 describe the experimental procedure followed in Phase 1. Section A.3.1.4 outlines the modifications made to this procedure in Phase 2.

A.3.1.1 Test Material

The Alloy 182 weld metal used for this test was prepared with the same Alloy 182 heat and the same welding procedure that were used in a previous study [68]. Figure A-117 shows a weld deposit similar to that used in this project, and Table A-10 gives the composition of the Alloy 182 used to manufacture it.

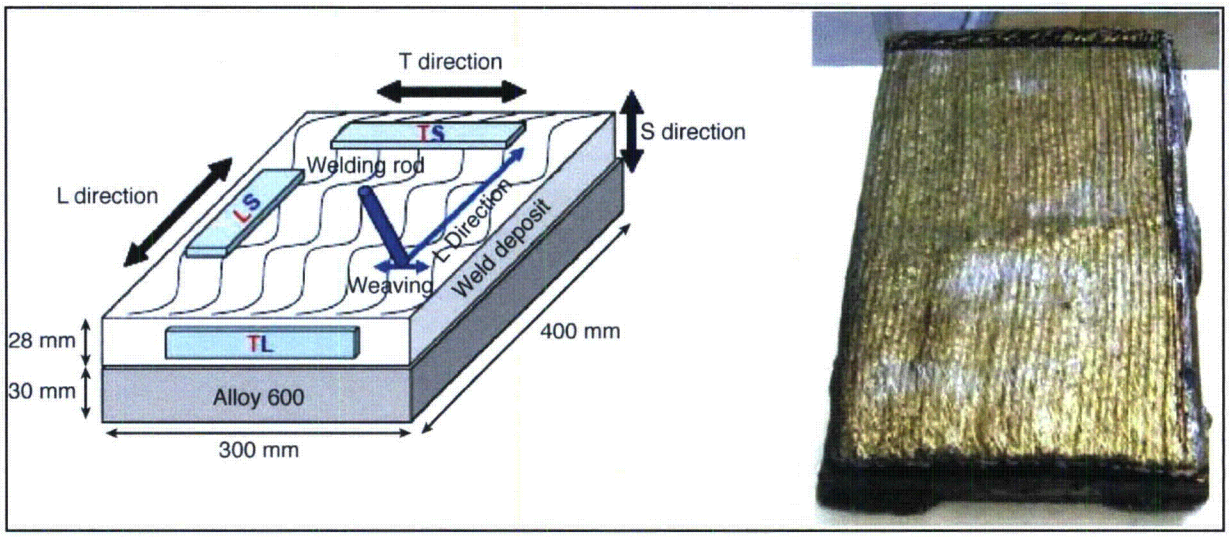

Figure A-117
As-manufactured Alloy 182 weld deposit on an Alloy 600 plate [68]

Table A-10
Chemical analysis of Soudonel CQ5 welding rods used to manufacture the Alloy 182 weld deposit

Element	Chemical Analysis (%)
C	0.026
S	0.002
P	0.006
Si	0.33
Mn	6.49
Ni	68.94
Cr	14.67
Cu	0.01
Co	0.01
V	0.028
Nb + Ta	1.879
Ti	0.06
Fe	6.89

A.3.1.2 Test Specimens

It was determined in a prior study [68] that the greatest susceptibility to PWSCC was obtained under the following conditions:

- Alloy 182 strips with thickness of 2 mm and 3 mm were machined in the T-L direction relative to the weld passes (Figure A-117).
- So-called "heavy grinding" was applied to the U-bend surfaces in the transverse direction relative to the applied strain/stress direction (Table A-11). This grinding procedure creates an average surface roughness, Ra, of 2.2 μm and a cold-worked layer about 30 μm thick, composed of an external layer of ~10 μm, which is so heavily cold-worked that it cannot be characterized by electron back scattered diffraction (EBSD), and an internal layer within which the cold work progressively decreases in intensity with depth (Figure A-118 and Figure A-119).
- X-ray diffraction measurements gave a similar result for the depth of the cold-worked surface layer. Vickers hardness (25 g) profiles in cross section indicated a slightly higher thickness, close to 50 μm, and revealed very hard external layers (Figure A-120).
- A reversed strain cycle (-3%/+ 9% for 3 mm-thick coupons and -2%/+ 6% for 2 mm-thick coupons) was applied during formation of the U-bend (Figure A-121).

- A spring was used to maintain a reproducible stress on the U-bend and avoid significant stress relaxation during exposure to PWR primary water (Figure A-122).
- With this specimen preparation procedure, the longitudinal stress at the apex of the "heavily ground" TL U-bends is around 1000/1100 MPa and the transverse stress is low.

Table A-11
Grinding parameters for transverse laboratory heavy grinding [68]

Rotation Speed	Transverse Sweep Rate	Longitudinal Sweep Rate	Depth of Pass	Grade
1500 t/min	80 mm/min	No	5 µm	60

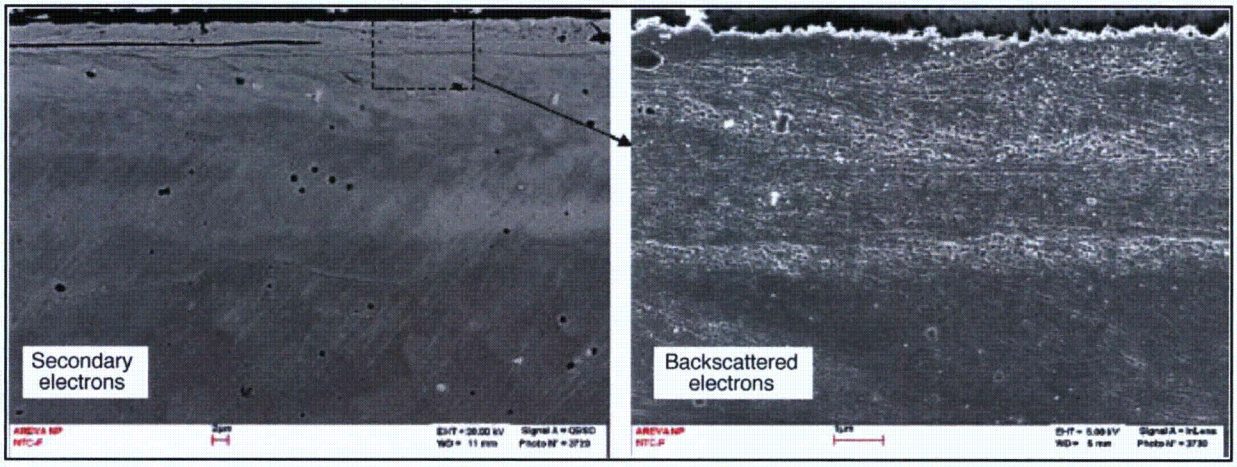

Figure A-118
SEM view of cold worked layer induced by "heavy grinding" [68]

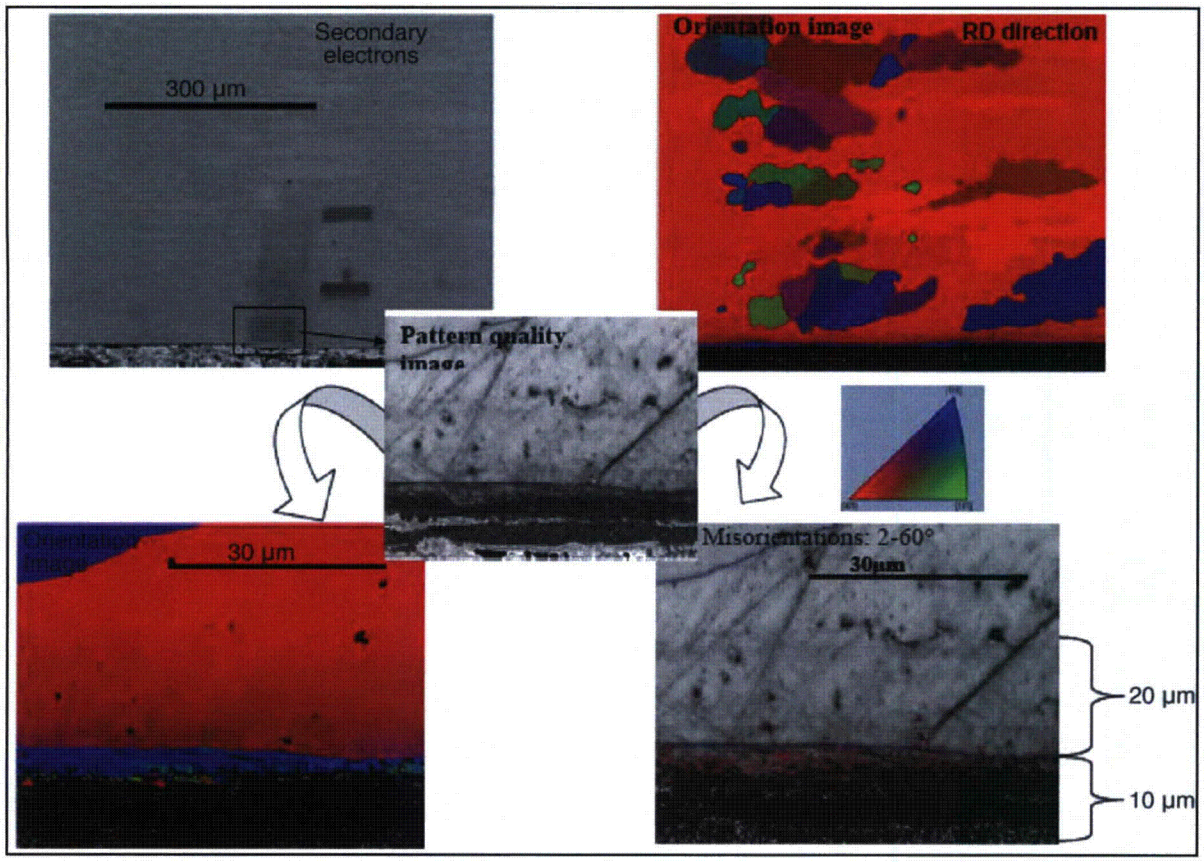

Figure A-119
EBSD analysis of cold worked layer induced by "heavy grinding"

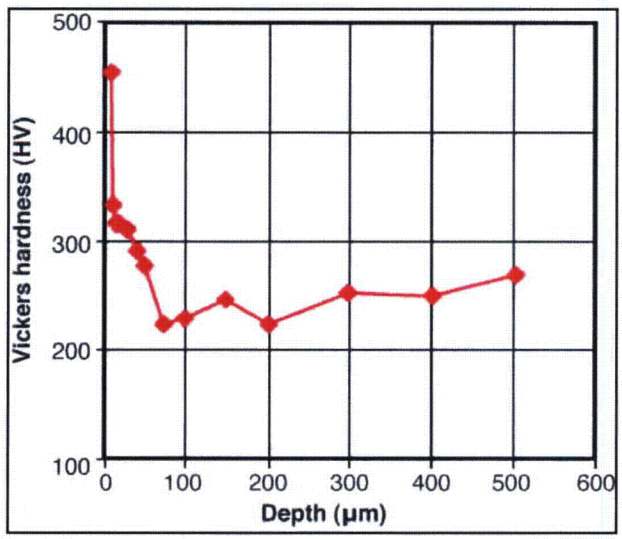

Figure A-120
Vickers hardness (25 g) profile of "heavily ground" surface

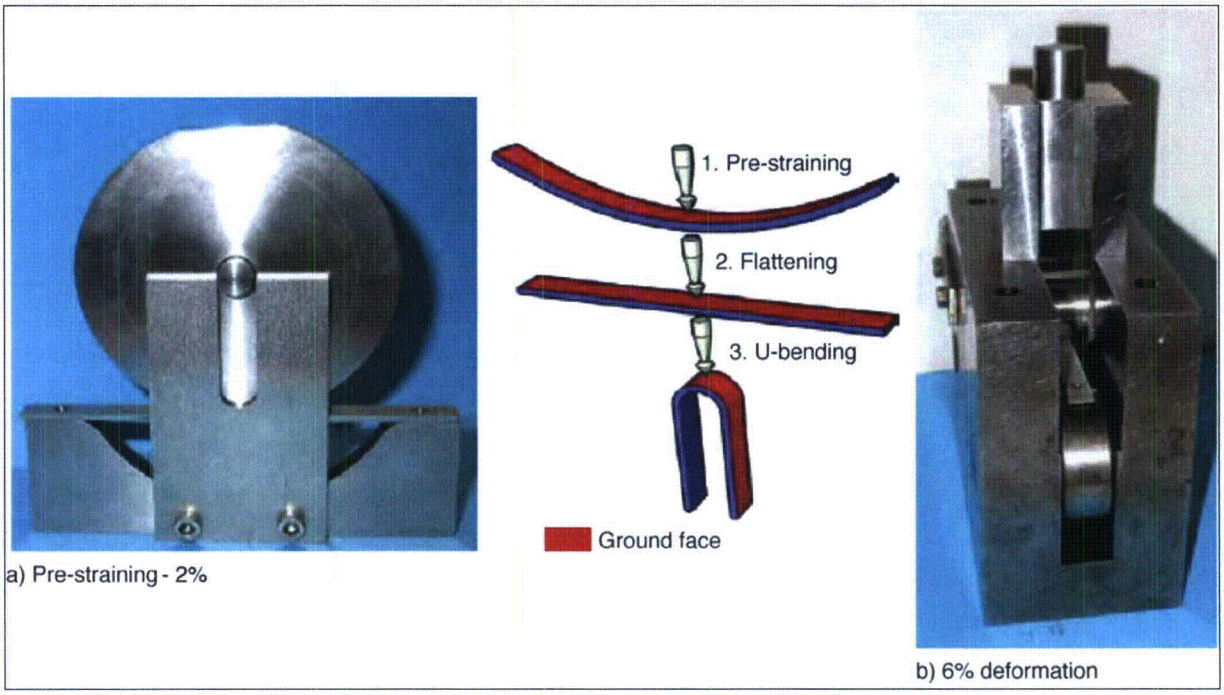

Figure A-121
Loading steps for U-bend specimens (ground face shown in red) [68]

Figure A-122
Spring loaded U-bend [68]

A.3.1.3 Test Environment and Duration

The simulated PWR primary water environment used in the previous research [68] on Alloy 182 was also used for this test project—that is, a solution of 1200 mg/kg B (added as boric acid) and 2 mg/kg Li (added as lithium hydroxide), deaerated, partial pressure of hydrogen of 30 kPa (controlled via a Pd-Ag thimble), 360°C, and static autoclave.

In past tests these conditions led to PWSCC initiation on more than 50% of the U-bends prepared according to the procedure described in Section A.3.1.2 after only 125 h of exposure. For each

test period, a new reference reversed U-bend (RUB) specimen from WF 422 steam generator tube was exposed in order to validate the test conditions.

A.3.1.4 Modifications to Experimental Procedure in Phase 2

In the second phase of experimentation, air laser peening (ALP) was introduced as a new mitigation method for investigation, along with particle peening, cavitation peening and rotopeening, which are not described in this report. Also, the mitigation methods investigated in the first phase of experimentation were further investigated. At the end of Phase 2, all mitigated U-bends had been subjected to a cumulative exposure of 3000 h to simulated primary water.

The Alloy 182 weld used for these tests was prepared by Shielded Metal Arc Welding following the same welding procedure that was employed in the previous phase of experimentation (see EPRI report 1015016, August 2007). Although this deposit was not the same as that used in the previous project, the composition of the welding rods was the same as in Phase 1 and the same welding specifications were employed (same rod batch and same welding parameters) to ensure that the new weld deposit was representative.

The procedure described above in Section A.3.1.2 for preparing U-bends was reproduced in Phase 2 of experimentation. However, in comparison with the previous phase, new thicker U-Bends (3mm thick instead of 2mm) were tested to avoid any deleterious effects induced by "mechanical" peening methods that could result in cold working up to 1mm on these specimens which are comparatively thin compared to field components.

With this specimen preparation procedure, the longitudinal stress at the apex of the "heavily ground" TL U-bends was ~800/1000MPa and the transverse stress was in compression at about -300 to -500 MPa.

Bolt-loaded U-bend specimens were introduced in this project since the resulting surface compressive stress after mitigation was expected to be intermediate between spring-loaded U-bends and more massive components.

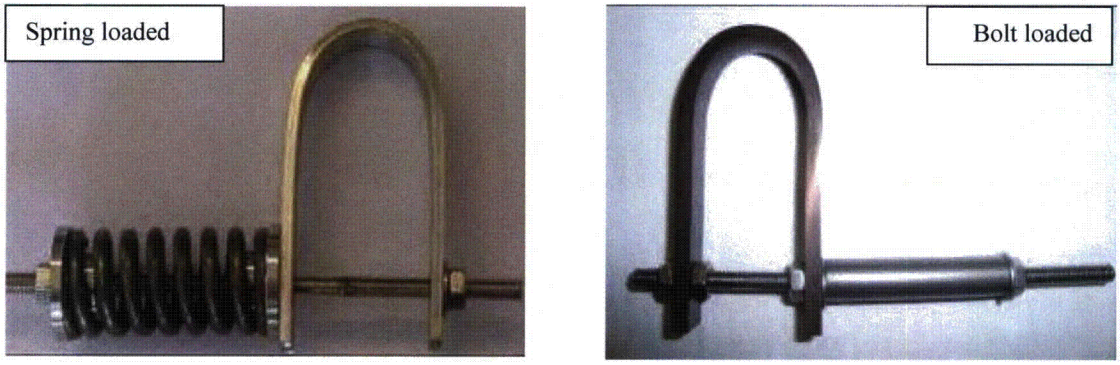

Figure A-123
Comparison of Spring loaded and bolt loaded U-bend specimens

The test environment described in Section A.3.1.3, which was used for Phase 1, was also used for Phase 2. Also, an initial pre-ageing period of 500 hours was carried out at 360°C in simulated PWR Primary Water. For this purpose, the specimens were just pre-formed to -2% or -3% to

generate relatively low residual tensile stresses. After forming into U-bends and applying surface mitigation treatments, the efficiency of the mitigation treatments was evaluated in two successive test periods of 1000 and 2000 h under similar test conditions.

A.3.2 Surface Stress Improvement Mitigation Methods

A.3.2.1 Mitigation Methods examined in Phase 1

As mentioned in the beginning of Section A.3, two surface stress improvement (SSI) treatments were included in Phase 1 of this test:

- Underwater laser peening performed by Toshiba
- Water jet peening performed by Hitachi-GE and by Mitsubishi, respectively

All the surface treatments were applied to the loaded U-bends.

The surface strains induced by these treatments resulted in a significant decrease of the distance between the legs of the U-bends, as shown in Table A-12 and Figure A-124. The significance of this observation is analyzed in the later discussion.

Table A-12
Distance between legs of spring-loaded U-bend after surface treatments

Distance Between U-Bend Legs	2-mm-Thick U-Bends	3-mm-Thick U-Bends
Initial	22 ± 0.5 mm	23 ± 1 mm
After Toshiba ULP	15.22 to 16.01 mm	16.27 to 16.94 mm
After Mitsubishi WJP	16.67 to 18.32 mm	15.84 to 16.39 mm
After Hitachi-GE WJP	16.10 to 17.09 mm	11.84 to 12.05 mm

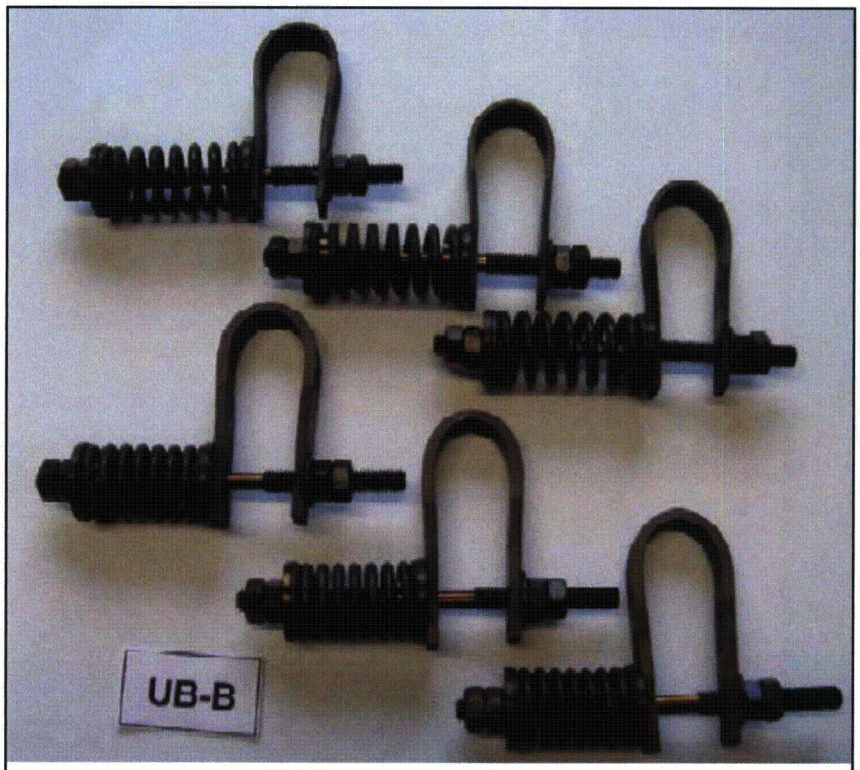

Fiber laser peening by Toshiba

Figure A-124
2-mm-thick and 3-mm-thick spring-loaded U-bends after surface treatments

A.3.2.2 Mitigation Methods examined in Phase 2

As outlined in the beginning of Section A.3, all mitigation methods investigated in Phase 1 were continued in Phase 2, namely underwater laser peening by Toshiba and water jet peening. The mitigation methods added to the investigation were particle peening, cavitation peening, air laser peening, and rotopeening. Of the four surface treatment methods new to Phase 2, only data for the U-bends treated with air laser peening is presented in this report.

Some of these treatments were performed on spring loaded U-Bends with the result that the distance between legs of the U-Bends significantly decreased after the introduction of surface compressive stresses (see Table A-13).

Table A-13
Displacement of legs of spring-loaded U-Bend specimens after mechanical surface mitigation treatments.

Displacement of U-bend legs	SPRING LOADED U-BENDS	
	2mm thick	3 mm thick
After Toshiba ULP	-5.99 to -6.78 mm	-6.06 to -6.73 mm
After Mitsubishi WJP	-3.68 to -5.33 mm	-6.61 to -7.16 mm
After Hitachi-GE WJP	-4.91 to -5.9 mm	-10.95 to -11.16 mm
After Metal Improvement ALP	----	-8.64 to -11.69 mm

A.3.3 Observations of U-Bend Surfaces before PWSCC Testing

A.3.3.1 U-Bend Pre-Peening Inspection for Experimentation Phase 1

After completing preparation of the Alloy 182 U-bends, a surface examination was performed in order to detect any surface defects that are sometimes present on the surface as a consequence of the relatively large applied strains to the weld deposit. Only three U-bends were found to have detectable surface defects (see Figure A-125)

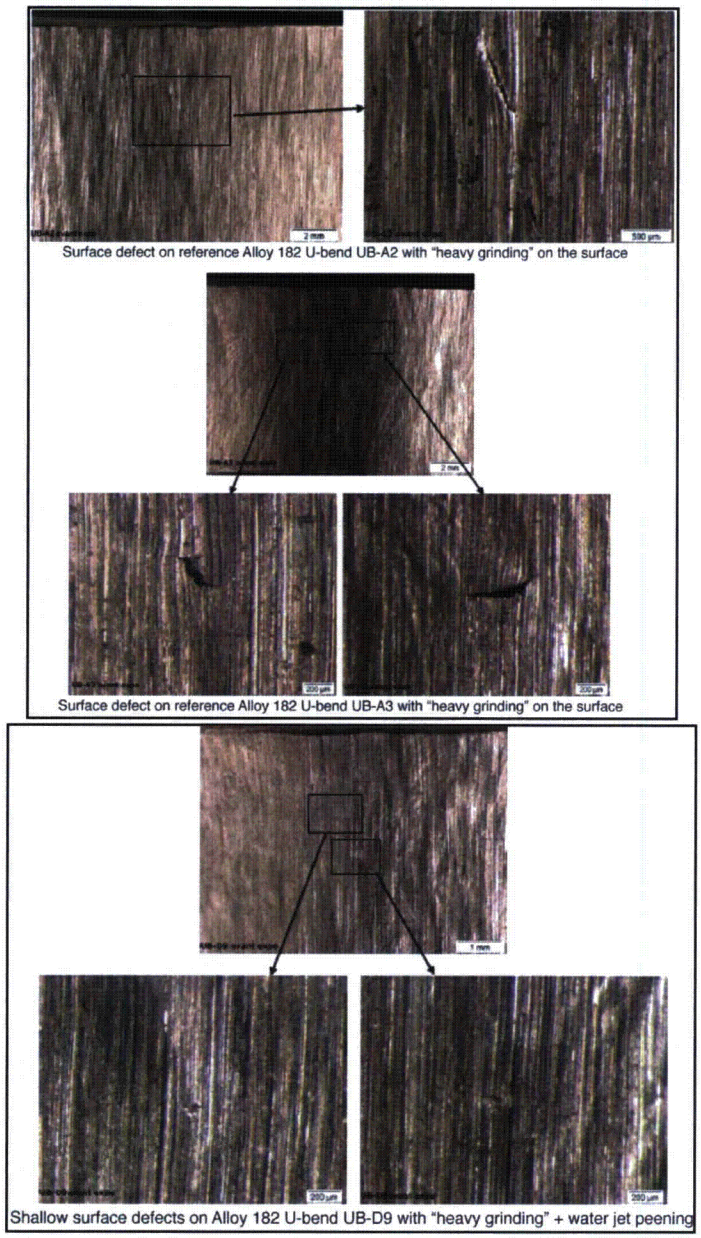

Figure A-125
Surface defects observed on U-bend surfaces before exposure to primary water

A.3.3.2 U-Bend Pre-Peening Inspection for Experimentation Phase 2

Similar surface examinations (by binocular optical microscopy) were performed in the second phase of experimentation following pre-aging and forming of the U-bends to detect any possible flaws such as hot cracks, mechanical openings of grain boundaries, or slag inclusions. Only two U-bends were found to have detectable surface defects, one of which was subsequently treated with ALP. This defect was probably a slag inclusion. (see Figure A-126)

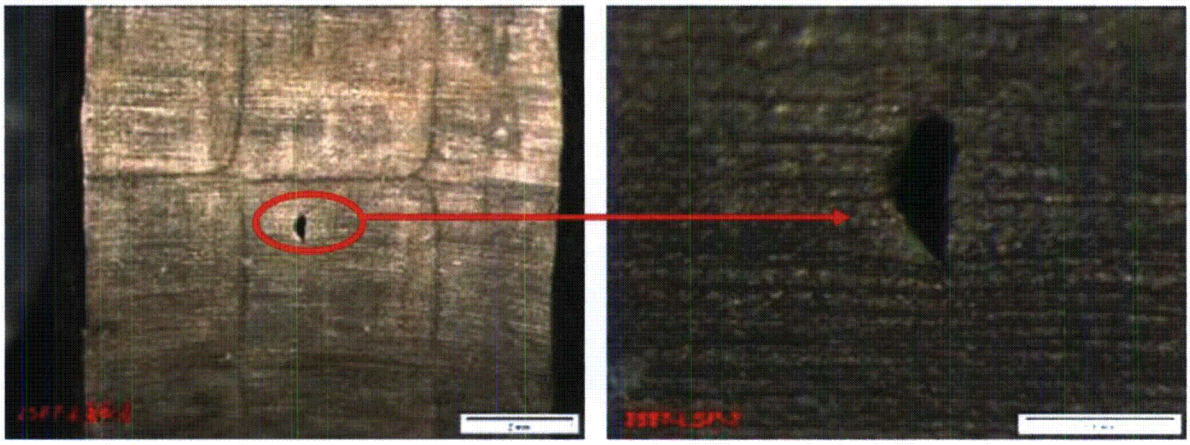

Surface defect on reference Alloy 182 U-bend UB-LSP-3 with "heavy grinding" + Air Laser Peening

Figure A-126
Surface defects observed after pre-ageing period in Primary Water and treatment of U-Bends surface

A.3.4 Test Matrices

A.3.4.1 Test Matrix for Phase 1

Table A-14 presents the PWSCC test matrix for Phase 1. Reference Alloy 182 U-bends without any mitigation technique applied were included to allow a comparison of the behavior of surface treated and untreated U-bends. In addition to the Alloy 182 specimens, a series of Alloy 600 spring-loaded U-bends were also prepared according the same procedures described in Section A.2.2 in order to check the effect of the surface preparation condition (that is, transverse grinding plus reverse straining) on Alloy 600.

It was initially planned to perform three successive test periods of 250, 250, and 500 h for a total exposure time of 1000 h. However, because the surface treatments of the test specimens took much longer than expected, only 1000-hour tests were performed.

Table A-14
Complete test matrix for "mechanical" remedial methods

Surface Condition	U-Bends		RUB
	2 mm thick	3 mm thick	
Alloy 182			
Reference "Heavy Grinding"	3 – Spring loaded	3 – Spring loaded	
Underwater Laser Peening by Toshiba	3 – Spring loaded	3 – Spring loaded	
Water Jet Peening by Mitsubishi	3 – Spring loaded	3 – Spring loaded	
Water Jet Peening by Hitachi-GE	3 – Spring loaded	3 – Spring loaded	
Alloy 600 – BMN Bar			
Reference "Heavy Grinding"	3 – Spring loaded	3 – Spring loaded	
Alloy 600 Reference SG Tube (Heat WF 422)			
As Received			1

A.3.4.2 Test Matrix for Phase 2

Table A-15 presents a partial PWSCC test matrix for both parts of Phase 2: testing of new mitigation treatments and re-exposure of 2000 h of U-Bends from the previous phase. Only the subset of peening methods discussed in this report is shown in the test matrix. Reference Alloy 182 U-bends without any mechanical mitigation treatment were included to allow a comparison of the behavior of surfaces treated and untreated.

The PWSCC testing of the U-bends treated with new mitigation methods specimens consisted of two successive test periods of 1000 h and 2000 h. A direct comparison of a large range of "mechanical" treatments was possible by including mechanically mitigated U-Bends from Phase 1 in the second exposure period of 2000 h.

Table A-15
Complete test matrix for "mechanical" remedial methods

Surface Condition	U-Bends		RUB
	2 mm thick	3 mm thick	
Alloy 182 specimens new to Phase 2 (exposed for a total period of 3000 h)			
Reference "Heavy Grinding"	–	3 – Spring loaded 3 – Bolt loaded	
Air Laser Peening by MIC	–	4 – Spring loaded 5 – Bolt loaded	
Alloy 182 specimens from Phase 1 (exposed for an additional period of 2000 h)			
Reference "Heavy Grinding"	3 – Spring loaded	3 – Spring loaded	
Underwater Laser Peening by Toshiba	3 – Spring loaded	3 – Spring loaded	
Water Jet Peening by Mitsubishi	3 – Spring loaded	3 – Spring loaded	
Water Jet Peening by Hitachi-GE	3 – Spring loaded	3 – Spring loaded	
Alloy 600 Reference SG Tube (Heat WF 422)			
As Received			1 / period

A.3.5 Results and Analysis

A.3.5.1 Phase 1 Surface Stresses and Cold Work of U-Bends

The surface stresses measured by XRD on the apexes of the U-bends after surface mitigation treatments are given in Table A-16. Valid measurements could not be obtained for all specimens, but those that were obtained showed that, on Alloy 182 U-bends:

- Tensile surface stresses on untreated 2-mm-thick U-bends were consistent with past measurements [68].
- Surface stresses on untreated 3-mm-thick U-bends were of the same order of magnitude as on 2-mm U-bends.
- Surface stresses were compressive on all U-bends treated with a "mechanical" mitigation method.
- On spring-loaded U-bends, compressive stresses after surface mitigation treatments tended to be higher in the transverse direction than in the longitudinal direction.

- On spring-loaded U-bends, there is no correlation between the surface stresses and the displacement of the legs during surface treatments (as expected).
- Surface cold work, evaluated from the half-width of the x-ray diffraction peak, was slightly higher on 3-mm-thick U-bends than on 2-mm-thick U-bends, which is consistent with the higher strains applied during forming (-3/+9 % instead of -2/+6%).
- Unexpectedly, the diffraction peak half-width was lower after all surface mitigation treatments, compared to initial surface cold work from "heavy grinding."

These results will be discussed in Section A.3.5.2.

On Alloy 600 U-bends, surface stresses, as well as surface cold work, were significantly lower than on Alloy 182 U-bends, which is consistent with the lower initial strength of Alloy 600.

Table A-16
XRD measurements of surface stress and cold work on U-bends before and after "mechanical" surface mitigation treatments

Surface Condition	Thickness	Δd[1] (mm)	#	Surface Stress (MPa)		Diffraction Peak Half Width (°)	
				Long.	Transv.	Long.	Transv.
Alloy 182							
Reference "Heavy Grinding"	2 mm		UB-A1	1070	NV[4]	4.15	NV
			UB-B6[2]	1195	-105		
	3 mm		UB-A5	975	NV	4.64	NV
			UB-B12[2]	1225	500		
Underwater Laser Peening by Toshiba	2 mm	~ 6/7	UB-B1	NV	NV	NV	NV
		~ 5	UB-B6[3]	-310	-45		
	3 mm	~ 5/6	UB-B14	NV	NV	NV	NV
		~ 10	UB-B12[3]	-360	-575		
Water Jet Peening by Mitsubishi	2 mm	~ 4/5	UB-C4	-250	-570	3.71	3.57
	3 mm	~ 6	UB-C11	-325	-740	3.51	3.62
Water Jet Peening by Hitachi-GE	2 mm	~ 5/6	UB-D1	-470	-595	3.48	3.51
	3 mm	~ 10	UB-D14	-360	-720	3.65	3.70
Alloy 600 – BMN Bar							
"Heavy Grinding"	2 mm		UB-F1	685	-330	3.92	3.98
	3 mm		UB-F5	630	-380	3.90	3.87

(1) Variation of leg distance during surface treatment
(2) Measurements by Toshiba before underwater laser peening
(3) Measurements by Toshiba after underwater laser peening
(4) NV = No valid measurement available

A.3.5.2 Phase 1 PWSCC Test Results

After 1000 h of exposure at 360°C, the control RUB specimen (SG tube heat WF 422) exhibited large cracks (Figure A-127) thus showing that the PWR primary water test conditions were as severe as expected.

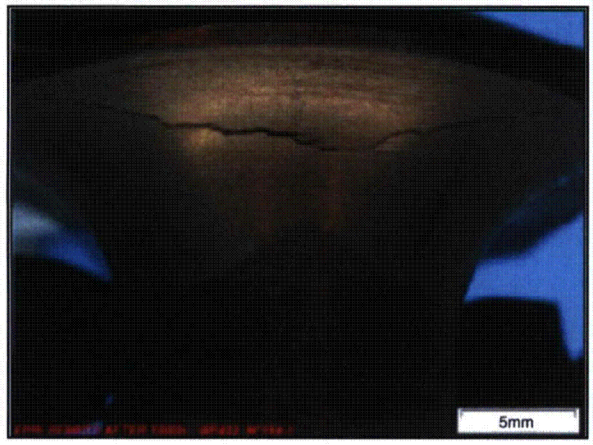

Figure A-127
RUB from steam generator (SG) tube WF 422 after 1000 h of exposure to PWR primary water at 360°C

Table A-17 summarizes all the observations on the U-bend test specimens, from which the following points are drawn:

- Reference Alloy 182 U-bends with "heavily ground" surfaces suffered extensive cracking (Figure A-128). This is in agreement with past results and, in addition to the extensive cracking observed on the reference WF 422 RUB, confirmed the severity of the test conditions.
- The 3-mm-thick U-bends that were strained to a greater degree than the 2-mm-thick specimens were, however, surprisingly less cracked than the 2-mm-thick UNTCC-bends. More tests are required to validate and understand this counterintuitive trend.
- None of the U-bends with remedial mechanical surface treatment exhibited cracking. This result is obviously consistent with the presence of compressive stresses on the external surfaces of the U-bends as shown by x-ray diffraction. Importantly, this also shows that there were no local tensile stress peaks induced by the surface treatments that were able to initiate cracking.
- Alloy 600 U-bends did not suffer from any cracking even though the surface condition and the applied strains were similar to those of the Alloy 182 U-bends. This may be due both to lower surface stresses present on Alloy 600 U-bend surfaces and to the finer microstructure of the wrought material that results in less strain/stress concentration during formation of the U-bend specimens.
- Accordingly, it is concluded that Alloy 600 U-bends are not a satisfactory specimen test configuration to evaluate the effect of surface mitigation methods on Alloy 600.

Table A-17
Results of 1000 h exposure test on Alloy 182 and Alloy 600 U-bends

Surface Condition	Thickness	#	Initial Surface Defects	Crack
Alloy 182				
Reference "Heavy Grinding"	2 mm	UB-A2 UB-A3 UB-A4	Yes Yes No	Large cracks Large cracks Large cracks
	3 mm	UB-A6 UB-A7 UB-A8	No No No	Small cracks No cracks Large cracks
Underwater Laser Peening by Toshiba	2 mm	UB-B3 UB-B4 UB-B5	No No No	No cracks
	3 mm	UB-B8 UB-B10 UB-B11	No No No	No cracks
Water Jet Peening by Mitsubishi	2 mm	UB-C1 UB-C2 UB-C3	No No No	No cracks
	3 mm	UB-C8 UB-C9 UB-C10	No No No	No cracks
Water Jet Peening by Hitachi-GE	2 mm	UB-D2 UB-D3 UB-D7	No No No	No cracks
	3 mm	UB-D8 UB-D9 UB-D10	No Yes—very shallow No	No cracks
Alloy 600 – BMN Bar				
"Heavy Grinding"	2 mm	UB-F2 UB-F3 UB-F4	No No No	No cracks
	3 mm	UB-F6 UB-F7 UB-F8	No No No	No cracks Probably cracked No cracks

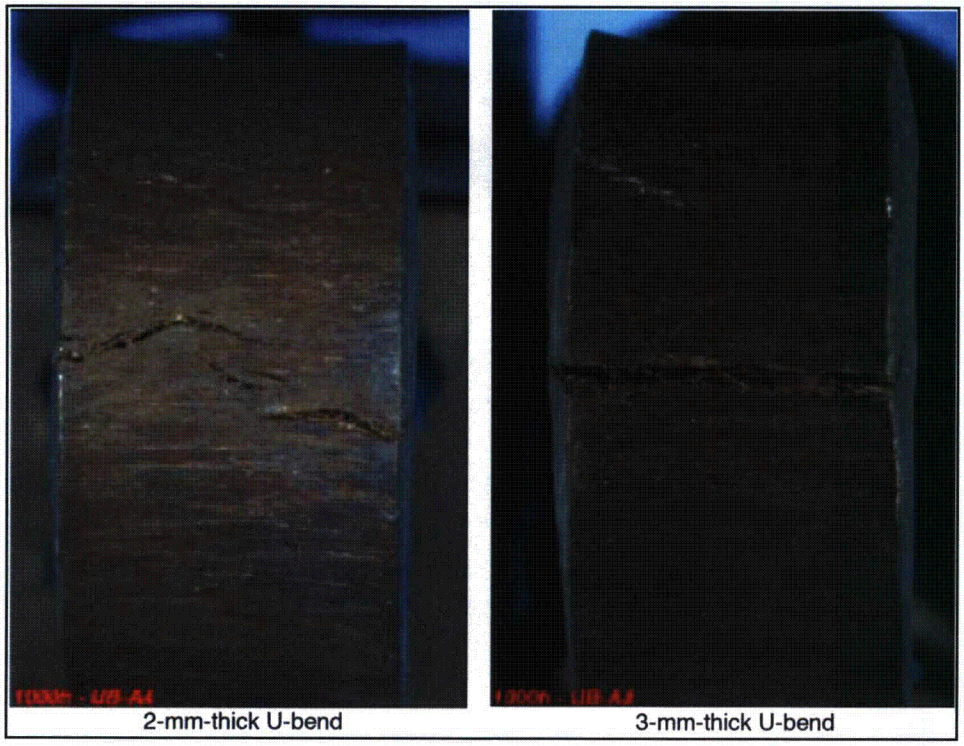

Figure A-128
U-bends with "heavily ground" surfaces after 1000 h of exposure to PWR primary water at 360°C

A.3.5.3 Surface Stresses and Cold Work of U-Bends in Phase 2

The surface stresses measured by XRD at the apexes of the U-bend specimens after mechanical surface mitigation treatments in Phase 2 are summarized in Table A-18. These measurements were performed before and after exposure for 3000h to simulated PWR primary water at 360°C. The conventional XRD measurement uncertainty for such a material is about ±50 MPa. Thus, any evolution of stresses of less than 100 MPa before and after exposure cannot be considered as real trends.

Valid residual stress measurements could not be obtained for all specimens. Nevertheless, when it was possible, the measurements showed that:

- surface stresses on untreated 3mm thick U-bends were of the same order of magnitude as on 2mm U-bends;
- all U-bends treated with a mechanical mitigation method exhibited compressive surface stresses in both transverse and longitudinal directions, with the exception of the 3mm specimens treated by Air Laser Peening (see Figure A-130).
- on spring loaded U-bends, there was no correlation between the surface stresses and the displacement of the legs that was observed during the surface mitigation treatments. This is due to the fact that the different mechanical treatments introduce compressive stresses on

different thicknesses. Only stress profile measurements by XRD would account for the leg displacements.

- For all specimens, the exposure tests caused significant decrease of both tensile (reference ground specimens) and compressive stresses (mitigated specimens) (see Figure A-129 and Figure A-131)

Table A-18
XRD measurements of surface stresses on U-Bends before and after corrosion test.

Surface Treatment	Thickness	Loading	Exposure	Surface Stress (MPa)	
				Longitudinal	Transverse
Phase 1 Specimens					
Reference "heavy grinding" (HG) – REMEDIATION 3	2 mm	spring	Before	1070	No Value
			Before (measurement by Toshiba)	1195	-105
			After 1000 h	Not valid since all specimens were cracked after 1000 h	
			After 3000 h		
	3 mm	spring	Before	975	No Value
			Before (measurement by Toshiba)	1225	500
			After 1000 h	700	-160
			After 3000 h	645	No Value
HG + Underwater Laser Peening (Toshiba)	2 mm	spring	Before	-310	-45
			After 1000 h	-480	No Value
			After 3000 h	-570	-405
	3 mm	spring	Before	-360	-575
			After 1000 h	-180	-380
			After 3000 h	-225	-400
HG + Water Jet Peening (MHI)	2 mm	spring	Before	-250	-570
			After 1000 h	-160	-440
			After 3000 h	-155	-355

Table A-18(continued)
XRD measurements of surface stresses on U-Bends before and after corrosion test.

Surface Treatment	Thickness	Loading	Exposure	Surface Stress (MPa)	
HG + Water Jet Peening (MHI) (continued)	3 mm	spring	Before	-325	-740
			After 1000 h	-40	-460
			After 3000 h	-50	-495
HG + Water Jet Peening (Hitachi-GE)	2 mm	spring	Before	-470	-595
			After 1000 h	-310	-500
			After 3000 h	-370	-480
	3 mm	spring	Before	-360	-720
			After 1000 h	-410	-600
			After 3000 h	-455	-590
Phase 2 Specimens					
Reference "heavy grinding" (HG)	3 mm	spring	Before	820	-270
			After 3000 h	465	-105
	3 mm	bolt	Before	670	-540
			After 3000 h	505	-250
HG + Air Laser Peening (MIC)	3 mm	spring	Before	Not available	Not available
			After 3000 h	685	490
	3 mm	bolt	Before	390	320
			After 3000 h	300	No Value

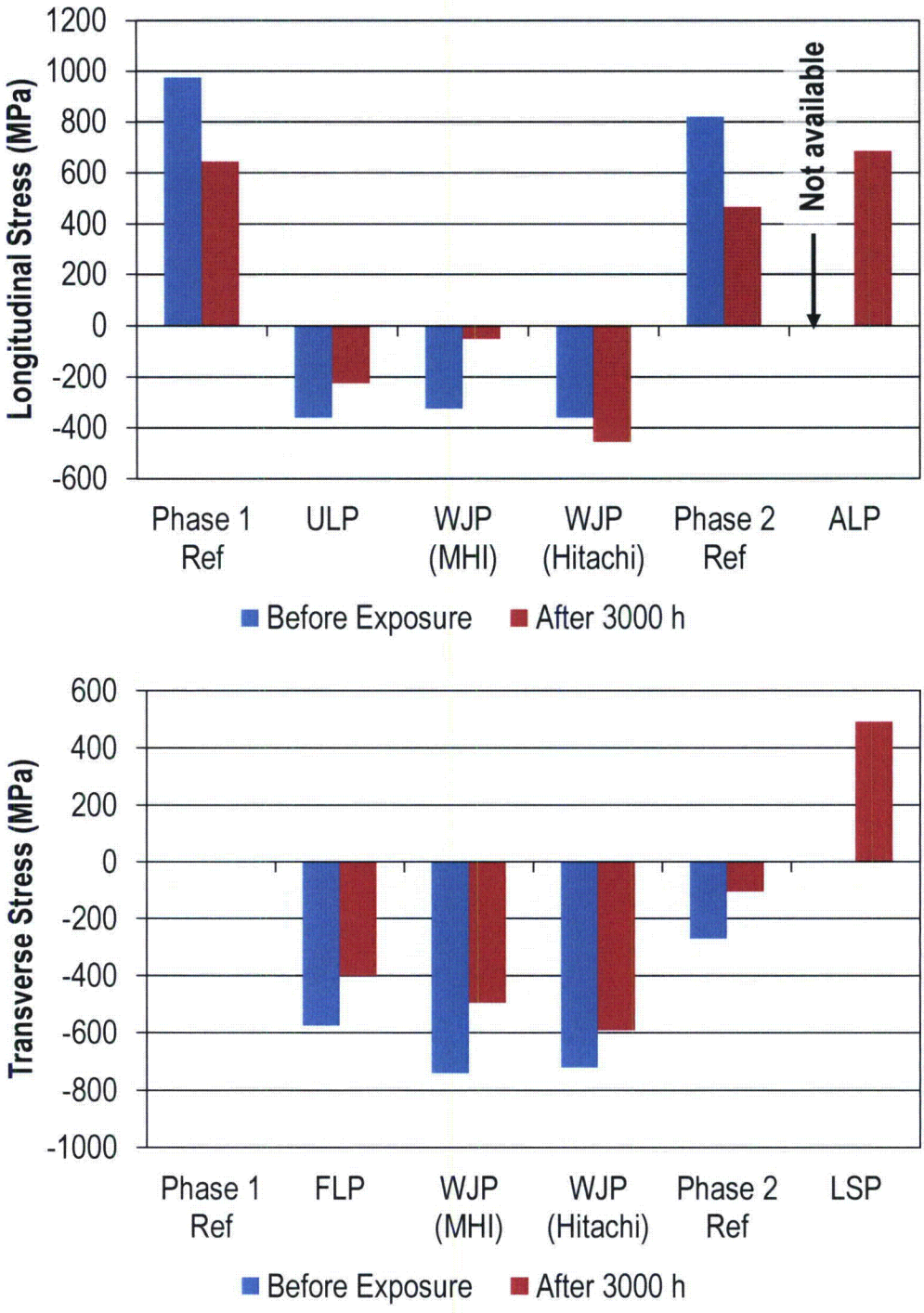

Figure A-129
Stress measurement at the Apex of 3mm thick spring-loaded U-bend

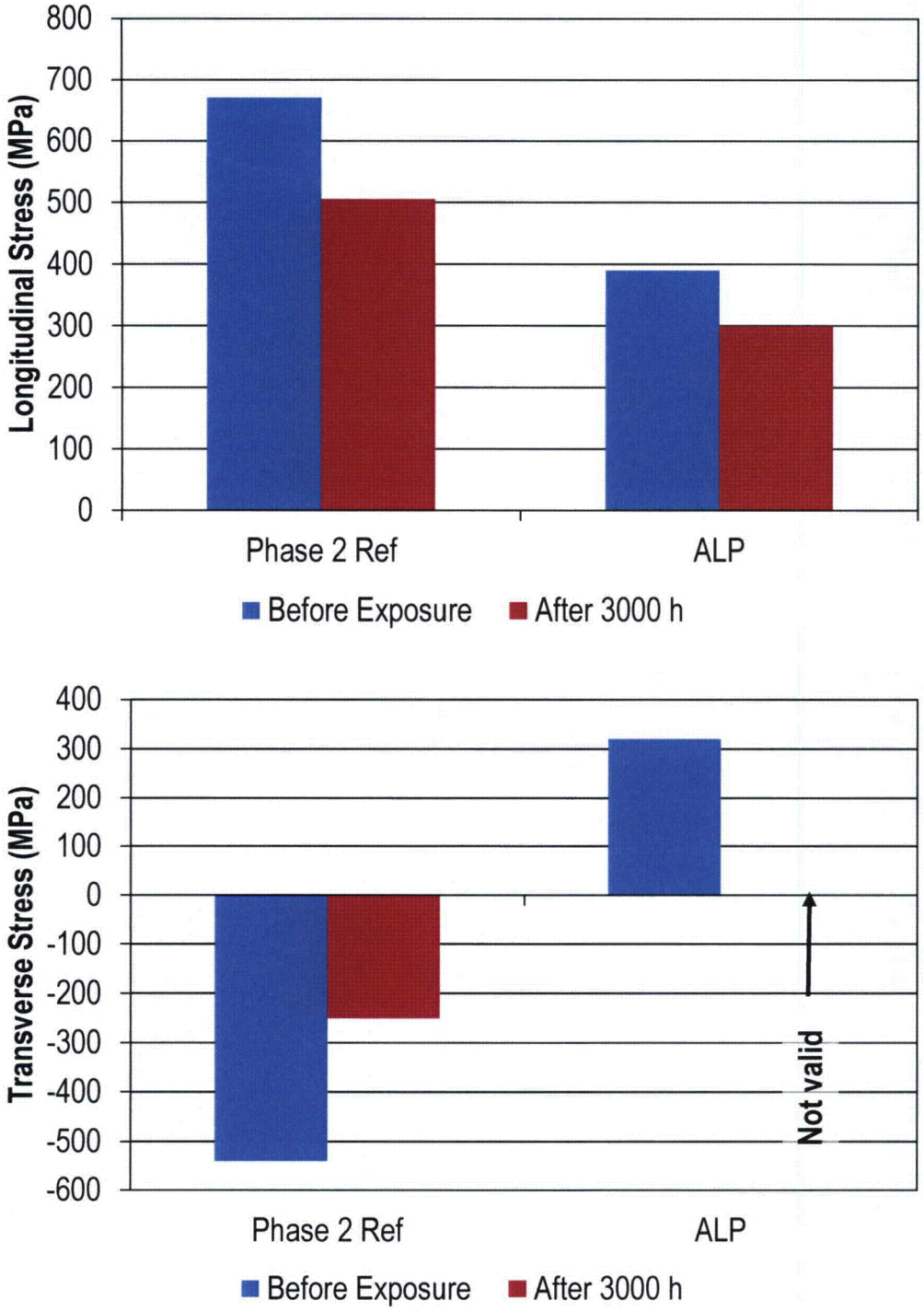

Figure A-130
Stress measurement at the Apex of 3mm thick bolt-loaded U-bend

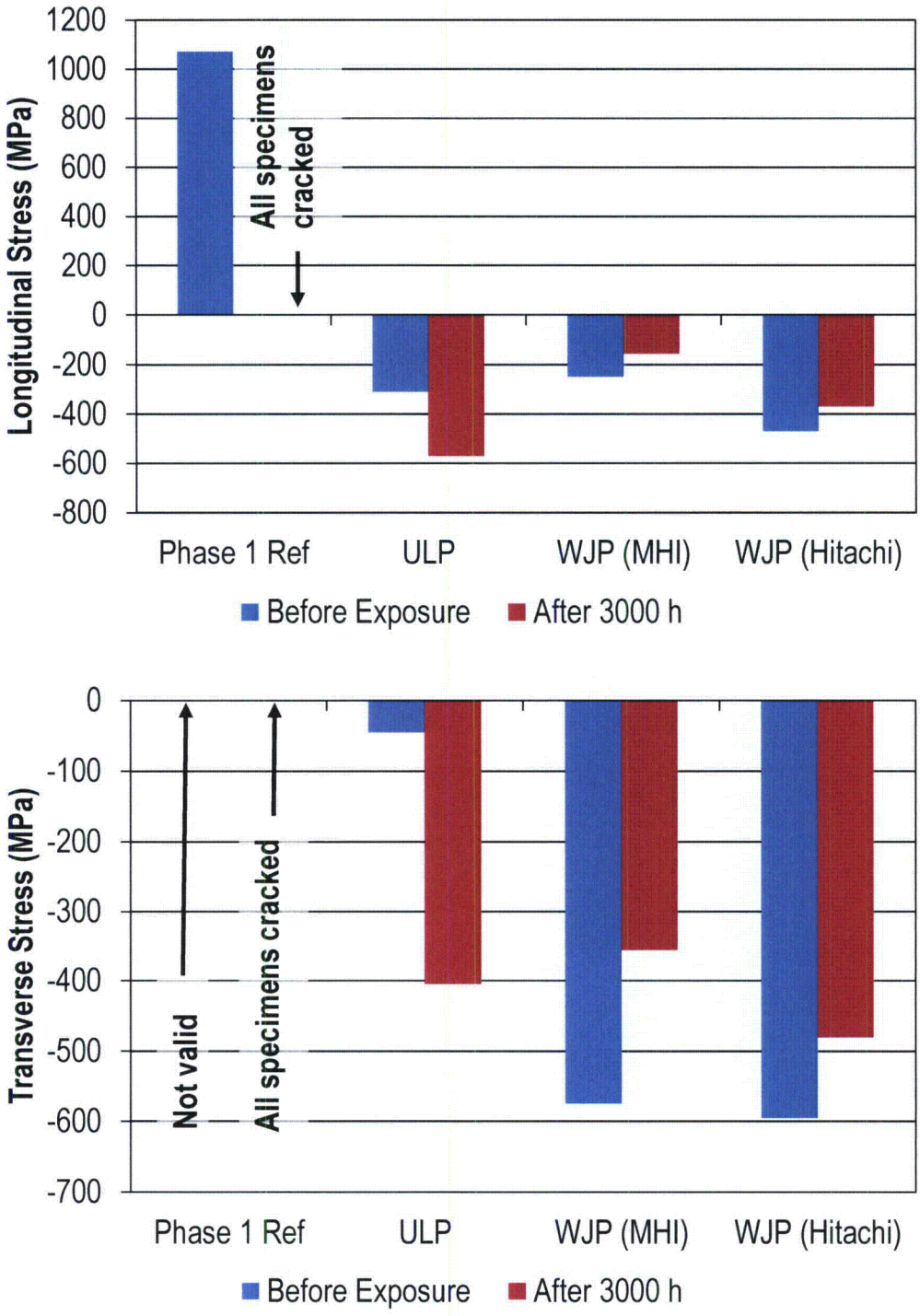

Figure A-131
Stress measurement at the Apex of 2mm thick spring-loaded U-bend

A.3.5.4 PWSCC Test Results in Phase 2

The test U-bends were exposed for two successive test periods of 1000 and 2000h in simulated PWR primary water at 360°C. For each period, a control RUB specimen (SG tube heat WF 422) was introduced to validate the SCC severity. The mechanically mitigated U-Bends from Phase 1 were only re-exposed during the second test period of 2000h (to enable a comparison for a cumulative exposure time of 3000h).

Table A-19 and Table A-20 respectively summarize all the observations on the U-bends for the new set of specimens and those from the previous phase of experimentation, respectively. Figure A-132, defines a reference system for the zones of the U-Bends where defects or cracks in the surface might be detected.

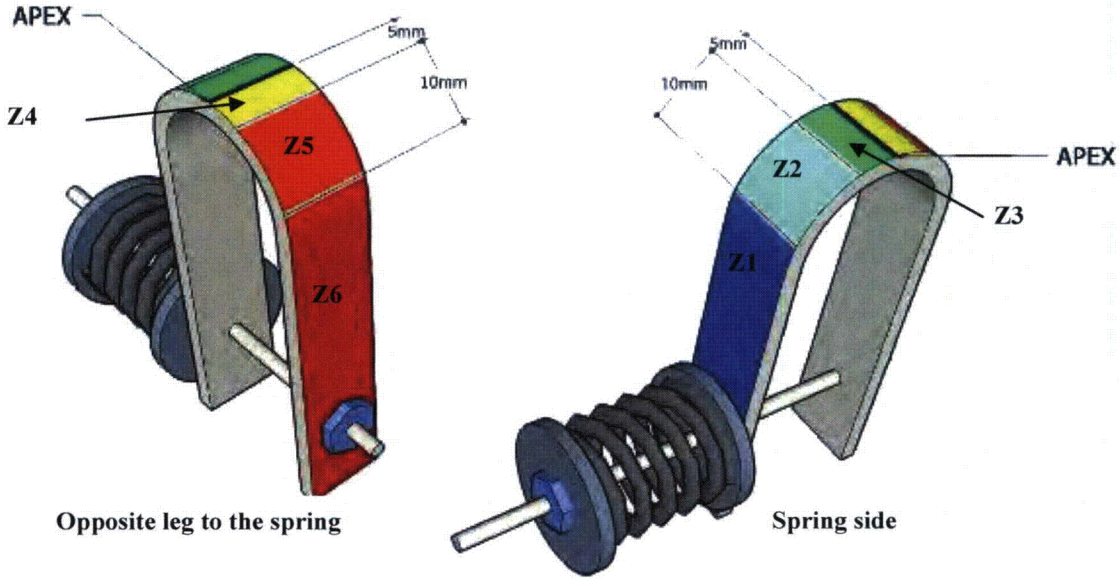

Figure A-132
Reference system for cracking zones of U-Bend specimens.

After each period of 1000 and 2000h at 360° C, the control RUB specimens (new RUB for each test period) exhibited large cracks (Figure A-133) thus showing that the simulated PWR primary water test conditions were as severe as expected.

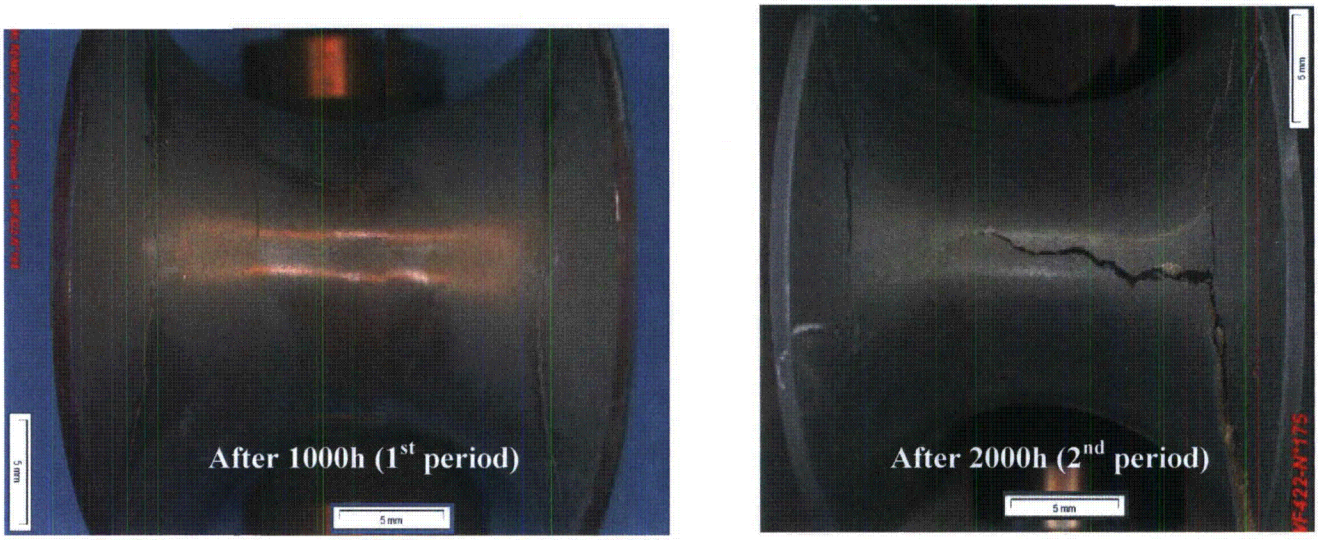

Figure A-133
RUBs from SG tube WF422 after 1000h and 2000h of exposure to PWR Primary Water at 360°C.

The following observations are drawn from the optical examinations of the U-bend specimens after a cumulative exposure time of 3000h:

- Reference Alloy 182 U-bends with "heavily ground" surfaces suffered extensive cracking (Figure A-134, Figure A-135 and Figure A-136 to Figure A-139). This is in agreement with past results and, in addition to the extensive cracking observed on the reference WF 422 RUB, confirmed the severity of the test conditions for PWSCC. The lower extent of cracking of the newly introduced "heavily ground" specimens compared to those in the first project could be attributed to the normal statistical scatter in PWSCC initiation time or to a somewhat more resistant weld deposit. However the extensive cracking of the RUB specimens in this specific case confirmed the severity of the test conditions.
- The 3mm thick U-bends that were strained to a greater degree than the 2 mm thick specimens were, however, surprisingly less cracked (see Table A-20) than the 2mm thick U-bends. More tests would be required to validate and understand this counter-intuitive trend.
- None of the U-bends with remedial mechanical surface treatment exhibited cracking. This result is obviously consistent with the presence of compressive stresses on the external surfaces of the U-bends, as shown by X-Ray Diffraction. Importantly, this also shows that there were no localized tensile stress peaks induced by the surface treatments that might have been able to initiate cracking.
- On one 3mm thick ground U-Bend specimen, a new PWSCC crack had initiated during the second exposure in the vicinity of large cracks initiated during the first exposure period of 1000h (see Figure A-134).
- Two defects were observed on water jet peened surfaces (longitudinal and linear defects in Figure A-140 and a slag inclusion in Figure A-141) whose nature could not be clearly determined.

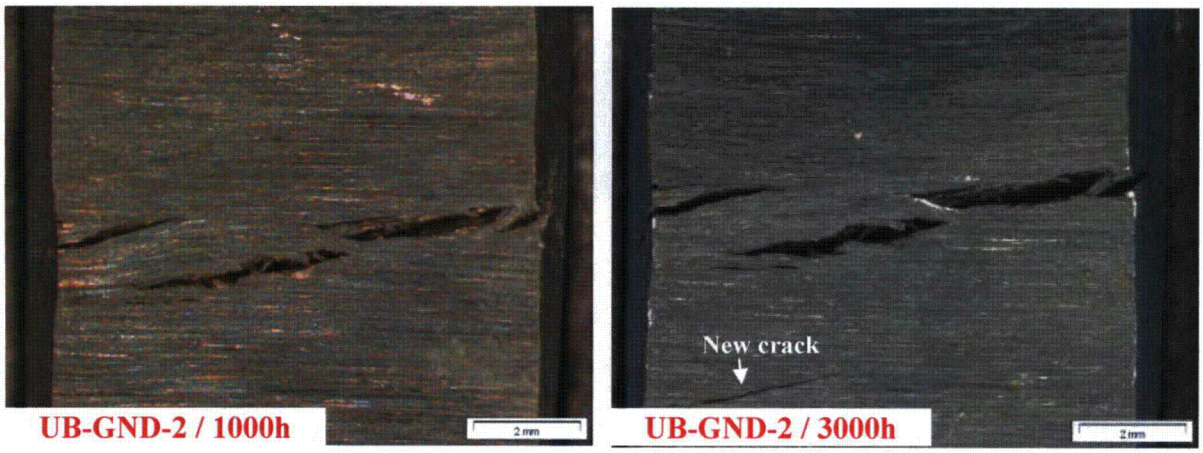

Figure A-134
UB-GND-2 with "heavily ground" surfaces after 1000 and 3000h exposure to PWR primary water at 360°C.

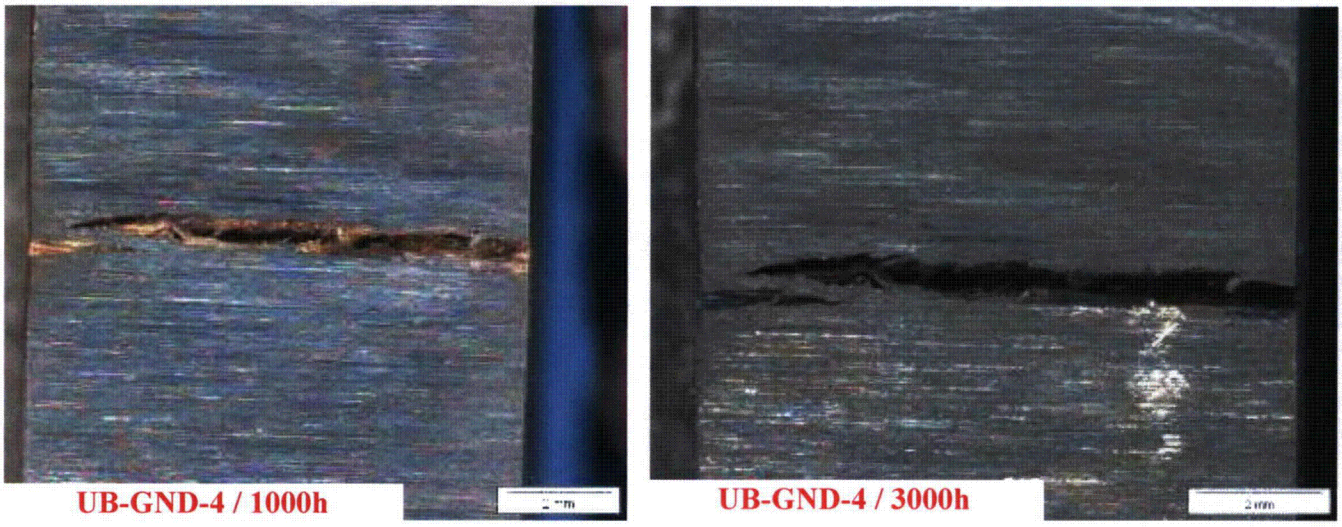

Figure A-135
UB-GND-4 with "heavily ground" surfaces after 1000 and 3000h exposure to PWR primary water at 360°C.

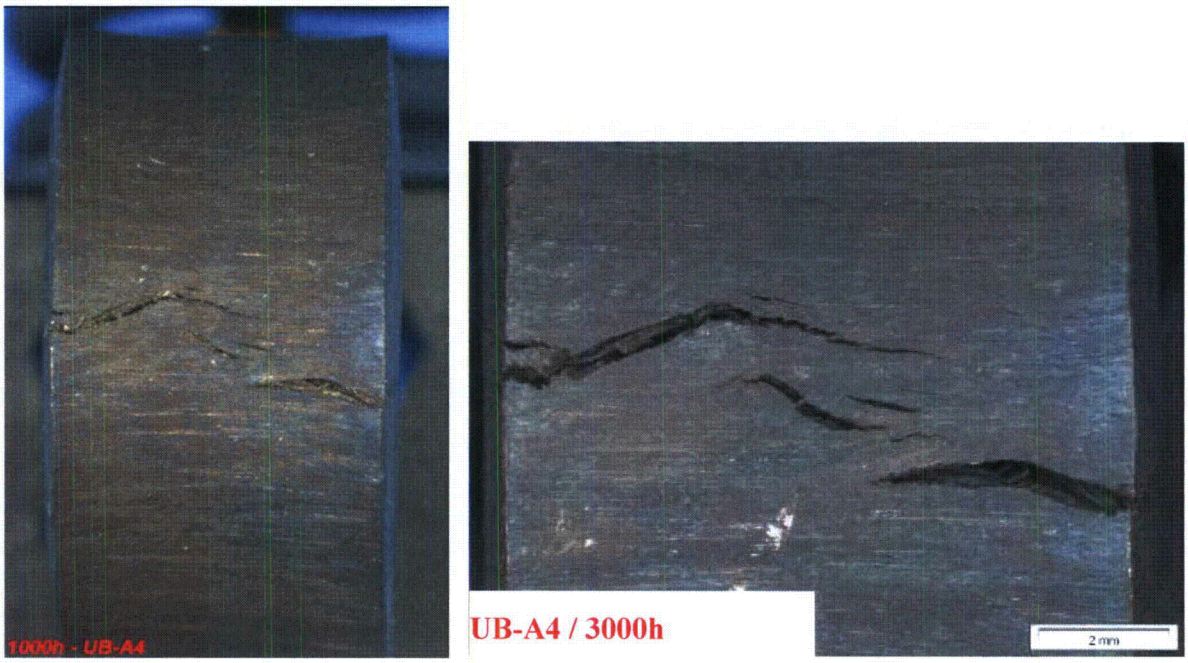

Figure A-136
UB-A4 with "heavily ground" surfaces after 1000 and 3000h exposure to PWR primary water at 360°C.

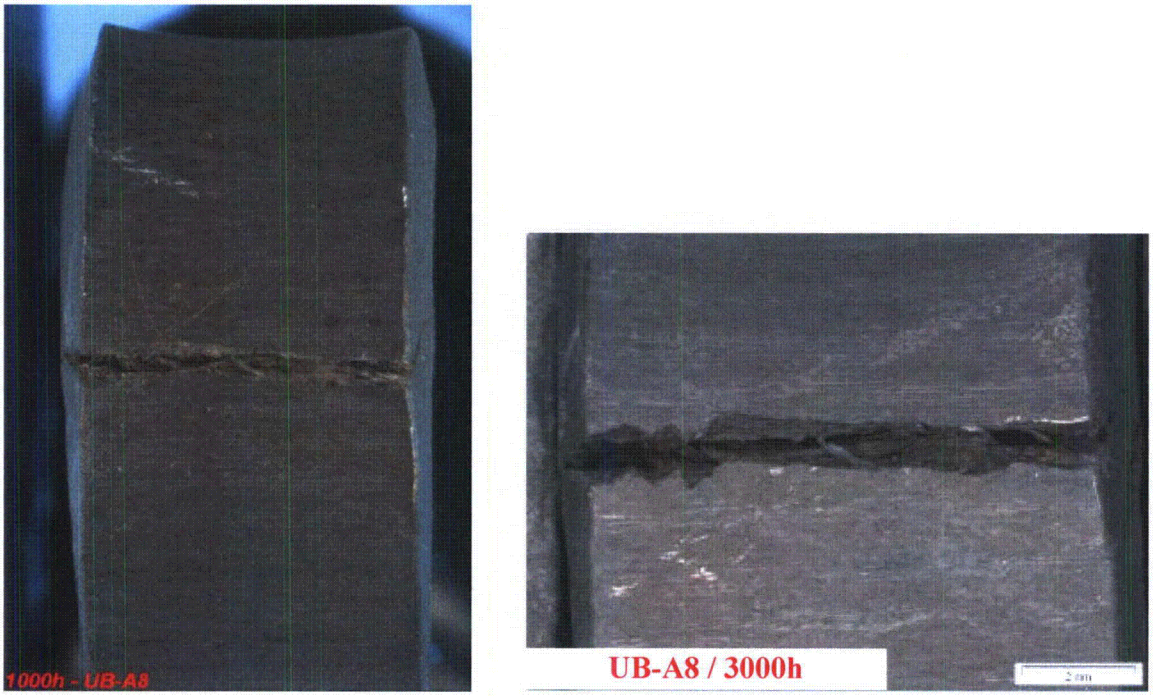

Figure A-137
UB-A8 with "heavily ground" surfaces after 1000 h exposure to PWR primary water at 360°C.

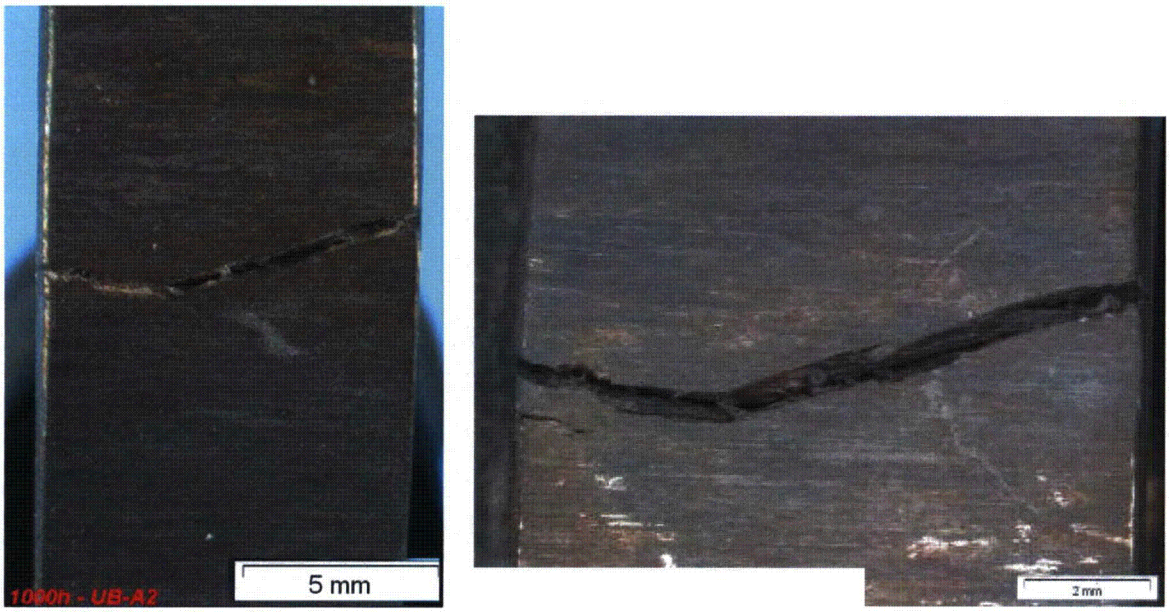

Figure A-138
UB-A2 with "heavily ground" surfaces after 1000 and 3000h exposure to PWR primary water at 360°C.

Figure A-139
UB-A3 with "heavily ground" surfaces after 1000 h exposure to PWR primary water at 360°C.

Figure A-140
UB-D3 with "Water Jet Peening" surfaces after 3000 h exposure to PWR primary water at 360°C.

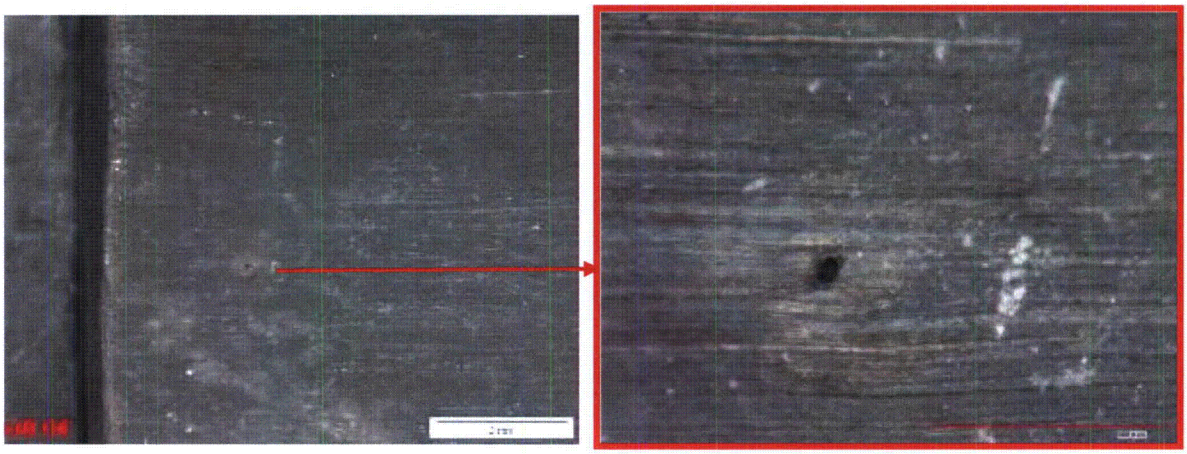

Figure A-141
UB-D8 with "Water Jet Peening" surfaces after 3000 h exposure to PWR primary water at 360°C.

Table A-19
Results of 1000+2000 h of exposure on Alloy 182 U-bends / new mechanical mitigation methods.

Surface Condition	Thickness	Loading Type	Specimen reference	Initial surface defects	After 1000 h in PWR conditions	After 3000 h in PWR conditions
Reference "Heavy Grinding" (HG)	3 mm	spring	UB-GND-1	No	No crack	No crack
			UB-GND-2	No	Large cracking in Z2/Z3	Large cracking in Z2/Z3 New Crack initiated in Z2/Z3
			UB-GND-3	No	No crack	No crack
	3 mm	bolt	UB-GND-4	No	Large cracking in Z5/Z6	Large cracking in Z5/Z6
			UB-GND-5	No	No crack	No crack
			UB-GND-6	No	No crack	No crack
HG + Air Laser Peening (MIC)	3 mm	spring	UB-ALP-1	No	No crack	No crack
			UB-ALP-2	No	No crack	No crack
			UB-ALP-3	No	No crack	No crack
			UB-ALP-4	No	No crack	No crack
	3 mm	bolt	UB-ALP-5	No	No crack	No crack
			UB-ALP-6	No	No crack	No crack
			UB-ALP-7	No	No crack	No crack
			UB-ALP-8	No	No crack	No crack
			UB-ALP-9	No	No crack	No crack

Table A-20
Results of 1000+2000 h of exposure on Alloy 182 U-bends / new mechanical mitigation methods.

Surface Condition	Thickness	Loading Type	Specimen reference	Initial surface defects	After 1000 h in PWR conditions	After 3000 h in PWR conditions
Reference "Heavy Grinding" (HG)	2 mm	spring	UB-A2	Yes	Large cracking	Large cracking
			UB-A3	Yes	Large cracking	Large cracking
			UB-A4	No	Large cracking at the apex	Large cracking at the apex
	3 mm	spring	UB-A6	No	Small cracks	Small cracks
			UB-A7	No	No crack	No crack
			UB-A8	No	Large cracking at the apex	Large cracking at the apex
HG + Under-water Laser Peening (Toshiba)	2 mm	spring	UB-B3	No	No crack	No crack
			UB-B4	No	No crack	No crack
			UB-B5	No	No crack	No crack
	3 mm	spring	UB-B8	No	No crack	No crack
			UB-B10	No	No crack	No crack
			UB-B11	No	No crack	No crack
HG + Water Jet Peening (MHI)	2 mm	spring	UB-C1	No	No crack	No crack
			UB-C2	No	No crack	No crack
			UB-C3	No	No crack	No crack
	3 mm	spring	UB-C8	No	No crack	No crack
			UB-C9	No	No crack	No crack
			UB-C10	No	No crack	No crack
HG + Water Jet Peening (Hitachi-GE)	2 mm	spring	UB-D7	No	No crack	No crack
			UB-D2	No	No crack	No crack
			UB-D3	No	No crack	Defect in Z6 that was not initially identified
	3 mm	spring	UB-D8	No	No crack	Slag inclusion in Z4
			UB-D9	Yes – Very shallow	No crack	No crack
			UB-D10	No	No crack	No crack

A.3.6 Discussion

A.3.6.1 Surface Stress Improvement Mitigation Methods

All SSI treatments tested in this project inhibited PWSCC initiation, at least for the exposure time used in this study. In addition, the use of U-bends to validate such remedial processes can be considered conservative relative to use of thicker specimens or component mock-ups. Significant deformation was observed in spring-loaded U-bends during peening, because peening relaxed the surface stresses to some extent. In other words, the compressive surface stresses induced by peening are partly relieved by deformation of the spring loaded U-bend, whereas this partial relief is not possible on rigid components.

In Table A-16, the compressive stresses measured by x-ray diffraction in the 2 mm-thick U-bends treated by ULP and WJP were lower than the stress measured in 3 mm-thick specimens with similar surface treatments. It also shows that, except in one case that needs to be verified, the compressive stresses are significantly higher in the transverse direction. This is consistent with the fact that, during surface treatment, the longitudinal deformations of the U-bends are larger than the transverse deformations, so that the stress relaxation in the longitudinal direction is more severe than that in the transverse direction.

The use of spring-loaded U-bends is a conservative method of evaluating the effectiveness of surface stress improvement techniques in plant configurations. Surface stresses induced on bolt loaded U-bends, used in the second phase of experimentation, should be intermediate between spring loaded U-bends and component mock-ups. Some deformation of the legs is possible, but not to the same extent as in spring loaded U-bends. For the peening methods discussed in this section, there are not enough stress measurements to verify this statement.

The U-bends treated with ALP developed tensile surface residual stress. As discussed in Section A.1.1.3 and MRP-162 [66], applying ALP in the absence of an ablative layer results in the ablation of a thin surface layer of the material. When this layer re-solidifies, it shrinks causing tensile stress at the surface, which becomes neutral at a very shallow depth before transitioning to highly compressive residual stresses. In the results presented in Section A.1.1.3, the residual stress becomes neutral at 0.025 mm (0.001 in). It is also worth noting that no PWSCC was found on these U-bends.

The results from Phase 1 and Phase 2 indicate that the mitigation methods investigated here inhibit or at least significantly delay PWSCC.

A.3.7 Summary and Perspectives

The results of this independent test have shown that ULP, WJP, and ALP improve resistance to PWSCC of Alloy 182 surfaces. Based on the previous PWSCC test data that crack initiation occurs in less than 250 h on U-bends with "heavily ground" reference surfaces, the present results show that the ULP and WJP surface stress improvement treatments bring a factor of improvement of at least 12 in resisting PWSCC initiation. (Because the ALP treated specimens were not included in the Phase 1 tests, the factor of improvement provided by ALP cannot be quantified from these tests.)

A.4 Experiments supporting No Unacceptable Side Effects from Peening

It is important to confirm that no unacceptable side effects are caused by peening a surface. Experiments performed by the vendors to assess the risk of unacceptable side effects resulting from peening, such as problems with inspectability by UT or excessive induced vibrations, are presented in this section. The effect of peening on the initiation of flaws and on the growth rate of pre-existing flaws was discussed in Section A.2 and A.3.

A.4.1 Effect of peening on inspectability by UT

Experiments were performed by Hitachi-GE to investigate the effect of WJP on inspectability by UT. SCC were initiated in a plate specimen of Type 304 stainless steel and a trough of Alloy 182 weld metal in an Alloy 600 plate, and phased array UT was used to determine the initial sizes of the cracks before peening. WJP was applied at parameters that give the maximum effect to assess inspectability in a worst case scenario. Phased array UT was performed again after peening, and the echo levels and measured crack depths from before and after WJP were compared. A summary of the experimental procedure can be found in Figure A-142. The measured crack depth comparisons are shown in Figure A-143, and there was no significant difference between before and after WJP suggesting that inspectability is not adversely affected by WJP.

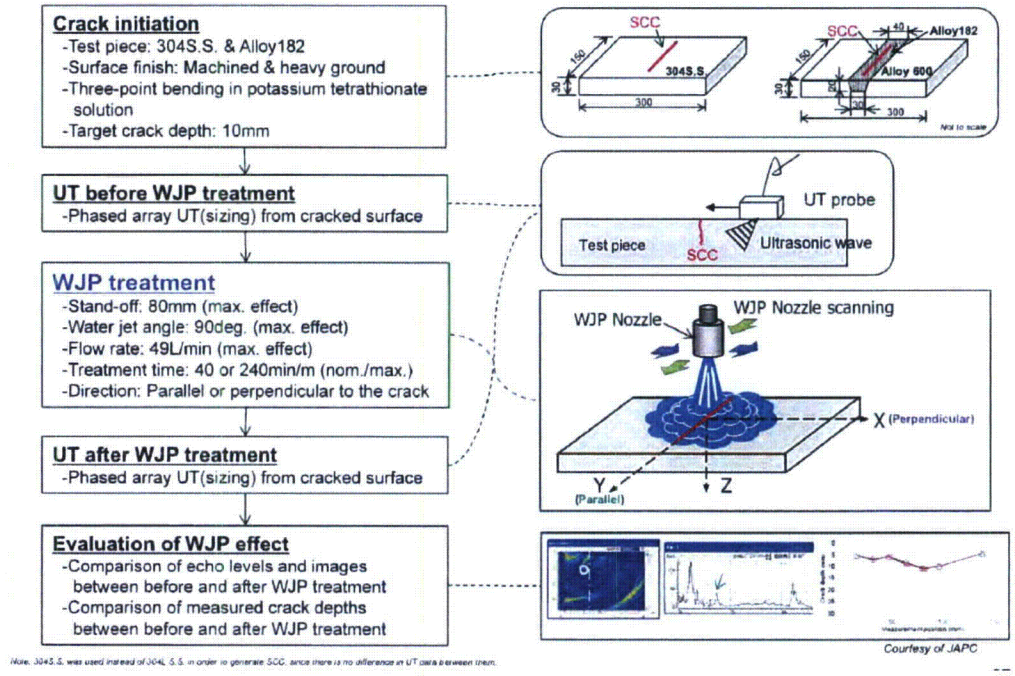

Figure A-142
Experimental procedure for investigation of effect of WJP on UT inspectability, provided by Hitachi-GE

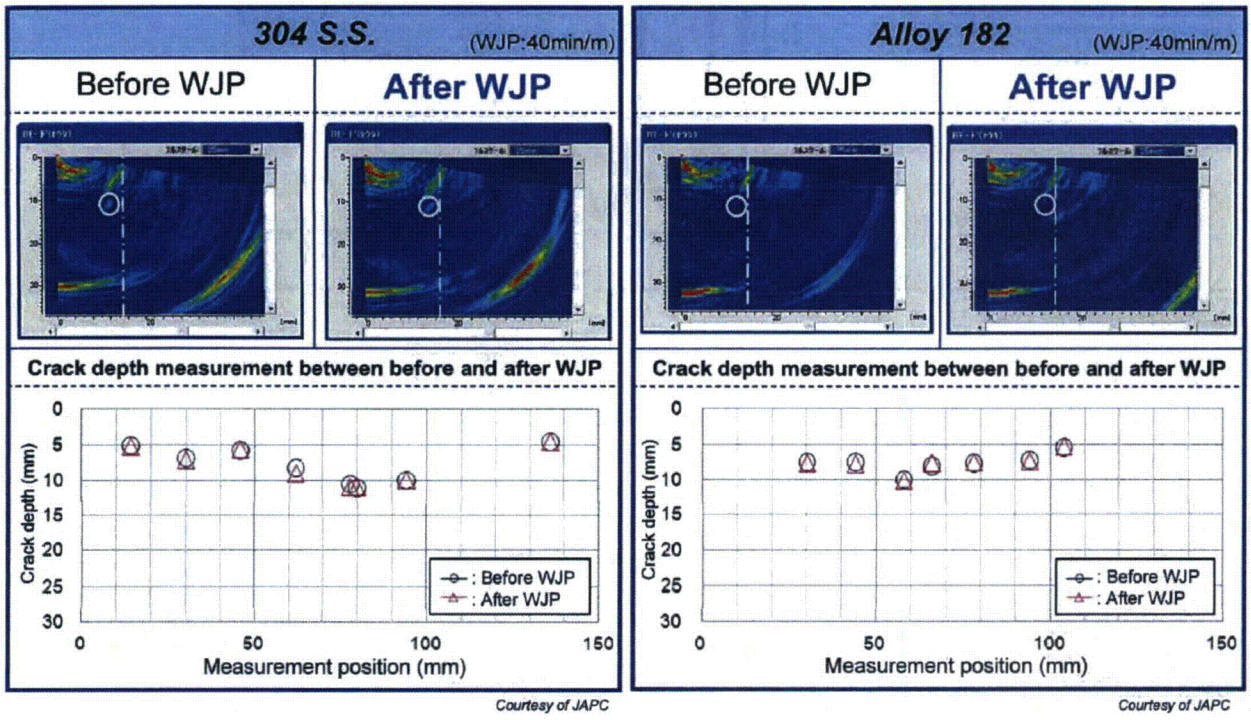

Figure A-143
Comparison of measured crack depth before and after WJP in Type 304 stainless steel and Alloy 182, provided by Hitachi-GE

A.4.2 Vibrational effect of WJP

Hitachi-GE quantified the vibrations that components, both target and surrounding, are subjected to under a range of normal WJP application conditions. The WJP parameters that were manipulated were the stand-off distance (80 – 200 mm) and the flow rate (41 – 49 L/min). The peak frequency for a set of peening conditions was determined by measuring the vibrational frequency of adjacent components. The peak frequency of applied load under typical WJP conditions was found to be approximately 450 Hz and ranges from 415 to 485 Hz over the full range of conditions investigated, as shown in Figure A-144. Hitachi-GE also states that it has techniques to reduce the amount of vibration if necessary.

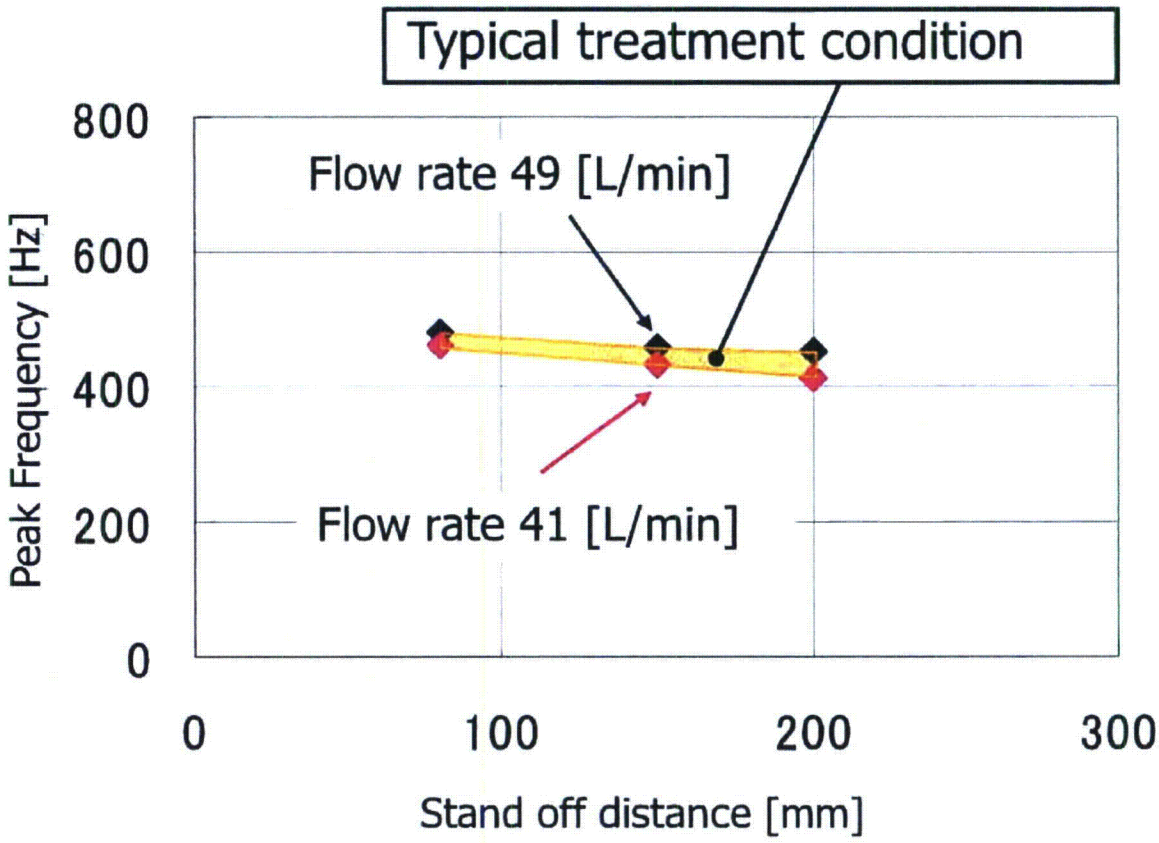

Figure A-144
Peak vibration frequency as a function of WJP application parameters (stand-off distance and flow rate), provided by Hitachi-GE

B
LONG-TERM EFFECTIVENESS OF SURFACE STRESS IMPROVEMENT

This appendix presents results of experiments conducted in order to assess the long term effectiveness of the residual stress profiles induced by the various peening methods. Given the elevated temperatures and mechanical load cycling applicable to plant operation, the compressive residual stress induced at a surface treated by SSI is subject to some degree of relaxation with time. Experiments performed by the vendors are included in Section B.1. Relaxation testing of ULP induced residual stress due to thermal relaxation is detailed in Section B.1.1, while relaxation testing of WJP induced residual stress due to load cycling or thermal relaxation is detailed in Section B.1.2. Independent testing was also commissioned by EPRI and performed by the Nuclear Research Institute in the Czech Republic to assess relaxation under conditions of high temperature and cyclic loading of specimens peened by all four vendors. The metallography, the microhardness depth profile and the surface stress were all measured, and the full results can be found in Section B.2.

B.1 Vendors' Tests on Sustainability

B.1.1 Sustainability of Stress Improvement by ULP

To demonstrate the sustainability of stress improvement by ULP, Toshiba performed tests on reversed U-bend specimens after ULP treatment. Surface residual stress was measured on reversed U-bend (RUB) specimens of Alloy 600 before and after laser peening to confirm the applicability of ULP to material with extremely high tensile stress on the surface. The tests were conducted in a high-temperature primary water environment at 360°C for 1000 hours. The temperature of 360°C acts to accelerate the effects of stress relaxation via creep effects compared to the operating temperature range of about 285-320°C for PWR components of interest for SSI treatment.

The test procedures and the test results are summarized in Figure B-1 and Figure B-2, respectively. The results demonstrate that underwater laser peening introduced high compressive residual stresses onto the specimens and that the compressive stress remained relatively unchanged for 1000 hours at 360°C.

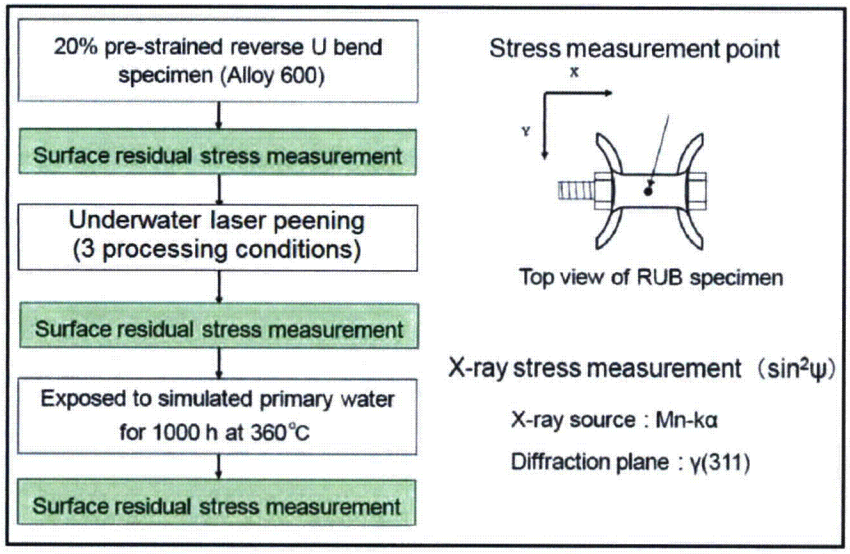

Figure B-1
Procedures for confirmation of residual stress stability on Alloy 600, provided by Toshiba

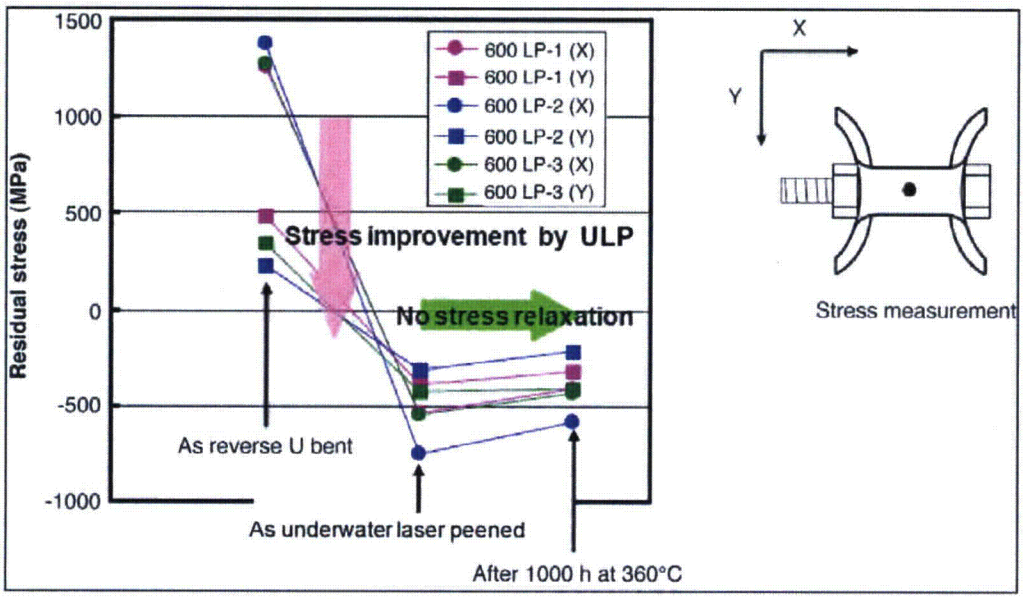

Figure B-2
Test results on residual stress stability on Alloy 600, provided by Toshiba

Toshiba also provided some further thermal relaxation data on an Alloy 600 specimen. The residual stress profile was measured in both directions to a depth of 1 mm before and after the specimens were held at elevated temperature. The Alloy 600 specimen was held at 350°C for 1646 h. The data are depicted in Figure B-3.

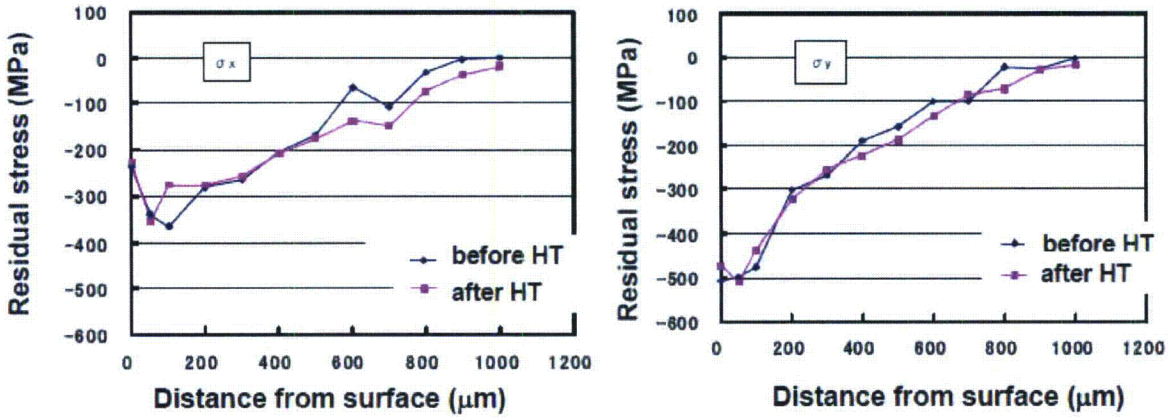

Figure B-3
Thermal Stress Relaxation test on Alloy 600 at 350°C for 1646 h

B.1.2 Sustainability of Stress Improvement by WJP

B.1.2.1 Stress Shakedown by Load Cycling

Separately, both Hitachi-GE and Mitsubishi investigated the long-term sustainability of stress improvement by WJP under cyclic loading and under the condition of elevated temperature. To investigate stress shakedown, tests by Hitachi-GE under cyclic strain that simulated the transient loading in a reactor were performed. With the specimens treated with WJP, a 100-cycle straining test revealed reduction of compressive stress in the first 10 cycles, but no further significant reduction throughout the remaining 90 cycles, Figure B-4. The specimens with WJP treatment sustained compressive stress throughout the entire 100 straining cycles.

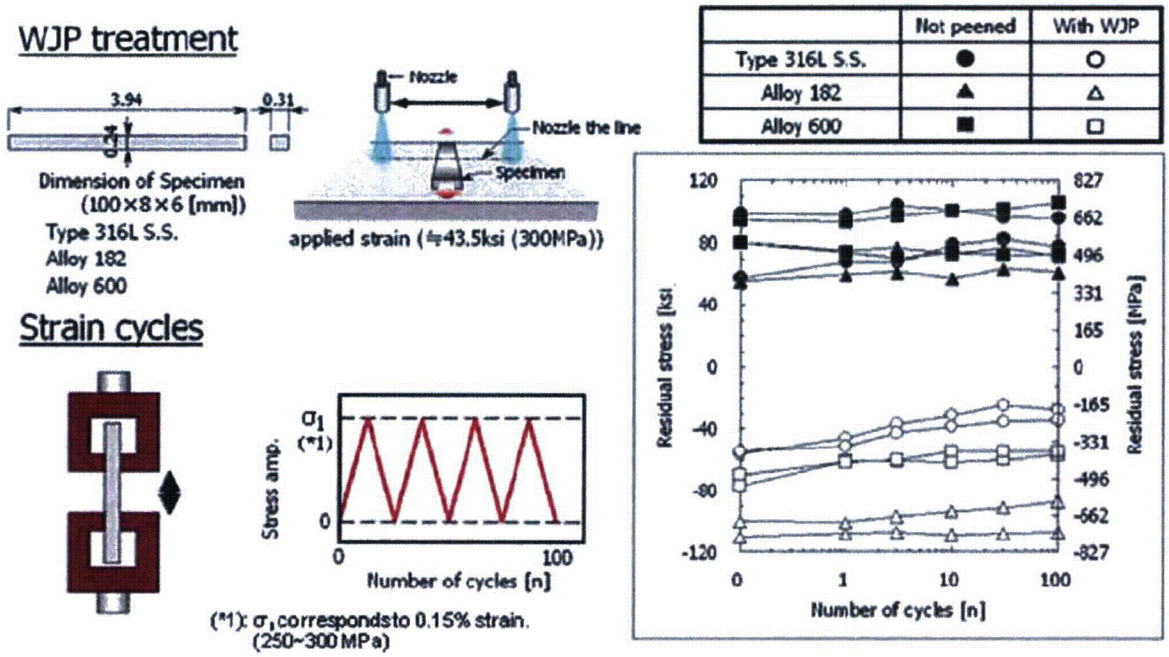

Figure B-4
Shakedown test (strain cycles (tensile)), Type 304 SS/Alloy 182/Alloy 600), provided by Hitachi-GE

Mitsubishi performed experiments to assess the cyclic stresses on components associated with start-up and shut-down on the residual stresses. In order to simulate the cyclic effect of plant start-up and shut-down, a tensile stress is applied to the peened surface of the Alloy 600 base metal test coupons treated with WJP by a three point bending method as shown in Figure B-5. Up to 2000 cycles were applied at stress ranges of up to 245 MPa (i.e. from a stress of 0 MPa to a maximum stress of 245 MPa tensile). The results of this testing, shown in Figure B-6, demonstrate that compressive residual stresses were sustained through 2000 cycles of high alternating stresses. The results from these tests under cyclic stress conditions support the long-term sustainability of the stress improvement provided by WJP treatment given plant startup and shutdown cycles.

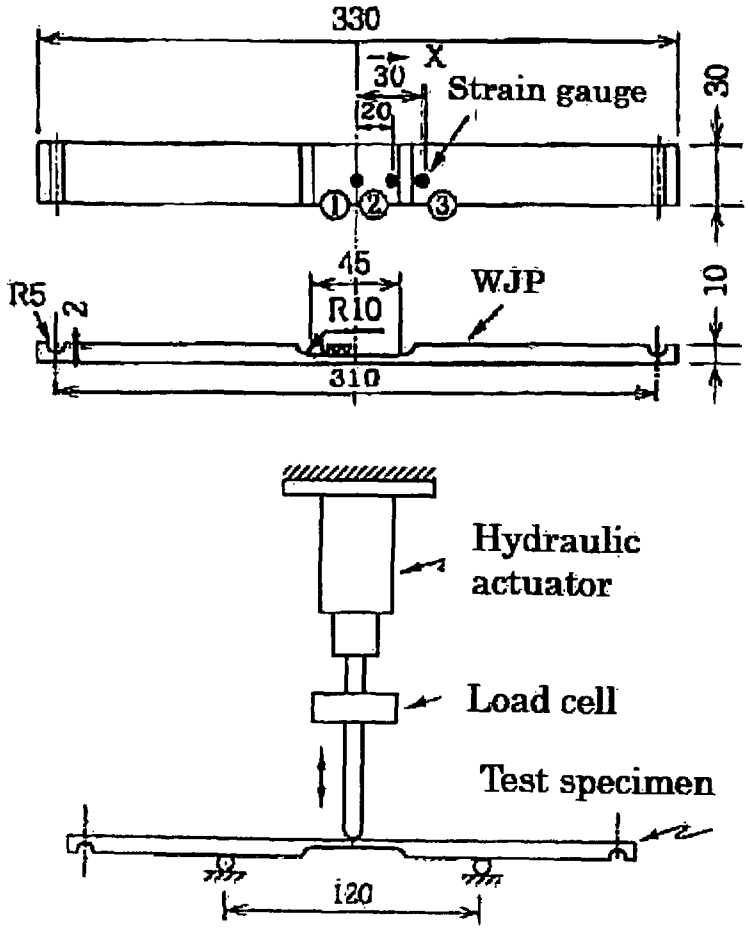

Figure B-5
Specimen for Cyclic Stress Relaxation Testing, provided by Mitsubishi

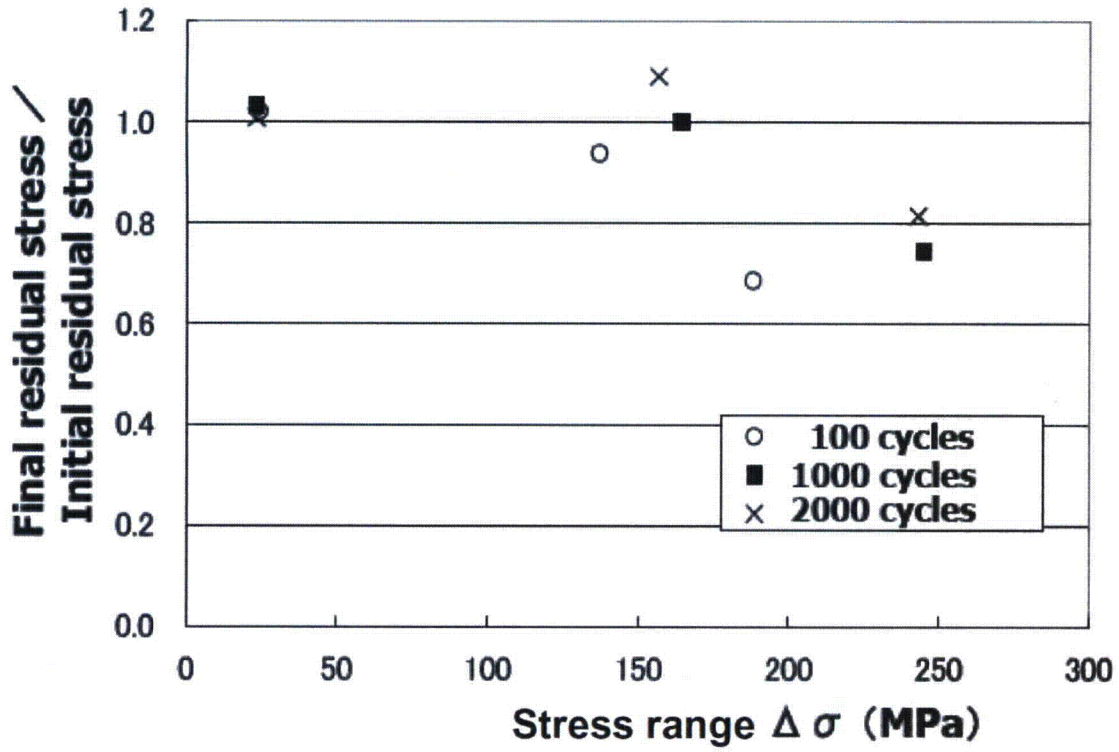

Figure B-6
Results of Cyclic Stress Relaxation Testing, provided by Mitsubishi

Experiments were also performed by Mitsubishi to assess the effect of load cycling at elevated temperature conditions. DM weld specimens of Alloy 600 and Type 316 SS butt welded together with Alloy 132 were treated with WJP or USP, and one specimen for each surface treatment was subjected to elevated temperature load cycling (130 MPa for 300 cycles at 1230 sec/cycle at 420°C) while the another specimen for each surface treatment was subjected to the elevated temperature without the load cycling. 300 cycles was chosen to account for 60 years of starting and stopping an actual plant assuming 5 starts/stops per year. Residual stress was measured by XRD in both specimens multiple times over the course of the experiment. The total time at temperature was 100 hours. The test procedure is shown in Figure B-7 and the result are presented in Figure B-8. For both surface treatment, the residual stress remained significantly compressive, and in the case of WJP, the difference in relaxation between the load cycled specimen and the specimen exposed only to elevated temperature was small.

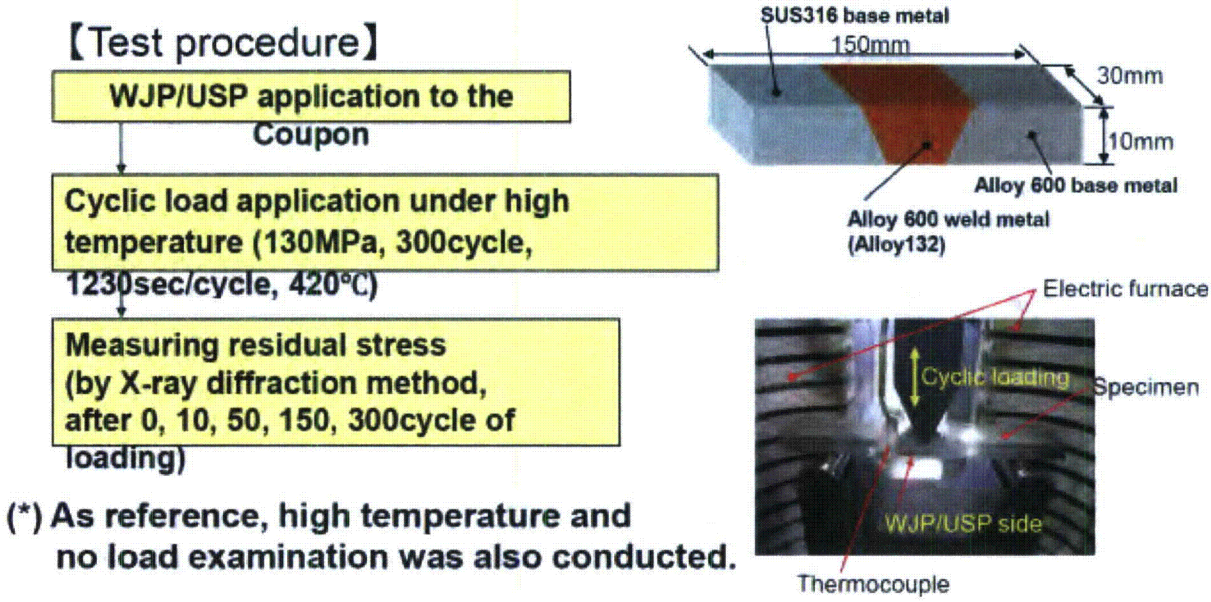

Figure B-7
Test Procedure for High Temperature Load Cycling Experiments by Mitsubishi

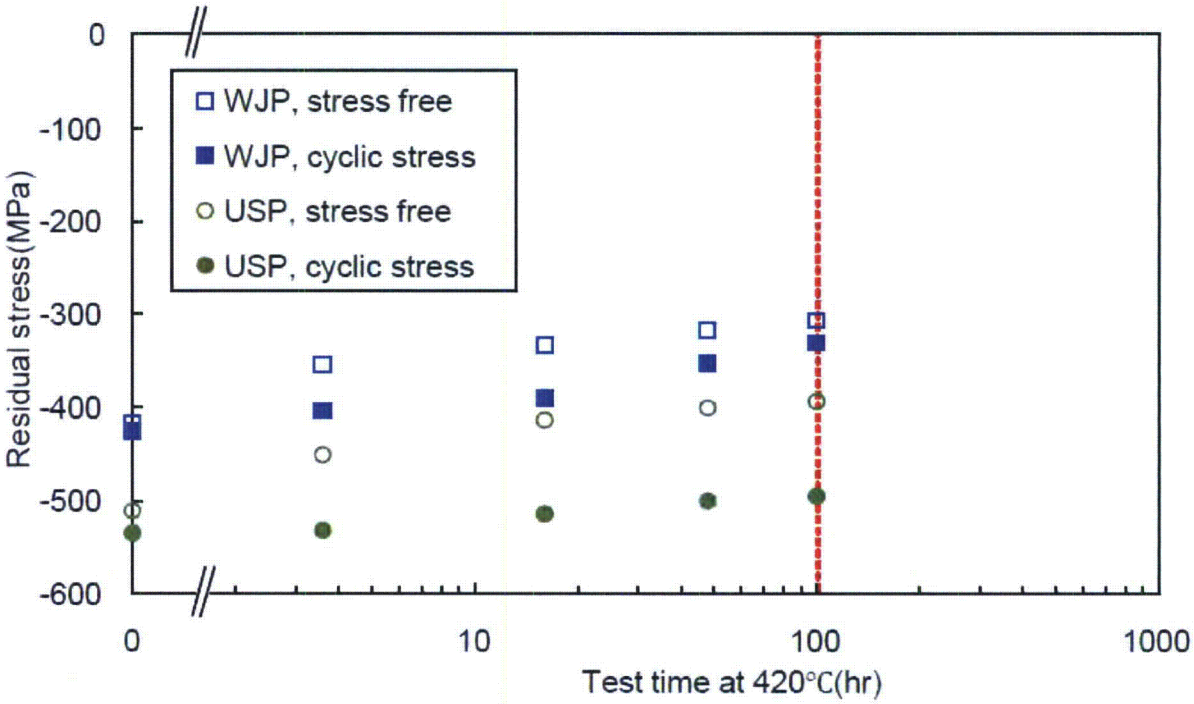

Figure B-8
Results of High Temperature Load cycling experiments by Mitsubishi

B.1.2.2 Thermal Stress Relaxation

To evaluate thermal relaxation in plant operation, an accelerated thermal relaxation test was performed at 450°C by Hitachi-GE. The temperature of 450°C acts to accelerate the effects of stress relaxation via creep effects compared to the operating temperature range of about 285-320°C for PWR components of interest for SSI treatment. Figure B-9 summarizes the test scheme and the test results. The WJP nozzle was scanned in the y-direction. For each material, three replicates were done, and the stress measurements for each replicate are shown in different colors on the plots. In the first hour of this test, a reduction in the level of compressive stress was observed. However, compressive stress remained at this reduced level for the rest of the test. Specimens with WJP treatment maintained their compressive status through the end of test. This result demonstrates that the compressive stress produced by WJP is stable for long-term operation.

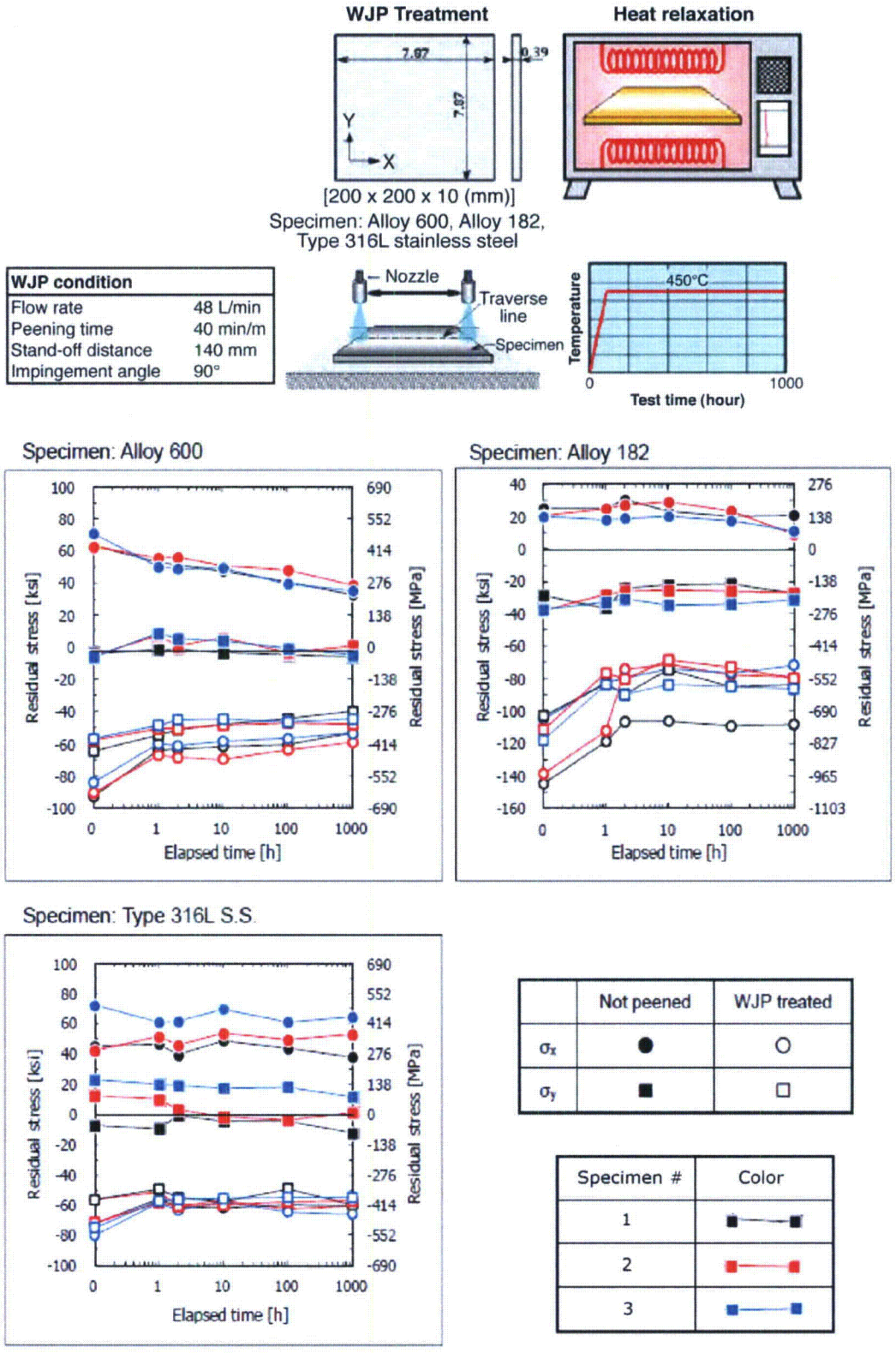

Figure B-9
Thermal relaxation test (Alloy 600 / Alloy 182 / 316L SS) at 450°C, provided by Hitachi-GE

Mitsubishi also performed thermal relaxation tests to investigate the effect of elevated temperature on the compressive residual stress produced via WJP. The potential concern is that the mitigated component may lose its compressive residual stresses over time and once again become susceptible to initiation of PWSCC. It is generally believed that stress relaxation is caused by creep phenomenon under a high temperature environment.

The Mitsubishi thermal aging tests were carried out at three different temperatures (320°C, 350°C, and 380°C) using the test coupon illustrated in Figure B-10. The upper two test temperatures act to accelerate the effects of stress relaxation via creep effects compared to the operating temperature range of about 285-320°C for PWR components of interest for SSI treatment. Three measurements of residual stress were taken at each of several aging times for each temperature. Table B-1 and Figure B-11 show the data that were obtained from this testing. These tests indicate that the compressive residual stresses imparted through the WJP process can be maintained under actual PWR operating conditions at a temperature of approximately 320°C (608°F), which is close to the upper end of temperatures of interest for SSI treatment in PWRs.

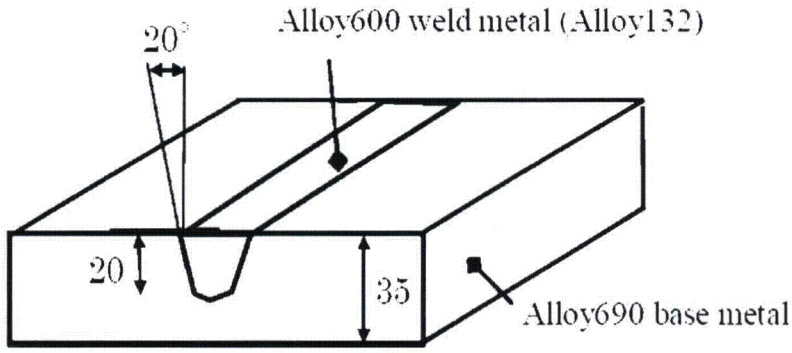

Figure B-10
Specimen for Relaxation Testing Under High Temperature Environment, provided by Mitsubishi

Table B-1
Data for Temperature Relaxation Testing, provided by Mitsubishi

Temperature	Time (hours)	Time (seconds)	Larson-Miller Parameter	Residual Stress (MPa)
380°C (716°F)	Initial State (After WJP)	Initial State (After WJP)	4000	-364
				-380
				-472
	1	3600	13100	-262
				-295
				-324
	10	36000	13755	-288
				-283
				-344
	100	360000	14410	-278
				-245
				-315
	1400	5040000	15161	-288
				-267
				-342
350°C (662°F)	Initial State (After WJP)	Initial State (After WJP)	4000	-366
				-311
				-354
	1	3600	12500	-282
				-238
				-275
	10	36000	13125	-286
				-249
				-297
	100	360000	12750	-366
				-263
				-293
	1400	5040000	14466	-275
				-267
				-298
320°C (608°F)	Initial State (After WJP)	Initial State (After WJP)	4000	-412
				-404
				-332
	1	3600	11900	-327
				-333
				-260
	10	36000	12495	-310
				-320
				-267
	100	360000	13090	-309
				-307
				-257

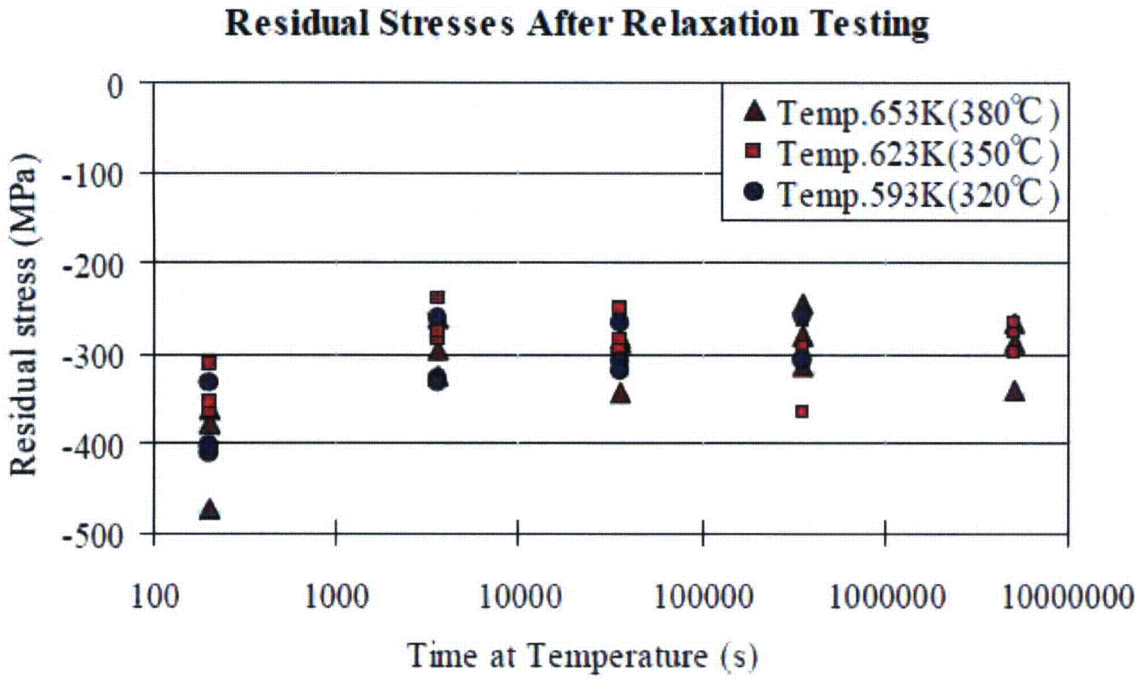

Figure B-11
Results of High Temperature Relaxation Testing, provided by Mitsubishi

B.2 Independent Testing by EPRI

B.2.1 Test Procedure

The objective of the EPRI testing was to evaluate the stress relaxation of a peening-induced compressive stress layer at and close to the sample surface under the influence of load cycling and operating temperature. The samples were manufactured at NRI from Alloy 600 plate material supplied by EPRI. They were subjected to different peening procedures by different vendors, with one set of samples left in the as-manufactured condition. Then the samples were exposed in an autoclave loop filled with PWR water at 300°C for different numbers of cycles. The loading pattern of one cycle consists of a slow ramp-up to three-fourths of yield strength, a holding period of 10 days, and a slow ramp-down to a load of zero.

In order to quickly assess the whole experiment prior to its start in the large autoclave, a small-scale test in a small Golem I autoclave was performed to check on the specimen dimensions, the applied forces, and the size of the specimen holders inside the autoclave. Three different methods were utilized to evaluate the test samples: metallography, microhardness depth profiling, and surface stress measurements. Each evaluation method was applied first on unexposed samples as the baseline measurement and then on exposed samples. The metallographic observation was used for a general description of the subsurface material microstructure and its alteration by peening procedures.

The microhardness depth profile measurement was used to evaluate the effect of the peening procedure on the material properties and to determine the hardness changes throughout the test. Although the data obtained by surface hardness measurement are less comprehensive, useful information can be derived through comparison with the nominal values defined in manufacturing specifications or standards. The most important part of the evaluation is surface stress measurements by x-ray diffraction, which determines the numerical value of surface stresses and their changes due to mechanical loading and thermal exposure.

B.2.1.1 Autoclave and Test Parameters

The IK-610 autoclave system used in the test consists of a heated recirculation flow autoclave vessel, an integrated bellows system for sample mechanical loading, and a water loop with a medium storage tank. The volumes for the autoclave tank and storage tank are 50 and 13 liters, respectively. The designed temperature inside the autoclave was 300°C, and the operational pressure was 9 MPa. Dedicated software was used to control the operation while all operational parameters (temperature, pressure, flow rate, electrochemical corrosion and redox/reduction potentials, outlet oxygen concentration, and outlet conductivity) were recorded throughout the test. A schematic of the autoclave and the loop is presented in Figure B-12. The autoclave internal tube is 186 mm in diameter and 4450 mm long.

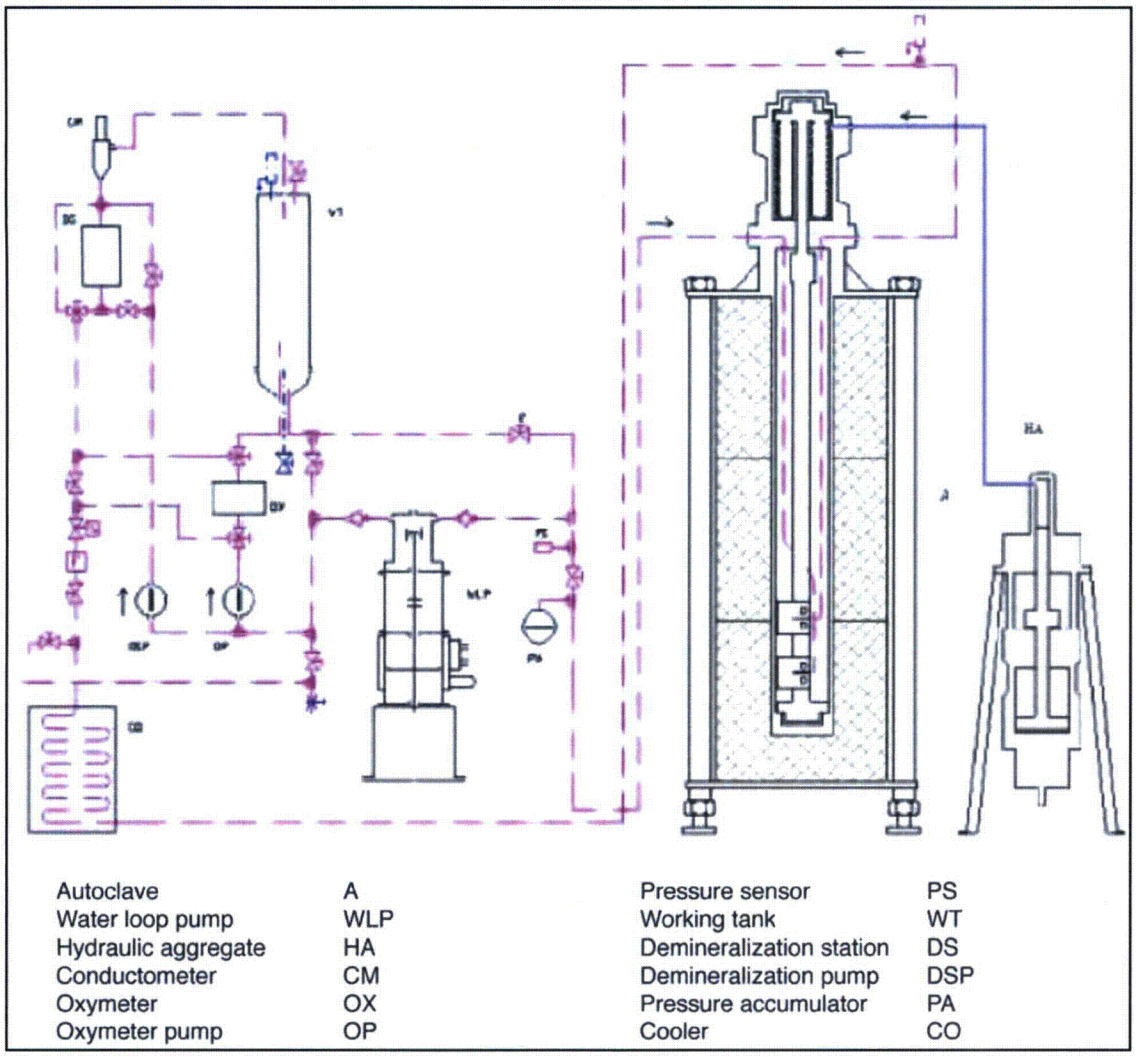

Figure B-12
Schematic drawing of the autoclave loop IK-610

The autoclave internals were modified to allow for simultaneous testing of eight tensile samples. The samples were arranged in a chain interconnected by special couplers, as shown in Figure B-13. As listed in Table B-2, the actual composition of the experimental water was measured and analyzed after each autoclave run.

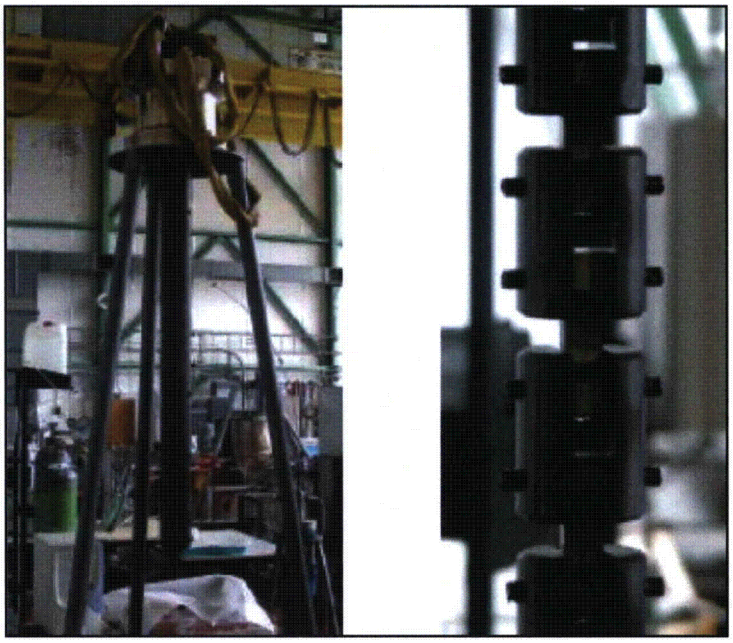

Figure B-13
General view of the autoclave internals and part of the chain with interconnected samples

Table B-2
Chemical analysis of the primary medium

Autoclave Run (hours)	Fluorides (µg/l)	Chlorides (µg/l)	Sulfates (µg/l)	Phosphates (µg/l)	Nitrates (µg/l)
Before exposure	16.21	157.31	365.48	378.27	250.88
4 cycles	14.10	36.94	153.03	37.51	103.66
8 cycles	12.98	71.22	573.58	37.51	44.23
Testing end	14.72	83.60	599.11	36.98	42.96

Similar experiments were performed at a later time by NRI for EPRI to assess the load cycling relaxation of a peening induced compressive stress layer in specimens treated with MIC's air laser peening with an ablative layer. The test arrangement and analytical equipment used for this project are the same and, as a result, are not described in detail here.

B.2.1.2 Test Samples

The material microstructure of the sample material used in the first set of experiments is shown in Figure B-14. Significant texture change caused by rolling is clearly visible by comparing the micrographs for Section 1 and Section 3. Small grains are precipitated at the large grain boundaries, where a large amount of fine precipitates as well as titanium carbides are visible.

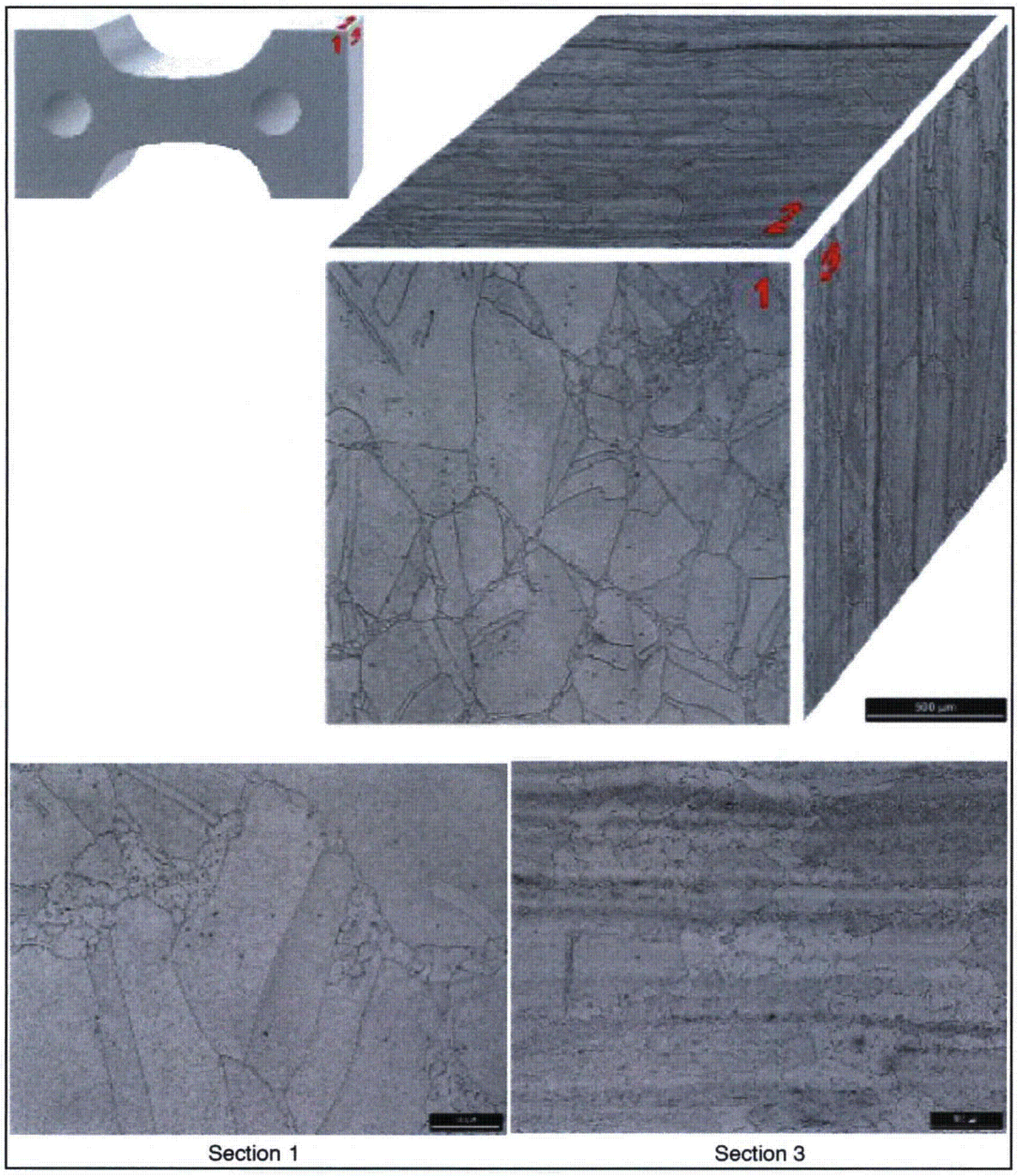

Figure B-14
Microstructure of the sample material

The samples were manufactured at NRI from Alloy 600 material supplied by EPRI. The material was produced by Jessop Specialty Products. The sample dimensions are shown in Figure B-15, and material characteristics provided in the certificate are listed in the Table B-3.

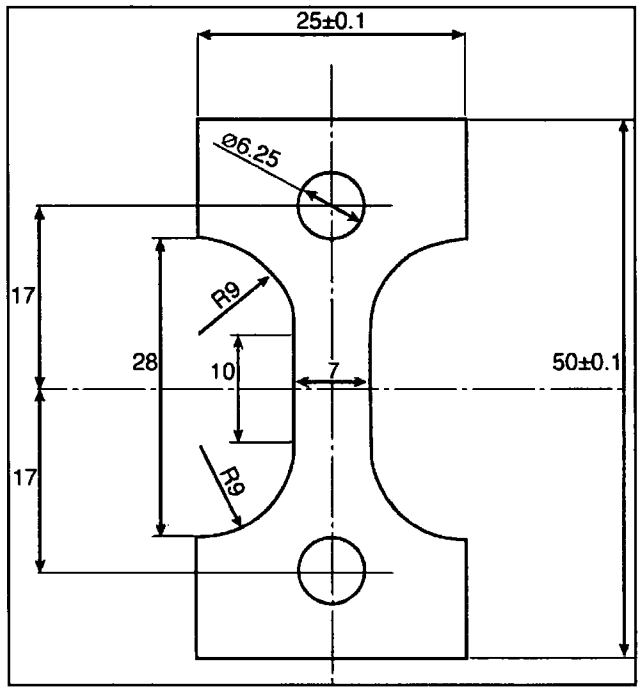

Figure B-15
Drawing of the test sample with dimensions in mm (sample thickness is 12.5 mm)

Table B-3
Alloy 600 chemical composition and mechanical properties provided in the certificate

Yield Strength			48.6 ksi / 335 MPa			Tensile Strength		97.5 ksi / 672 MPa						
Elongation			47.0%			Reduction of Area		56.0%						
C	Mn	P	S	Si	Ni	Cr	Co	Cu	Fe	N	Cb	Ta	Ti	Al
0.050	0.21	0.006	0.0003	0.20	74.97	16.00	0.06	0.03	7.80	0.002	0.03	0.003	0.28	0.29

All test samples were manufactured with the same procedure, which started with rough machining on a milling machine, after which both sides of the samples were processed on a grinding machine. After that, one set of samples was left untreated in the as-manufactured condition, and other samples were sent to four different vendors for surface treatment. Table B-4 summarizes the vendor assignment information for the first round of testing.

Table B-4
Vendors, peening processes, and samples used for first set of tests

Peening Vendor	Peening Type	Samples
Hitachi-GE	Water Jet Peening	F2, F3, F5, F7, F8
Mitsubishi	Water Jet Peening	F17, F20, F21, F22, F23
Toshiba	Underwater Laser Peening	F11, F12, F13, F14, F15
As manufactured	—	F27, F28, F29, F30, F31

The material used in the second set of experiments, involving MIC's air laser peening, had a material structure that was different from the one used in the first set of experiments. This fact is clearly visible on the macrophotographs and micrographs of the polished and etched perpendicular section through the central part of the dog bone sample, see Figure B-16. The material used for the former study is partially recrystallized with the smaller grains precipitating along the grain boundaries of larger grains (on the right). Material used in the second set of experiments has significant deformation bands parallel to the plate surface, indicating higher cold work (on the left). In general the hardness in the regions with smaller grains is higher, compared to the large grain size areas. This feature is clearly visible on the microhardness depth profile plots. A mostly gradual drop in the microhardness values is interrupted by repeated spikes, indicating positions where the microhardness indent was applied within the small grain area.

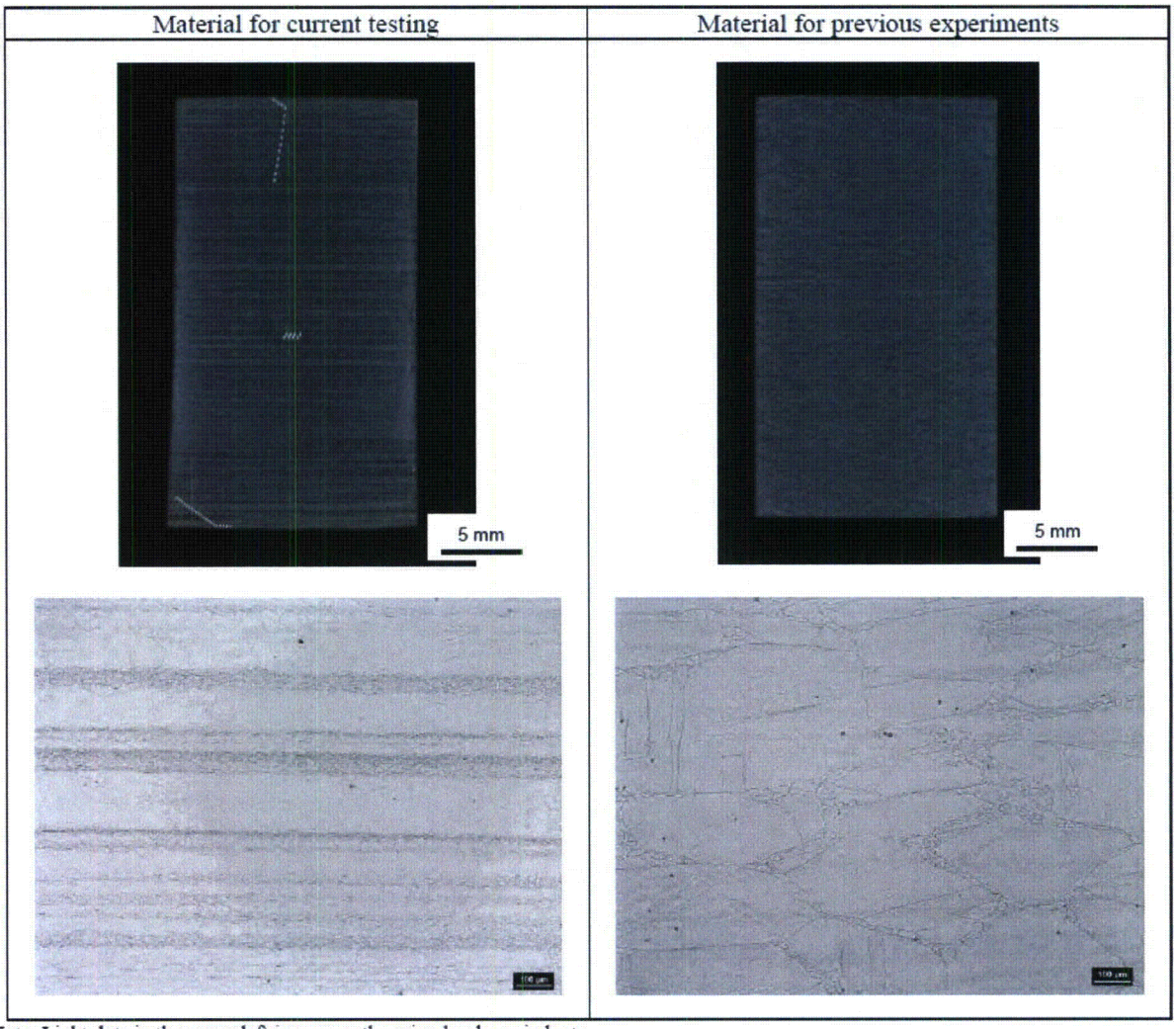

Note: Light dots in the upper left image are the microhardness indents.

Figure B-16
Comparison of the Microstructure of the Material Available for this Project (left) and the Material Used for the First Set of Experiments (right)

The differences in the microstructure represent the only significant change between the first and second set of experiments. They should be taken into account during final evaluation of the peening processes.

B.2.1.3 Test Procedure

After samples were installed inside the autoclave, the whole system was sealed and filled with medium before the flow pump was started. Due to the large dimensions of the autoclave, it took two days to heat the system up to the operational temperature.

During both sets of testing, samples were loaded with static stresses for different numbers of cycles. Each cycle consisted of a slow ramp-up to 20 kN in about 5 minutes, holding for 240

hours, a slow ramp-down to zero load in 5 minutes, and holding for 1 hour. The samples with various surface treatments were exposed to two, four, or eight cycles; the test matrix is shown in Table B-5 and Table B-6.

Table B-5
Stress relaxation test matrix

Peening Vendor	2 Cycles	4 Cycles	8 Cycles
Hitachi-GE–WJP	F5, F8	F3, F7	F2
Mitsubishi–WJP	F21, F23	F20, F22	F17
Toshiba–ULP	F14, F15	F12, F13	F11
As manufactured	F30, F31	F28, F29	F27

Table B-6
Sample Numbering for ALP treated specimens

Peening Vendor	Unexposed	2 cycles	4 cycles	8 cycles
MIC	AB13	AB7, AB8	AB9, AB11	AB2, AB10

B.2.2 Test Results and Analysis

The test results obtained from metallographic observation, microhardness depth profile measurement, and stress level measurement (before and after testing) are compared in this section. Visual appearance of the samples after peening and after testing is documented as well. There were five surface conditions tested over two sets of experimentation: as-manufactured, treated by underwater laser peening (Toshiba), treated with water jet peening (by Hitachi-GE and Mitsubishi, respectively), and treated by air laser peening (MIC). The data are presented with respect to the number of loading cycles.

B.2.2.1 As-Manufactured Samples

The purpose of as-manufactured sample testing was to obtain the benchmark values of standard material without any surface treatment. Their surfaces were ground only. The appearance of the samples prepared for exposure is shown in Figure B-17. Samples were randomly selected for the exposure of different cycles. Appearance of the samples after exposure is shown in Figure B-18. All samples are covered by high-temperature oxides originating mainly from the pins and also from the interconnecting fixtures as shown in Figure B-13. To check the dimensional change, the sample lengths were measured before and after each experiment. The difference was found to be within measurement tolerance, which confirms that the samples were not strained over the yield strength.

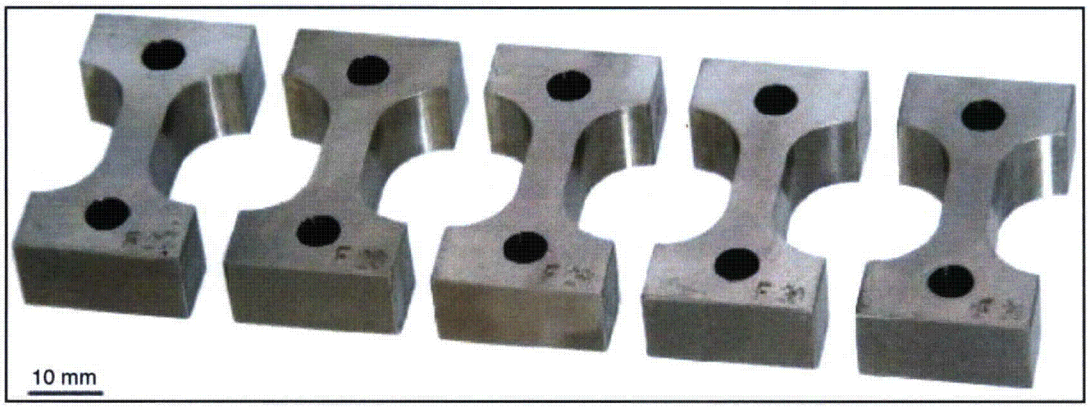

Figure B-17
All samples prepared for exposure

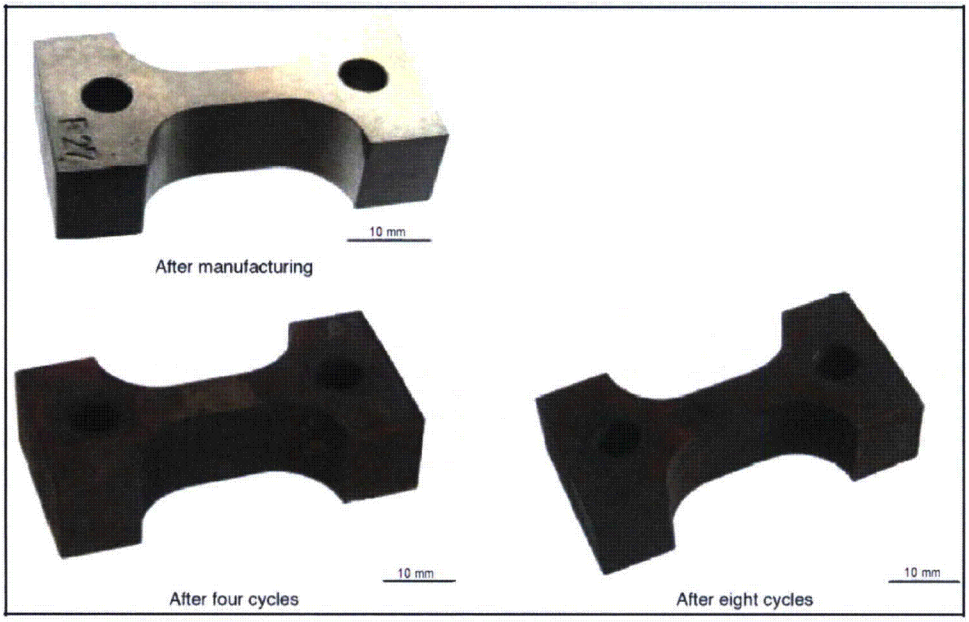

Figure B-18
Appearance of the as-manufactured samples after different stages of the experiment

The microstructure in the area under the surface is shown in Figure B-19. No visible change was observed in microstructure after exposure, in terms of grain size variations or carbide precipitation. In addition, the subsurface area of the sample does not show any significantly deformed layer that would indicate extensive cold working.

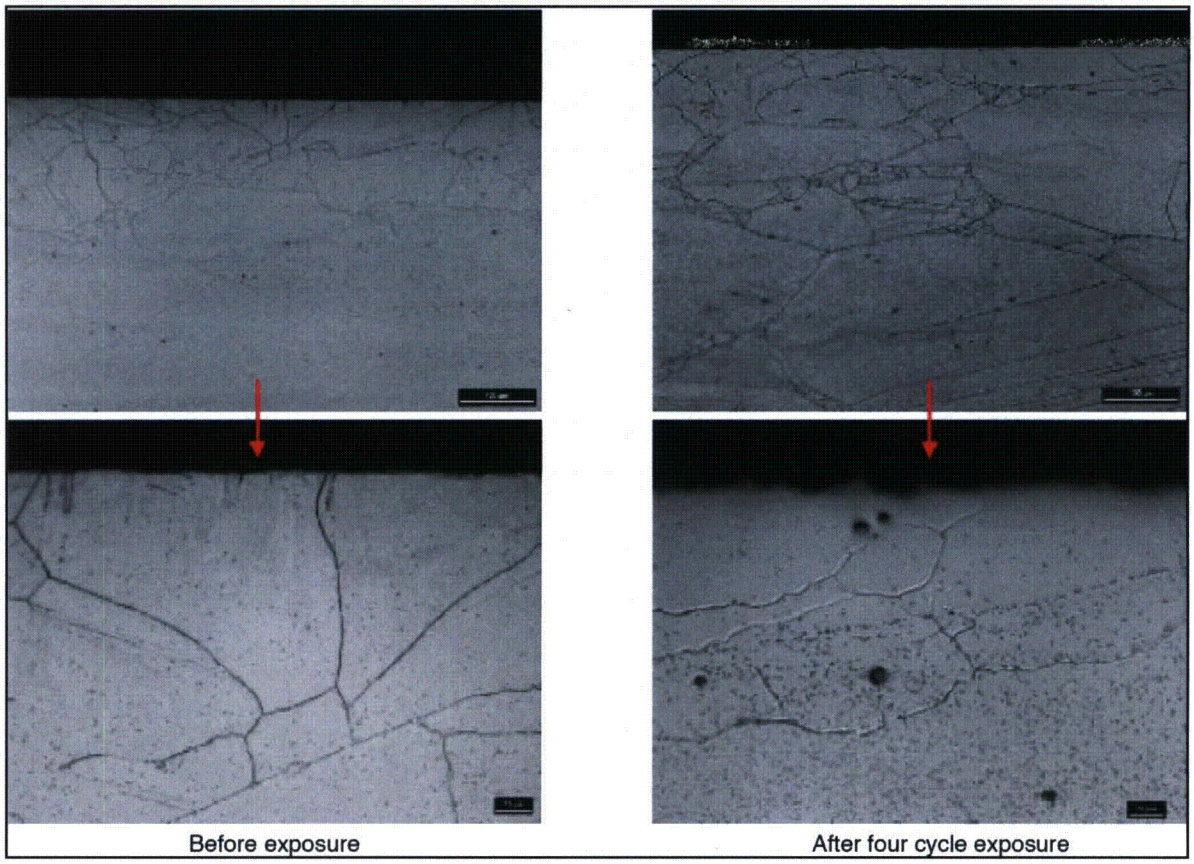

Figure B-19
Subsurface layer microstructure of the as-manufactured sample

The microhardness depth profile is shown in Figure B-20. The measurements were taken to the depth of about 700 μm under the surface for three types of samples: unexposed, exposed for four cycles, and exposed for eight cycles. The short horizontal line close to the location of the surface shows an average microhardness value directly beneath the surface, calculated from five measurements.

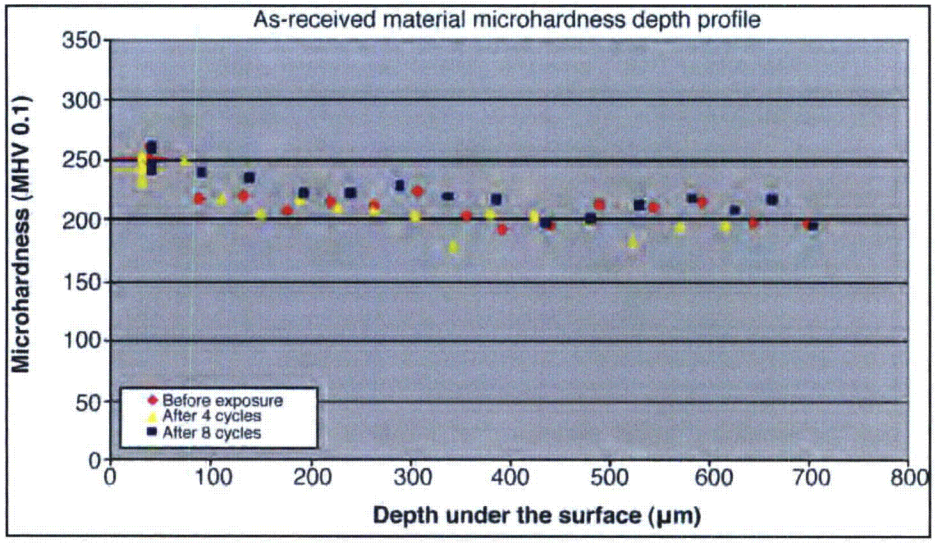

Figure B-20
Microhardness depth profile of the as-manufactured sample

No significant change between the unexposed and exposed samples was found with respect to inherent scatter of microhardness data. The surface microhardness is about 10% over the bulk material microhardness (MHV). This elevated value decreases rapidly to the bulk material value at approximately 100 µm under the surface. The variations of the individual MHV measurements deep in the material are caused by the fact that indents were imprinted into the grains with different orientations and generally cover various lengths of the grain boundaries.

The results of surface stress measurements are shown in Figure B-21, and individual values together with standard deviations are listed in Table B-7. Note that the first bar in the graph indicates the value before exposure; the second bar indicates the surface stress value measured on the same sample after exposure of a specific number of cycles.

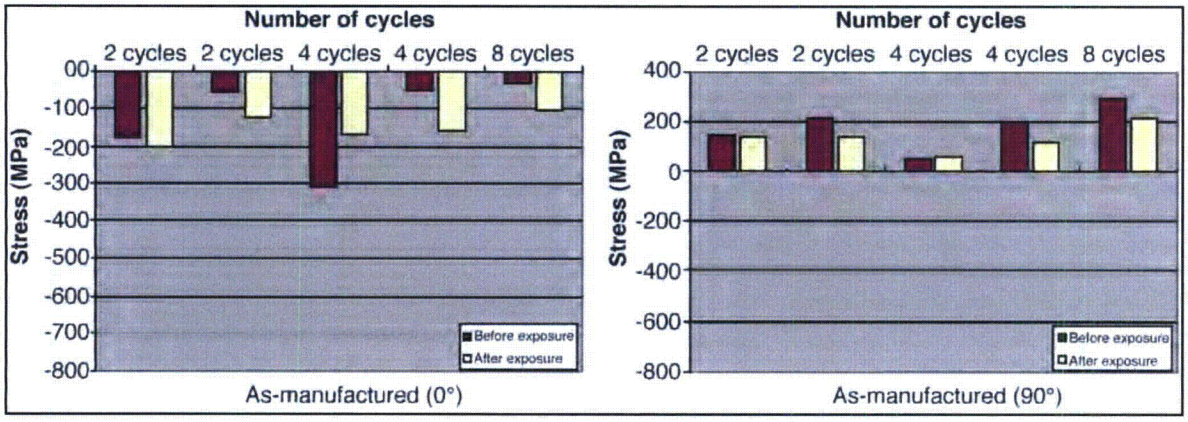

Figure B-21
Surface stresses measured parallel (left) and perpendicular (right) to the loading direction, as-manufactured

Table B-7
Results of the stress measurements: as-manufactured

		2 Cycles		2 Cycles		4 Cycles		4 Cycles		8 Cycles	
		σ (MPa)	*St. Dev.*	σ (MPa)	*St. Dev.*	σ (MPa)	*St. Dev.*	σ (MPa)	*St. Dev.*	σ (MPa)	*St. Dev.*
Before Exposure	0°	-179.3	*76.4*	-56.3	*27.4*	-309.6	*18.0*	-52.5	*30.4*	-30.5	*43.9*
	90°	149.5	*35.4*	210.4	*41.2*	56.1	*35.7*	199.8	*41.7*	296.1	*34.7*
After Exposure	0°	-200.8	*45.5*	-124.8	*51.3*	-169.7	*13.9*	-161.8	*36.0*	-103.5	*28.7*
	90°	142.3	*25.5*	141.2	*49.8*	58.9	*33.9*	121.7	*41.4*	211.3	*22.2*

The difference of stresses measured in two directions is obvious. The stresses in the direction parallel to the loading (along the main axis of the sample) are negative before and after testing, whereas the stresses in the other direction are positive. This variation is caused by the manufacturing procedure—grinding—which creates surface texture.

Another important fact is the substantial variation of surface stresses between test samples before exposure in both 0° and 90° directions. Those variations are likely caused by differences in the final grinding parameters (down pressure of the stone, amount of material reduction, and so on). Even though the surface stresses on other samples reserved for peening were not measured prior to peening, it is reasonable to expect a similar level of variation as well. The peening process will smooth the surface stress of samples such that the variation between the peened samples will be much lower, as shown in sections that follow.

B.2.2.2 Underwater Laser Peening by Toshiba

Appearance of all samples after peening is shown in Figure B-22. The peened surfaces are noticeably darker than as-manufactured surfaces. No dimpling or other surface unevenness has been observed.

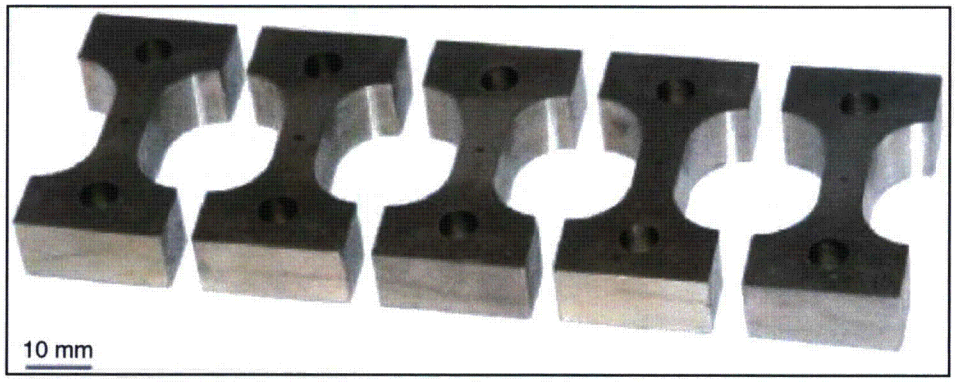

Figure B-22
All samples prepared for exposure after underwater laser peening by Toshiba

Appearance of the samples before exposure and after exposure for different numbers of cycles is shown in Figure B-23. All samples are covered with high-temperature oxides, originating mainly from the pins, interconnecting fixtures, and autoclave body. The dimensional check—measurement of the sample length—was performed before and after the experiment. No significant change was detected. This confirms that the samples were not strained over the yield strength value.

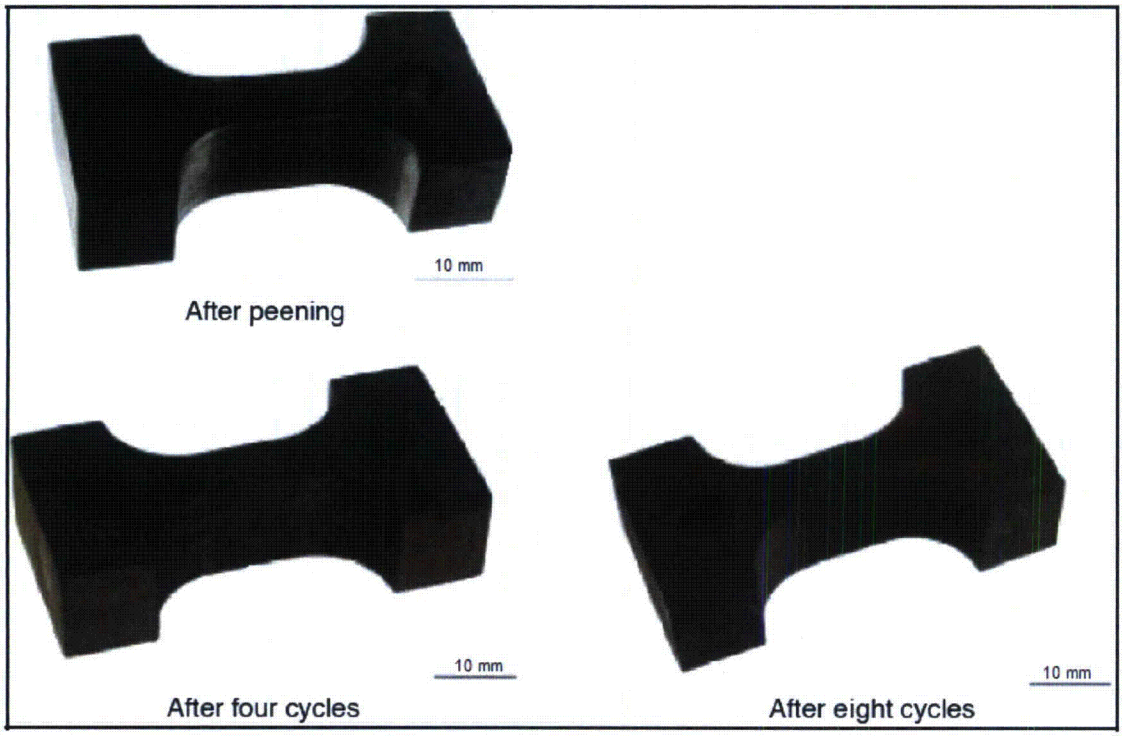

Figure B-23
Appearance of the samples after different stages of experiment: ULP by Toshiba

The microstructure of the material in the subsurface layer before and after exposure is shown in Figure B-24. The microstructure of peened samples before and after exposure appears to be similar. There are no changes either directly under the surface or deeper in the bulk material. Both the grain size and morphology or the amount and distribution of the carbides are equivalent. Also, no visible deformation bands could be observed under the surface of peened samples. An analogous situation is in the microstructure of the samples after exposure. One sample for each number of exposure cycles (2, 4, and 8) was sectioned; no visible change in the microstructure was detected.

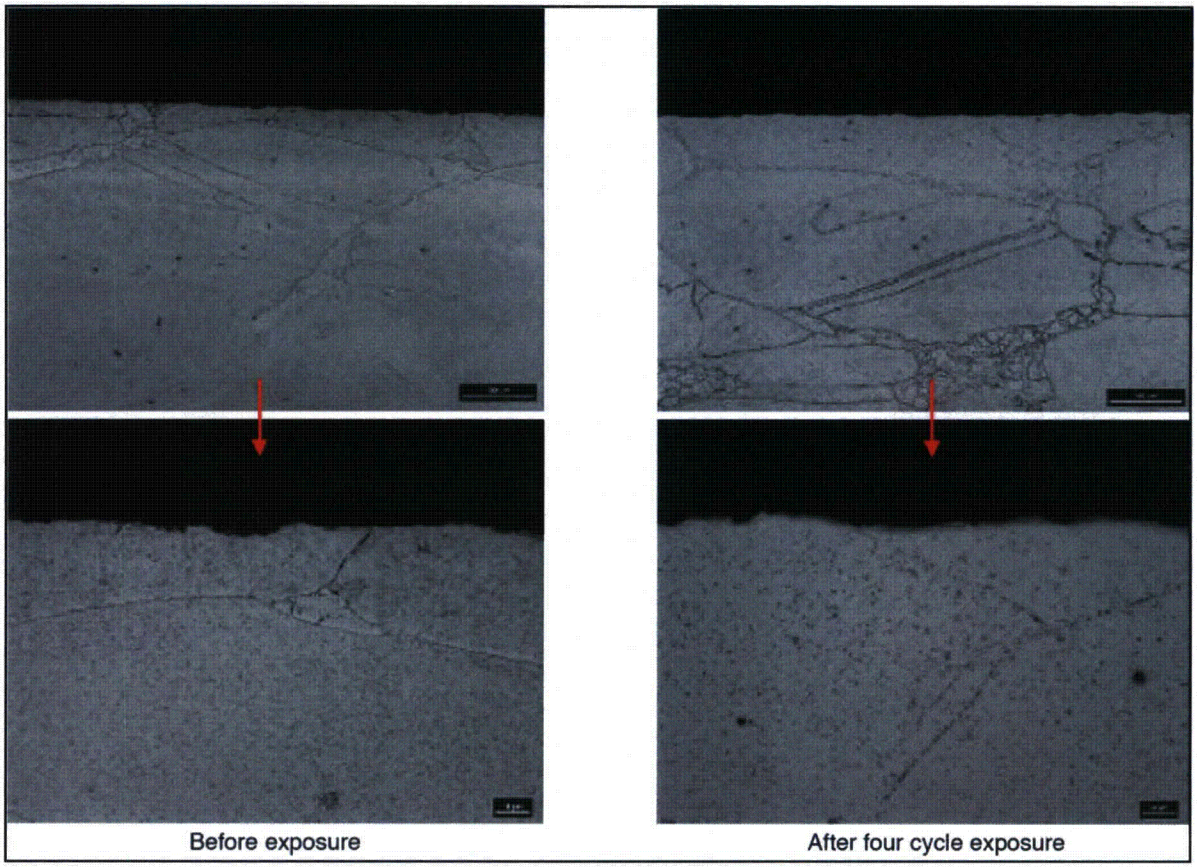

Figure B-24
Subsurface layer microstructure: ULP by Toshiba

The microhardness depth profile graph is shown in Figure B-25. The measurement has been made to about 700 μm under the sample surface for three types of samples: unexposed, exposed for four cycles, and exposed for eight cycles. The short horizontal line in position of the sample surface shows the average microhardness value directly beneath the surface, calculated from five measurements.

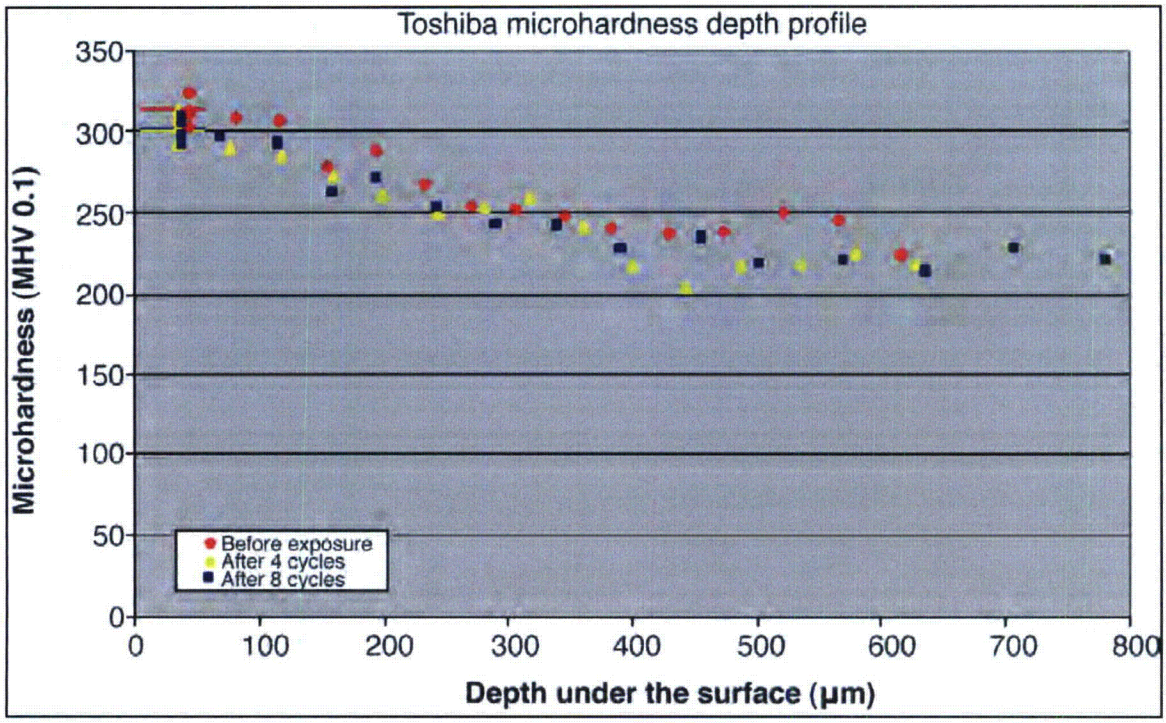

Figure B-25
Microhardness depth profile: ULP by Toshiba

The surface microhardness is about 20% above the bulk material MHV, compared to only about 10% increase for the unpeened material. This elevated value falls slowly to the bulk material value approximately 300 µm under the surface. This corresponds to the fact that this type of peening process influences material deeper than some other peening methods. MHV measured on the sample before exposure appears to be higher compared to hardness measured on both samples after exposure, but the difference is not substantial and could be explained by inherent scatter of microhardness measurement.

The results of the surface stress measurements are shown in Figure B-26. The first bar in the graph indicates the value before exposure; the second bar indicates the surface stress value measured on the same sample after exposure for the respective number of cycles.

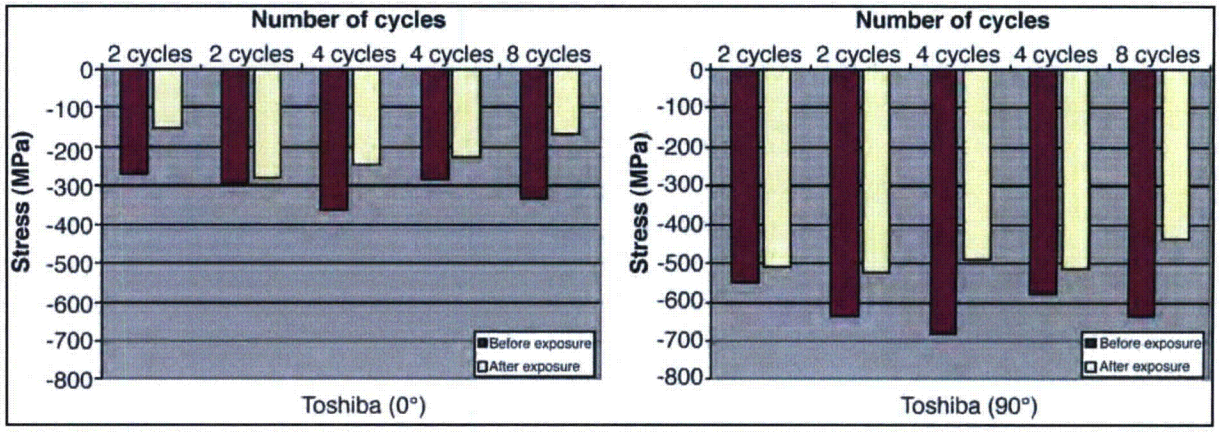

Figure B-26
Surface stresses measured parallel (left) and perpendicular (right) to the loading direction: ULP by Toshiba

The values in the graphs show that the surface stresses have been transformed into negative values—that is, compressive stresses. The significant difference in stresses measured in both directions is clearly visible. The stresses before testing in the direction parallel to the loading (along the main axis of the sample) are around -300 MPa, while the stresses in the other direction are about -600 MPa.

Note that the variance of all stress values measured in one direction is found to be mostly within the 100 MPa range after peening. In comparison, the as-manufactured samples have highly scattered surface stress values, as shown in Figure B-21. This indicates that the ULP process is not only able to convert the surface stresses into negative values, but is also able to "smooth" the sample surface with regard to the stress distribution.

The average drop of the surface stresses is 95 MPa for 0° measurement and 123 MPa for 90° after cyclic loading. These values are comparable to values associated with other peening methods, but given the relatively low pre-exposure stresses in 0° direction, the after-exposure stresses are significantly lower, a compressive stress of about -150 MPa. No consistent relation between the stress relaxation intensity and the number of cycles could be found.

The individual numerical values together with the standard deviations are shown in Table B-8. Almost all standard deviation values are below 10% of the measured value, indicating the high precision and reliability of stress measurement.

Table B-8
Results of the stress measurements: ULP, Toshiba

		2 Cycles		2 Cycles		4 Cycles		4 Cycles		8 Cycles	
		σ (MPa)	*St. Dev.*	σ (MPa)	*St. Dev.*	σ (MPa)	*St. Dev.*	σ (MPa)	*St. Dev.*	σ (MPa)	*St. Dev.*
Before Exposure	0°	-295.7	*23.5*	-270.9	*15.3*	-283.6	*19.0*	-362.0	*20.5*	-334.0	*37.0*
	90°	-635.4	*37.0*	-546.5	*52.3*	-577.4	*49.1*	-683.2	*27.2*	-640.4	*57.4*
After Exposure	0°	-280.4	*35.4*	-153.4	*18.1*	-225.8	*23.3*	-247.1	*21.9*	-166.4	*48.3*
	90°	-526.1	*17.4*	-505.9	*23.3*	-512.1	*37.9*	-487.2	*33.4*	-436.6	*36.7*

B.2.2.3 Water Jet Peening by Hitachi-GE

Appearance of the samples after peening is shown in Figure B-27. The color of the peened surface is not changed in comparison to as-manufactured samples, and the surface is slightly uneven. This can be better seen in Figure B-28, showing surface appearance before and after exposure in details. This unevenness is most likely caused by the various densities of cavitation bubbles.

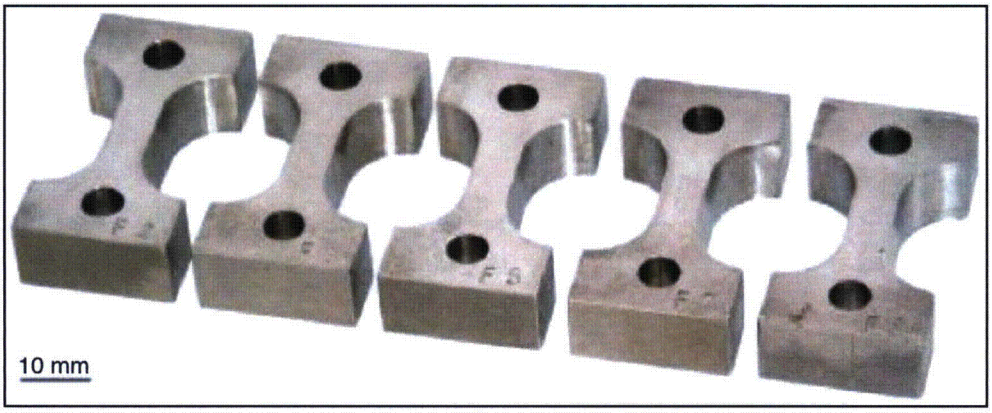

Figure B-27
All samples prepared for exposure after water jet peening by Hitachi-GE

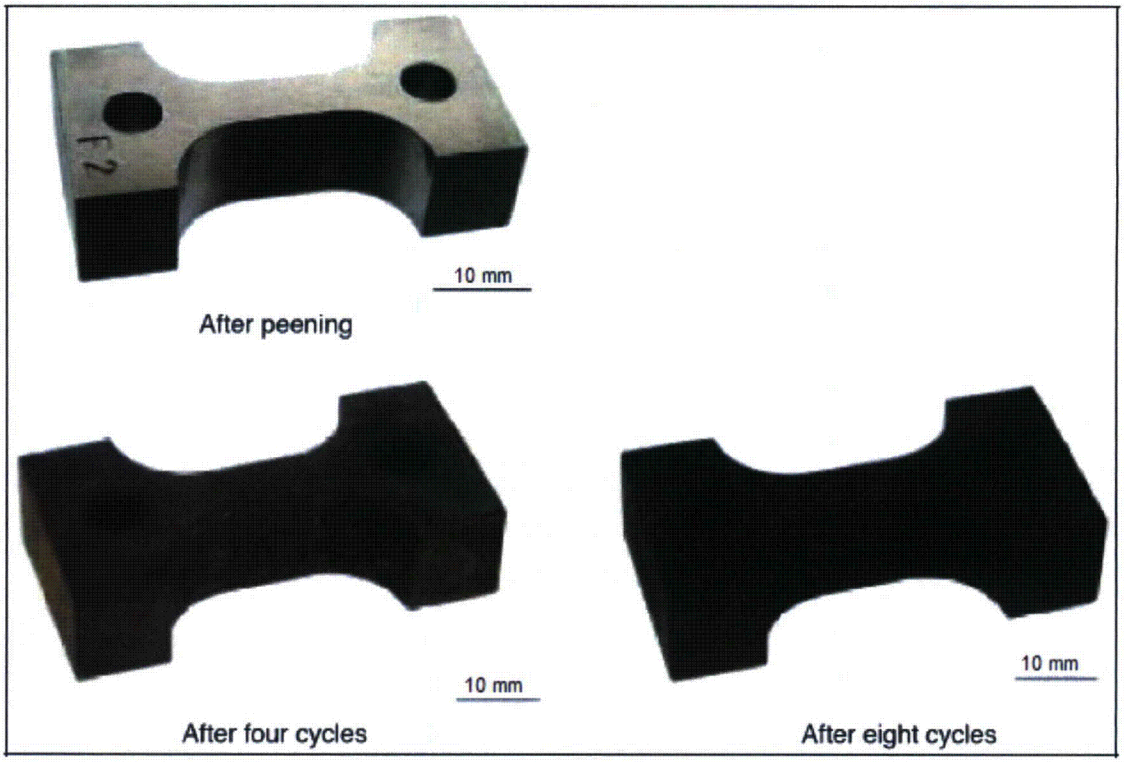

Figure B-28
Appearance of the samples after different stages of experiment: WJP by Hitachi-GE

The microstructure of the material in the subsurface layer before and after exposure is shown in Figure B-29. The measurements of the peened samples look similar to the as-manufactured samples before exposure. There was no visible change either directly under the surface or deeper in the bulk material. Both the grain size and morphology or the amount and distribution of the carbides are equivalent. Also, no visible deformation bands were found under the surface of peened samples. An analogous situation was found in the microstructure of the samples after exposure. One sample for each number of exposure cycles (2, 4, and 8) was sectioned; no visible change in the microstructure was detected.

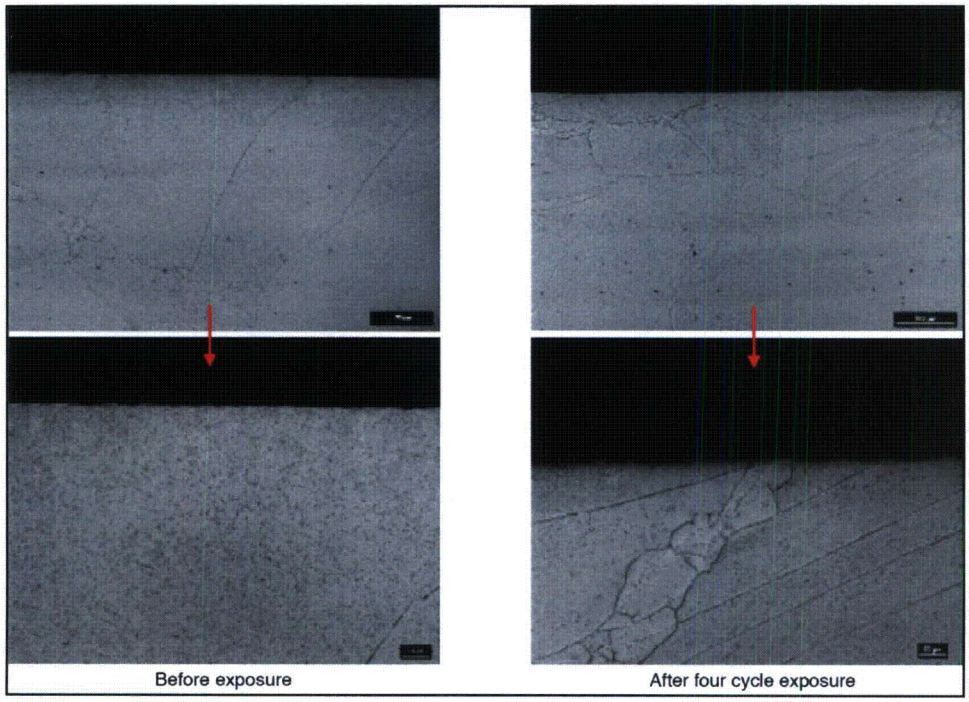

Figure B-29
Subsurface layer microstructure: WJP by Hitachi-GE

The microhardness depth profiles are shown in Figure B-30. The measurements were taken to about 700 μm under the sample surface for three types of samples: unexposed, exposed for four cycles, and exposed for eight cycles. The short horizontal line on the plot shows the average microhardness value directly beneath the surface, based on five measurements.

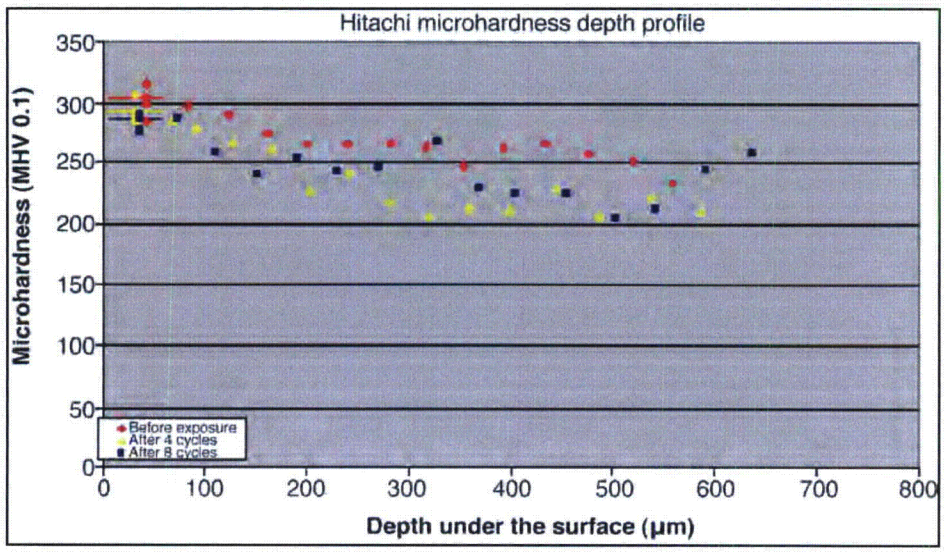

Figure B-30
Microhardness depth profile: WJP by Hitachi-GE

The surface microhardness is about 25% higher than the bulk material MHV, compared to only 10% increase for the unpeened material. This elevated value slowly decreases to the bulk material value at approximately 250 μm under the surface. No significant change of microhardness was found before and after exposure. Variations of the individual MHV measurements deeper in the material are caused by the fact that indents are imprinted into the grains with different orientation and generally cover various lengths of the grain boundaries.

The results of the surface stress measurements are shown in Figure B-31. The values on the graph show that the surface stresses have been converted into negative values—that is, compressive stresses. Similar surface stress measurements were found in both directions on all samples treated with different peening methods. The stresses in the direction parallel to the loading (along the main axis of the sample) before testing are slightly below -500 MPa, while the stresses are around -450 MPa in the other direction.

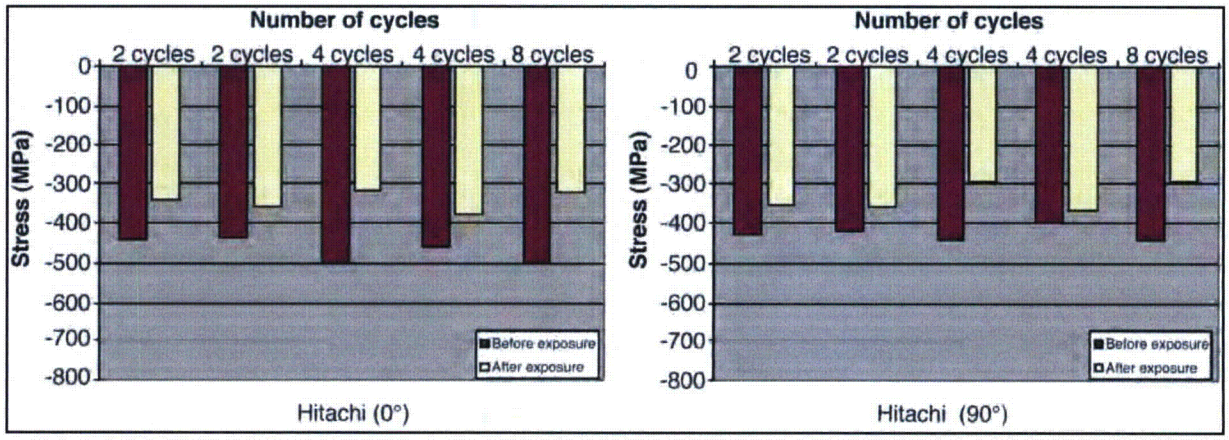

Figure B-31
Surface stresses measured parallel (left) and perpendicular (right) to the loading direction: WJP by Hitachi-GE

The variation of the stresses after peening measured in either one of the directions was found to be within 100 MPa, smaller than for the as-manufactured samples discussed above. This indicates that the peening processes not only altered the surface stresses into negative values, but also smoothed the distribution. The average drop of the surface stresses due to exposure is 126 MPa for the 0° direction and 92 MPa for the 90° direction. Those values are comparable to values associated with other peening procedures. No consistent relation between the relaxation intensity and the number of cycles could be found.

Individual stress values and the standard deviations are shown in Table B-9. Almost all standard deviation values are within 10% of the measured value, indicating the high precision and reliability of the surface stress measurement.

Table B-9
Results of the stress measurements: WJP, Hitachi-GE

		2 Cycles		2 Cycles		4 Cycles		4 Cycles		8 Cycles	
		σ (MPa)	*St. Dev.*	σ (MPa)	*St. Dev.*	σ (MPa)	*St. Dev.*	σ (MPa)	*St. Dev.*	σ (MPa)	*St. Dev.*
Before Exposure	0°	-443.7	*16.8*	-435.5	*22.7*	-501.9	*30.3*	-458.7	*22.2*	-501.0	*32.1*
	90°	-427.2	*10.3*	-414.8	*18.1*	-441.9	*18.0*	-399.0	*12.0*	-441.9	*40.5*
After Exposure	0°	-340.0	*22.2*	-354.8	*26.5*	-318.2	*24.0*	-375.3	*13.8*	-320.2	*24.7*
	90°	-353.2	*21.4*	-355.4	*8.3*	-293.4	*38.1*	-367.3	*13.8*	-293.2	*23.7*

B.2.2.4 Water Jet Peening by Mitsubishi

Appearance of all samples after peening is shown in Figure B-32. The color of the peened surface is not changed compared to as-manufactured samples; the surface is slightly uneven. This is seen better in Figure B-33, showing surface appearance before and after exposure in detail.

Figure B-32
Samples prepared for exposure after water jet peening, Mitsubishi

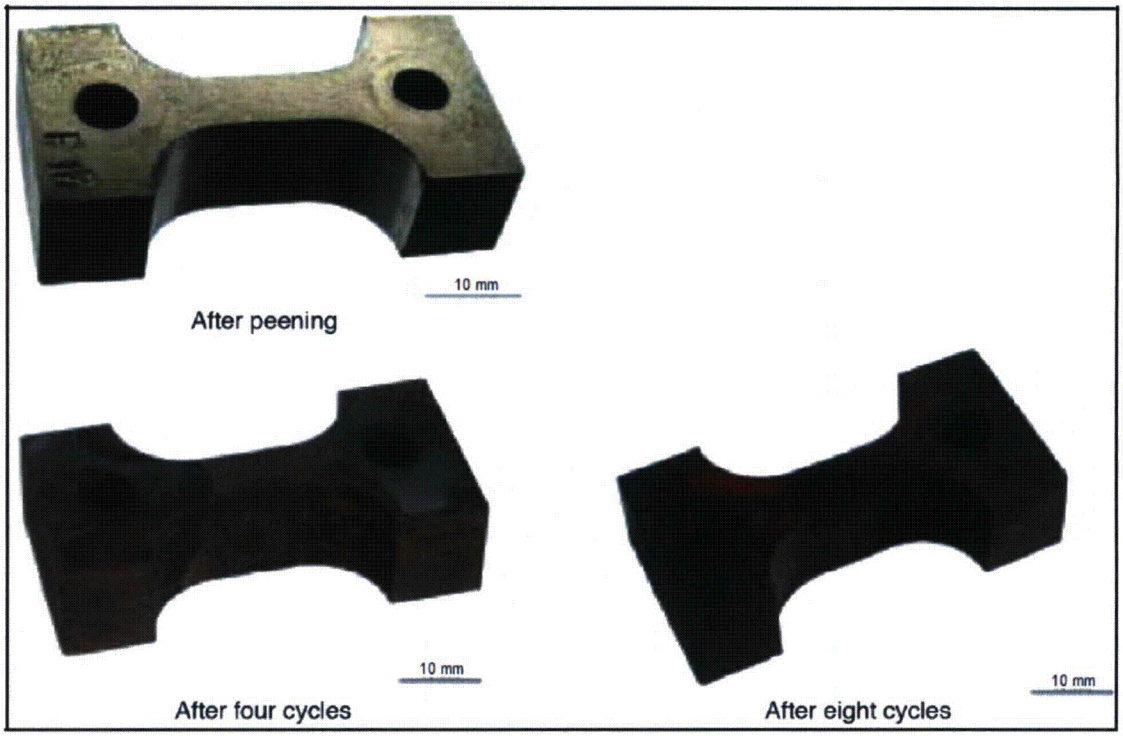

Figure B-33
Appearance of the samples after different stages of the experiment: WJP by Mitsubishi

The microstructure of the material in the subsurface layer before and after exposure is shown in Figure B-34. The microstructure of the as-manufactured sample, shown in Figure B-19, and the microstructure of the peened sample before exposure appear to be similar. There was no change either directly under the surface or deeper in the bulk material visible in low or high magnification. Both the grain size and morphology or the amount and distribution of the carbides are equivalent. Also, no deformation bands are visible under the surface of the peened sample. An analogous situation was found in the microstructure of the samples after exposure. One sample for each number of exposure cycles (2, 4, and 8) was sectioned; no visible change in the microstructure was detected.

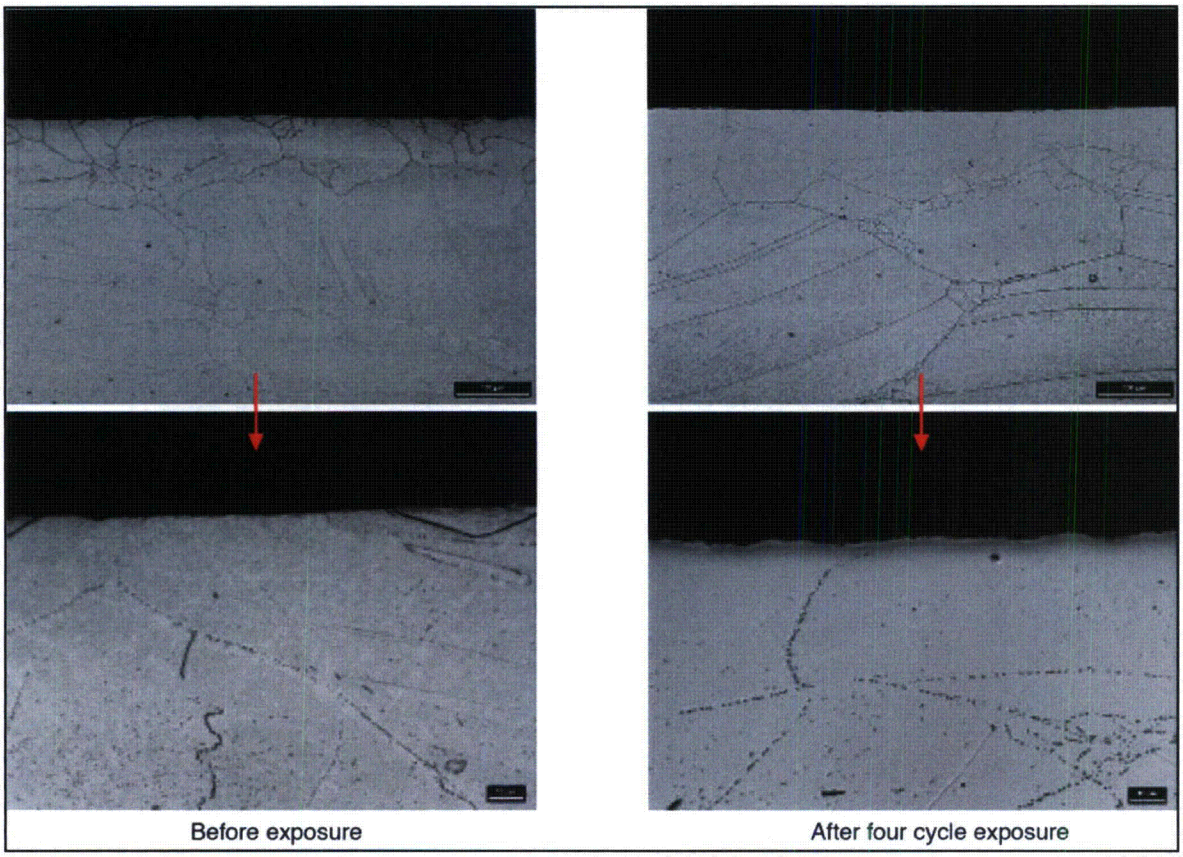

Figure B-34
Subsurface layer microstructure: WJP by Mitsubishi

The microhardness depth profiles are shown in Figure B-35. The measurements were made to about 700 μm under the surface for three types of samples: unexposed, exposed for four cycles, and exposed for eight cycles. The short horizontal line in the position of the sample surface shows the average microhardness value directly beneath the surface, calculated from five measurements. The surface microhardness is about 25% higher than the bulk material MHV, compared to only about 10% increase for the unpeened material. This elevated value decreases slowly to the bulk material value at approximately 200 μm under the surface. With respect to inherent scatter of microhardness data, no visible change between the unexposed and exposed samples was found.

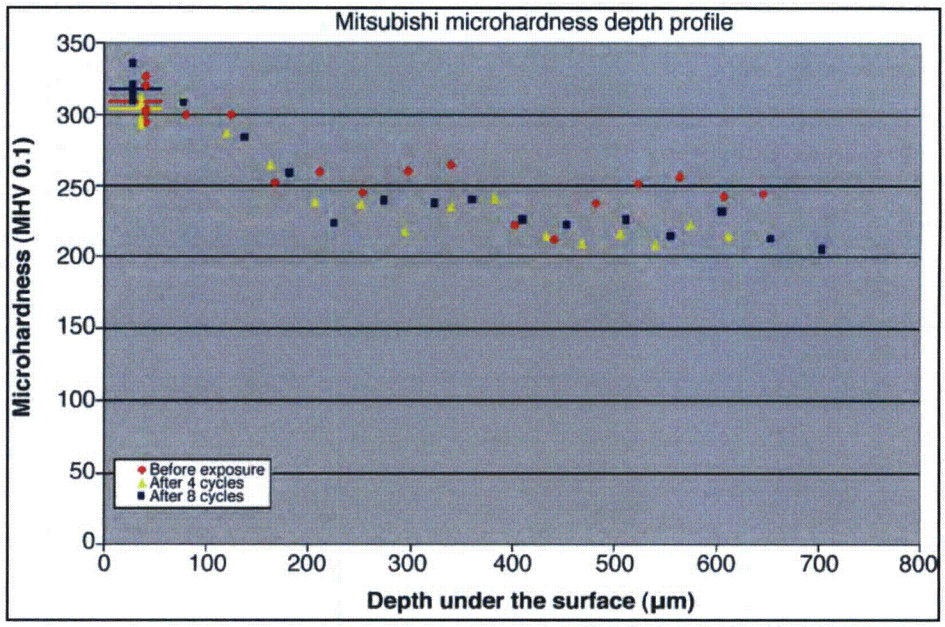

Figure B-35
Microhardness depth profile: WJP by Mitsubishi

The results of the surface stress measurements are shown in Figure B-36. The values in the graphs show that the surface stresses have been transformed into negative values—that is, compressive stresses. A significant difference in the stresses measured in the axial and transverse directions could be distinguished. The stresses before testing in the direction parallel to the loading (along the main axis of the sample) are slightly below -500 MPa, while the stresses in the transverse direction are around -350 MPa.

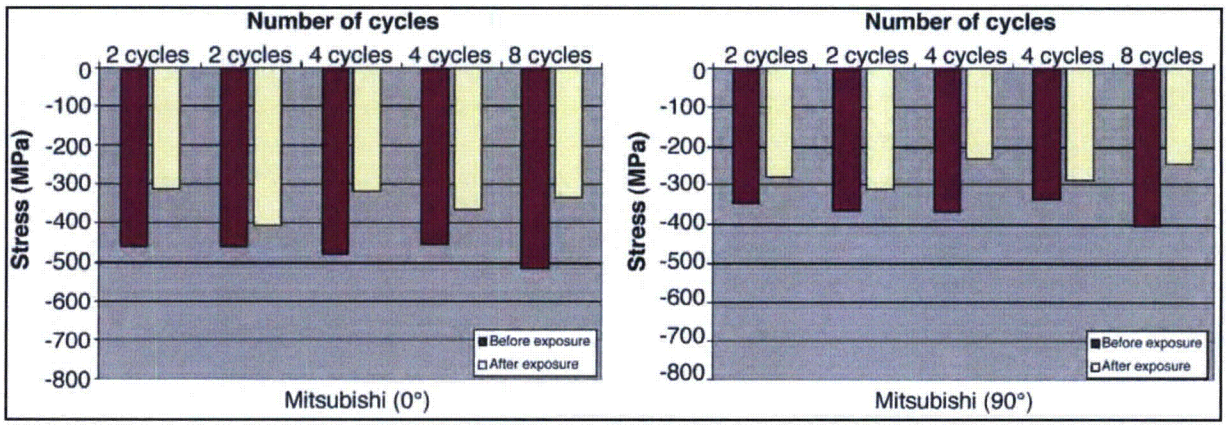

Figure B-36
Surface stresses measured parallel (left) and perpendicular (right) to the loading direction: WJP by Mitsubishi

The variation of the stresses after peening measured in one direction was found to be mostly within the 100 MPa range. In comparison, highly scattered surface stress values were found for

the as-manufactured samples, as discussed above. This indicates that the peening process not only changed the surface stress values, but also smoothed them. The average drop of the surface stresses due to cycling is 128 MPa in the 0° direction and 97 MPa in the 90° direction. No consistent relationship of the relaxation intensity with respect to the number of cycles was found. The stress values together with the standard deviations are shown in Table B-10. All standard deviations are within 10% of the average values.

Table B-10
Results of the stress measurements: WJP, Mitsubishi

		2 Cycles		2 Cycles		4 Cycles		4 Cycles		8 Cycles	
		σ (MPa)	St. Dev.	σ (MPa)	St. Dev.	σ (MPa)	St. Dev.	σ (MPa)	St. Dev.	σ (MPa)	St. Dev.
Before Exposure	0°	-463.0	19.4	-464.4	20.5	-453.4	25.8	-483.2	34.5	-371.1	12.1
	90°	-369.1	11.7	-349.2	25.2	-337.6	14.1	-371.3	12.1	-406.0	18.7
After Exposure	0°	-405.2	16.0	-310.3	25.6	-365.7	35.3	-319.0	26.7	-333.7	13.6
	90°	-307.3	24.2	-280.3	12.9	-287.0	18.4	-229.6	21.1	-241.6	17.7

B.2.2.5 Air Laser Peening by MIC

The samples described in this section were treated with MIC's air laser peening process using an ablative layer. The appearance of the peened surface for the samples both before and after exposure is shown on Figure B-37. The peened area is localized in the central part of the dog bone sample; both sides of the samples have been peened. The surface of the sample is visibly deformed in a wave-like pattern perpendicular to the main axis, indicating significant deformation of the subsurface layer. This deformation is confirmed by microhardness measurements. No changes in the surface morphology are visible after exposure.

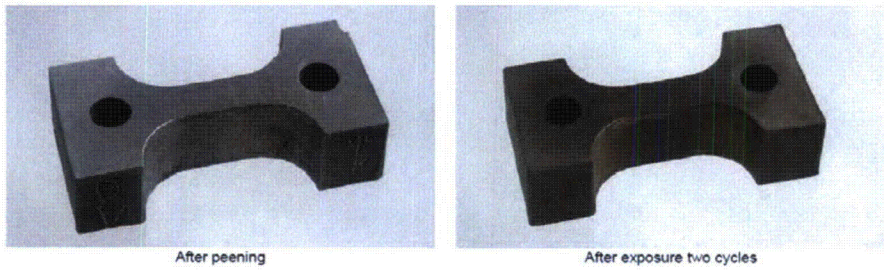

Figure B-37
Appearance of the samples after different stages of experiment: ALP by MIC

The material microstructure available for this testing is different from the material used in the first set of experiments. The material used for this testing has distinct parallel bands of large grains alternating with small grain bands with higher microhardness.

The microstructure of the unexposed sample AB13, available for destructive testing after peening, is shown on Figure B-38. The micrographs show that both surfaces of the sample are uneven. This is likely caused by the peening process itself, as indicated by the close up photograph of the sample surface. The surface morphology of this sample differs from all other samples, including the others exposed to the same ALP treatment.

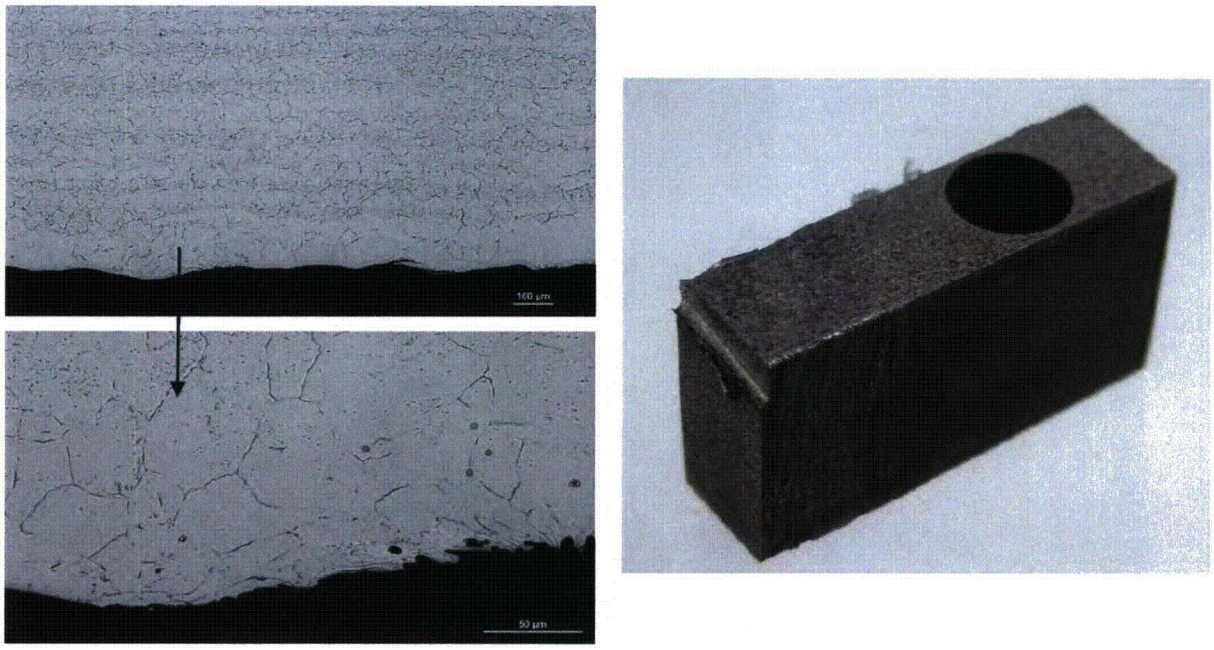

Figure B-38
Microstructure of the sample after peening and before exposure (micrographs on left) and close-up of the surface (right)

The surface of all other samples is relatively flat and even. There are no visible differences between samples exposed for different number of cycles.

The microstructures in the areas under the upper and lower surfaces of the sample exposed for 8 cycles are shown in Figure B-39. This particular sample had the large grain band positioned directly under the upper surface and small grain band under the lower surface. The micrographs show that there are no visible changes in microstructure after exposure as regards the grain size or microstructural deformations under both surfaces.

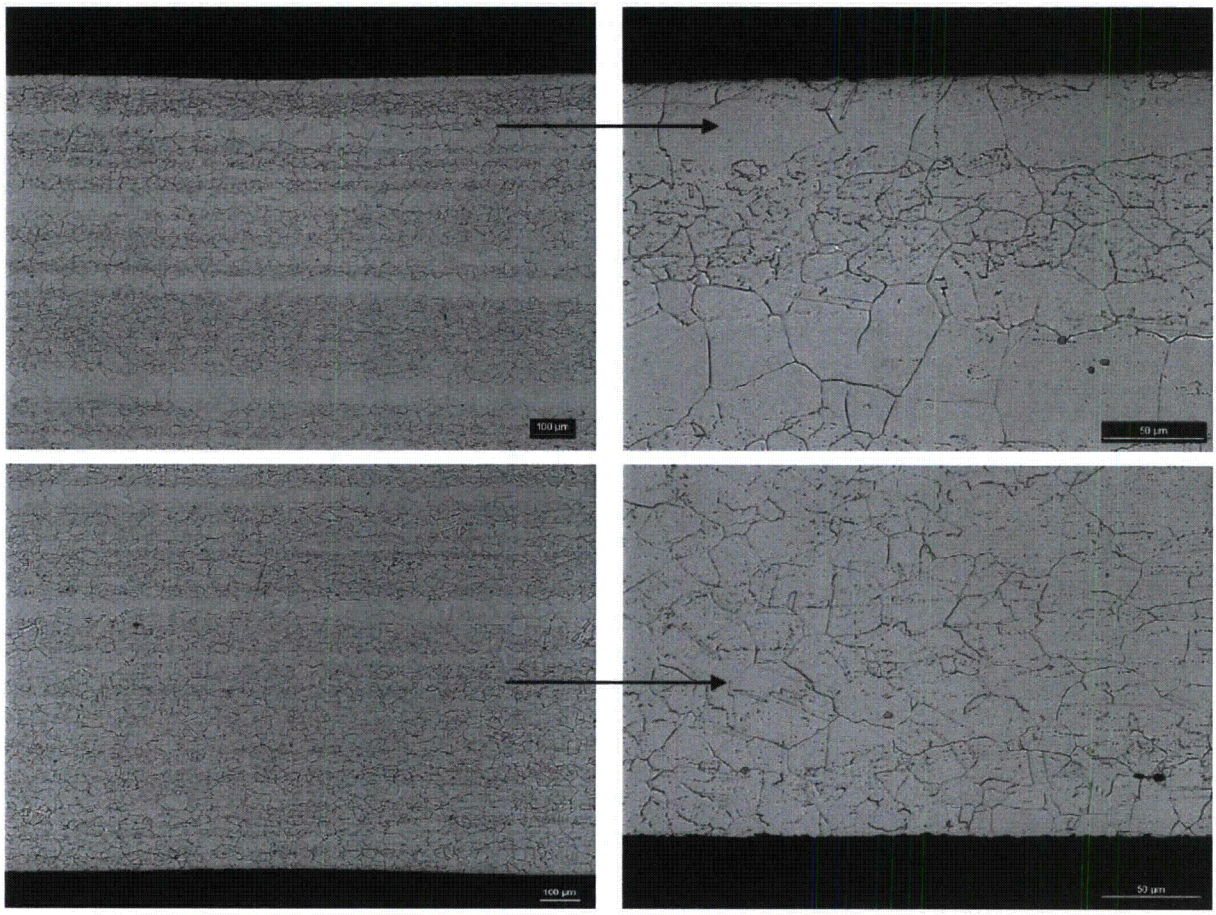

Figure B-39
Microstructure of the sample after exposure (8 cycles), upper and lower surface, different magnifications: ALP by MIC

The microhardness depth profile has been measured for all samples (unexposed, 2C, 4C and 8C) on both surfaces. All the data for the MIC peened samples are summarized in a the plot on Figure B-40. The short lines at the beginning of the plot indicate average microhardness values calculated from several indents just under the surface. This averaging helps to evaluate relatively the scattered values of subsurface indents.

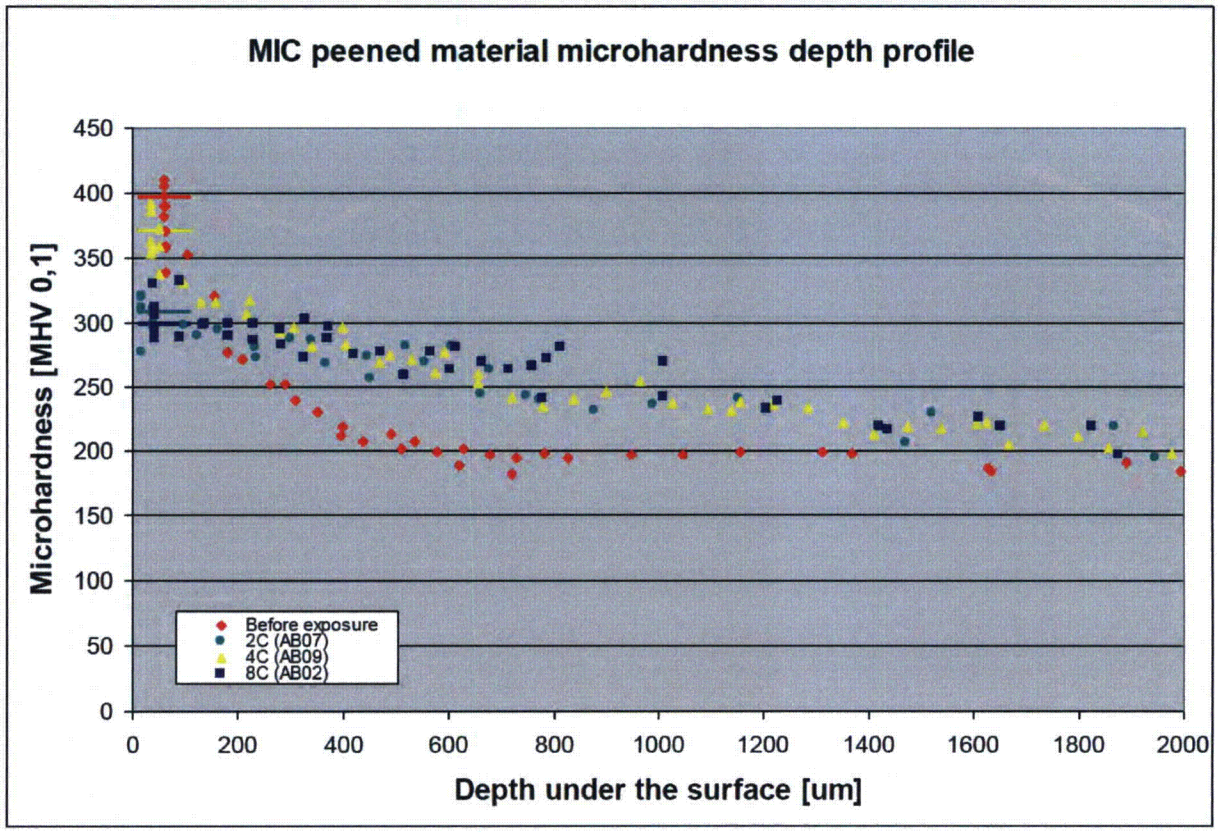

Figure B-40
Microhardness depth profile: ALP by MIC

The microhardness depth profile shows that the loading process decreases the surface microhardness values compared to unexposed sample, but increases the subsurface values. The bulk microhardness value of the exposed samples is also reached deeper under the surface (around 1500 μm) compared to the other peening methods or the unexposed sample in these experiments, which attained bulk microhardness at an average depth of 500 μm. This feature has not been observed on any of other three peening methods studied in the first set of experiments. The variations in the values measured deeper in the bulk material are caused by the bimodal microstructure, with alternating bands of large and small grains. The average value of microhardness of the large grain area, calculated from all samples, is 174 MHV. The average value of microhardness of the small grain bands is 203 MHV. The difference in indents sizes is visible on group of indents on Figure B-41.

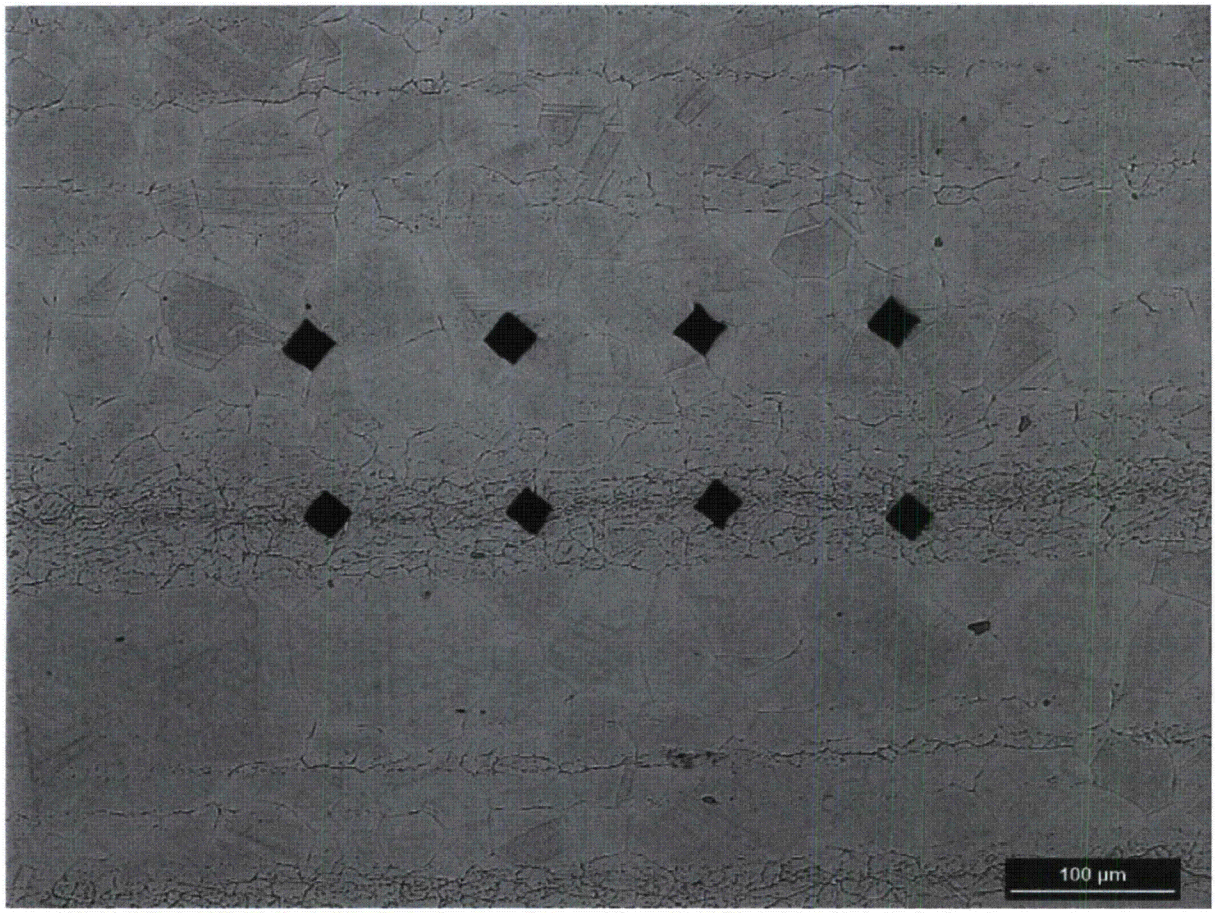

Figure B-41
Comparison of MHV Indent Sizes in Large and Small Grain Areas

The results of the surface stress measurements are shown on Figure B-42. The stresses are measured in both the axial direction (parallel to the loading direction, on the left) and the perpendicular direction (right). The bar on left indicates the surface stress before exposure, the bar on right shows the value after exposure to respective number of cycles. The plot provides information about the stress state both directly after application of the peening process and after loading in the autoclave.

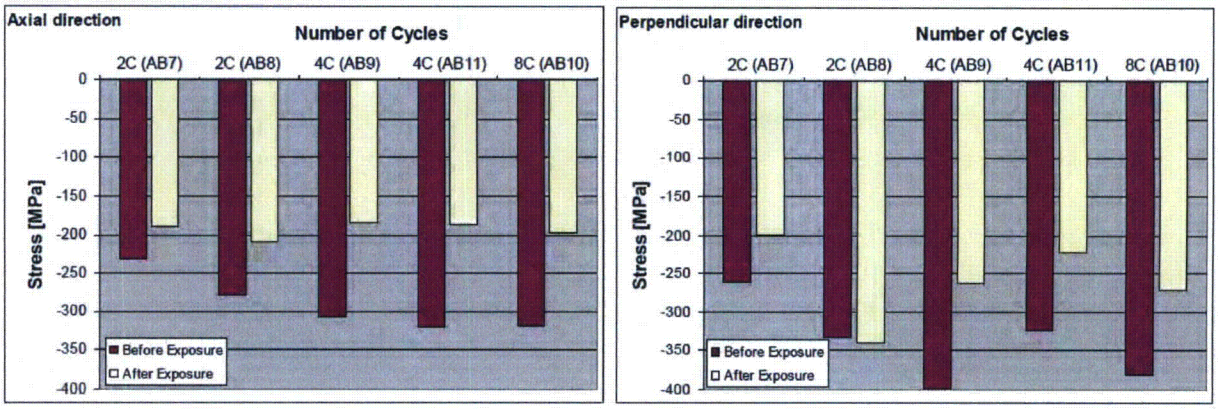

Figure B-42
Surface stresses measured parallel (left) and perpendicular (right) to the loading direction: ALP by MIC

The main conclusions of the surface stress measurement are in conformity with results of the first set of experiments: stress relaxation after loading has been detected, which is apparently independent of the number of loading cycles.

For all samples in both directions a relaxation in the range of 20-40% has been detected, which is similar to the relaxation that has been observed in the first set of experiments for the other three peening processes. Also, there appears to be no relation between the number of loading cycles the sample has been subjected to and the degree of relaxation. The drop in the surface stresses after the exposure appears to be rather uniform for all samples, about 30% (with exception of sample AB8, perpendicular direction). This conclusion is also similar to that based on the first set of experiments.

In order to facilitate further analysis of the stress measurement data all numerical values of the measurements together with standard deviation provided by the measuring system are given in Table B-11.

Table B-11
Results of the stress measurements: ALP, MIC

		2 Cycles		2 Cycles		4 Cycles		4 Cycles		8 Cycles	
		σ (MPa)	*St. dev.*	σ (MPa)	*St. dev.*	σ (MPa)	*St. dev.*	σ (MPa)	*St. dev.*	σ (MPa)	*St. dev.*
Before exp.	Axial	-230.8	*19.1*	-278.3	*22.0*	-306.3	*11.5*	-321.1	*14.6*	-318.8	*23.9*
	Perp.	-260.5	*25.9*	-333.8	*32.8*	-398.5	*32.0*	-323.9	*27.3*	-381.5	*27.8*
After exp.	Axial	-189.2	*17.6*	-208.8	*27.3*	-184.9	*15.9*	-186.9	*22.5*	-198.3	*14.4*
	Perp.	-199.8	*22.3*	-340.6	*23.0*	-261.9	*13.7*	-222.0	*31.3*	-272.1	*18.1*

B.2.2.6 Comparison of Results across the four peening vendors

Comparing the absolute values of the surface stresses between all four vendors, the MIC process produces the least compressive stresses on the surface. The average values are summarized on the Table B-12. The data also show that the average decrease after exposure for all peening processes is between 20 to 30%.

Table B-12
Comparison of Average Values of the Surface Stresses from the First and Second Set of Experiments

Vendor	Measurement Orientation	Average stress after peening (MPa)	Average stress decrease after exposure (%)
MIC	Axial	-291	-32
	Perpendicular	-339	-23
Hitachi-GE	Axial	-468	-27
	Perpendicular	-425	-22
Mitsubishi	Axial	-475	-27
	Perpendicular	-366	-27
Toshiba	Axial	-309	-31
	Perpendicular	-616	-20

Figure B-43 compares the results of the experiments on microhardness values of peened samples from all four vendors (in both sets of experiments). Significantly higher subsurface MHV values for the MIC peening process for the sample before exposure as well as after 4 cycles are clearly visible. After 8 cycles the subsurface MHV values equalize for all four peening processes, but MIC peening produces higher microhardness values deeper in material.

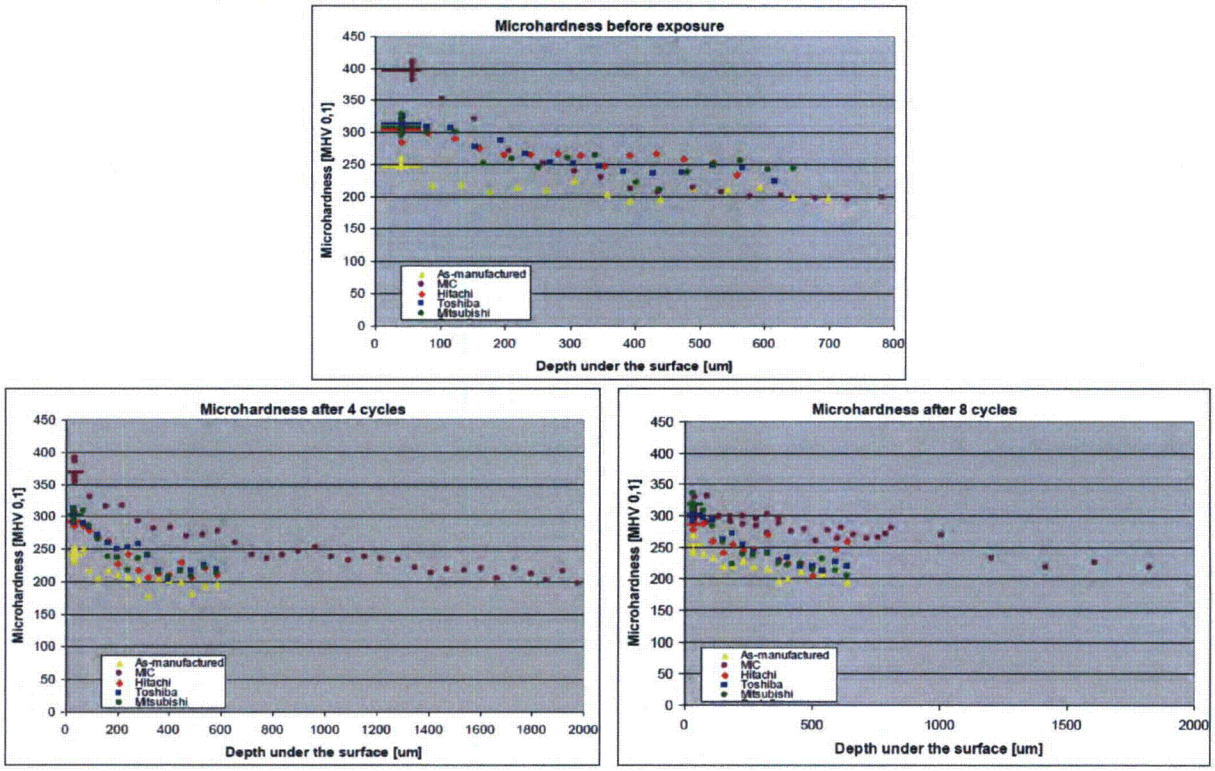

Figure B-43
Comparison of MHV Depth Profile Results in both sets of experiments

The bulk MHV values for MIC peening for the unexposed sample are reached at a relatively shallow depth, even compared to other peening methods On the other hand, there is a deeper-reaching increase of MHV in the exposed MIC samples. This is apparently an attribute of the peening process and is not related to the differences in the material microstructure.

Export Control Restrictions

Access to and use of EPRI Intellectual Property is granted with the specific understanding and requirement that responsibility for ensuring full compliance with all applicable U.S. and foreign export laws and regulations is being undertaken by you and your company. This includes an obligation to ensure that any individual receiving access hereunder who is not a U.S. citizen or permanent U.S. resident is permitted access under applicable U.S. and foreign export laws and regulations. In the event you are uncertain whether you or your company may lawfully obtain access to this EPRI Intellectual Property, you acknowledge that it is your obligation to consult with your company's legal counsel to determine whether this access is lawful. Although EPRI may make available on a case-by-case basis an informal assessment of the applicable U.S. export classification for specific EPRI Intellectual Property, you and your company acknowledge that this assessment is solely for informational purposes and not for reliance purposes. You and your company acknowledge that it is still the obligation of you and your company to make your own assessment of the applicable U.S. export classification and ensure compliance accordingly. You and your company understand and acknowledge your obligations to make a prompt report to EPRI and the appropriate authorities regarding any access to or use of EPRI Intellectual Property hereunder that may be in violation of applicable U.S. or foreign export laws or regulations.

The Electric Power Research Institute Inc., (EPRI, www.epri.com) conducts research and development relating to the generation, delivery and use of electricity for the benefit of the public. An independent, nonprofit organization, EPRI brings together its scientists and engineers as well as experts from academia and industry to help address challenges in electricity, including reliability, efficiency, health, safety and the environment. EPRI also provides technology, policy and economic analyses to drive long-range research and development planning, and supports research in emerging technologies. EPRI's members represent more than 90 percent of the electricity generated and delivered in the United States, and international participation extends to 40 countries. EPRI's principal offices and laboratories are located in Palo Alto, Calif.; Charlotte, N.C.; Knoxville, Tenn.; and Lenox, Mass.

Together...Shaping the Future of Electricity

Program:

Pressurized Water Reactor Materials Reliability Program

1025839

Electric Power Research Institute
3420 Hillview Avenue, Palo Alto, California 94304-1338 • PO Box 10412, Palo Alto, California 94303-0813 USA
800.313.3774 • 650.855.2121 • askepri@epri.com • www.epri.com